POLYTECHNIQUE MONTRÉAL
affiliée à l'Université de Montréal

Smart Charging Management of Electric Vehicles Through Optimization and Learning-Based Coordination

ARIAN SHAH KAMRANI
Département de mathématiques et de génie industriel

Thèse présentée en vue de l'obtention du diplôme de *Philosophiæ Doctor*
Mathématiques

Novembre 2025

POLYTECHNIQUE MONTRÉAL
affiliée à l'Université de Montréal

Cette thèse intitulée :

Smart Charging Management of Electric Vehicles Through Optimization and Learning-Based Coordination

présentée par **Arian SHAH KAMRANI**
en vue de l'obtention du diplôme de *Philosophiæ Doctor*
a été dûment acceptée par le jury d'examen constitué de :

Youssef DIOUANE, président
Hanane DAGDOUGUI, membre et directrice de recherche
Quentin CAPPART, membre
Zhanle WANG, membre externe

DEDICATION

To my parents, Fariba and Kamyar.

ACKNOWLEDGEMENTS

I would like to start by thanking Professor Hanane Dagdougui, my supervisor, for her constant support throughout my Ph.D. She saw potential in my work even when I doubted it myself, whether in steady times or during challenges, her support, encouragement, and understanding were always there. Her guidance helped shape this thesis and made a big impact on how I have grown as a researcher. I am truly grateful for everything she has done.

I also want to thank my lab friends and colleagues at Polytechnique, GERAD, and Mila, who made this journey much more enjoyable. Some days, just knowing I would see them was reason enough to come to the university. Their presence, conversations, and encouragements gave me energy and motivation when I needed it most. I am also grateful to Professor Keyhan Sheshyekani and Professor Samira Keivanpour for their kind support and guidance throughout this time.

This research was made possible thanks to the data and resources generously shared by Hydro-Québec and Circuit Électrique. Their contributions formed the foundation of this work and allowed me to explore real-world challenges in electric vehicle charging infrastructure. I am sincerely grateful for their trust and for enabling this research to stay grounded in practical relevance.

To my parents, I owe more than I can express. Your unconditional love, patience, and quiet strength carried me through every stage of this journey. You have always believed in me, and your support gave me the courage to keep going. For everything you have done — and everything you have been — I am deeply grateful.

I am also thankful for the friendships I built here in Montreal. They helped me get through the long winters with laughter, warmth, and shared memories. The time we spent together gave me a chance to step away from research and simply enjoy the moment, which brought a sense of balance to this journey.

Last but not least, I would like to thank my life partner Neda Shamaeian for being by my side through all the ups and downs of this journey. Whether it was listening, encouraging me, or simply being there, she helped more than she knows.

RÉSUMÉ

Les flottes de véhicules électriques (VE) sont appelées à jouer un rôle central dans la décarbonation des systèmes de transport urbain. Toutefois, l'intégration à grande échelle des VE pose d'importants défis à la stabilité du réseau électrique et aux systèmes de communication, en raison des incertitudes liées au comportement des conducteurs, de l'augmentation de la demande de puissance de pointe et de la complexité computationnelle associée à la coordination de millions de sessions de recharge. Les mécanismes de contrôle centralisé deviennent moins pratiques en raison des préoccupations relatives à la confidentialité des données des usagers (profils de consommation, habitudes de déplacement, etc.), et la surcharge de communication qui augmente la latence et fragilise la réactivité du système.

D'une part, les propriétaires de VE sont souvent réticents à partager des données personnelles détaillées, et d'autre part, le gestionnaire de réseau de distribution (GRD) n'est pas autorisé à divulguer des informations confidentielles sur la topologie du réseau ou les contraintes internes d'exploitation. Il devient donc nécessaire de développer des cadres de gestion de la recharge des VE qui soient évolutifs, distribués et hiérarchiques, tout en garantissant la protection de la vie privée et en réduisant les charges liées à l'échange d'information.

Cette thèse vise à concevoir des stratégies robustes, évolutives et interprétables pour la coordination de la recharge des VE, qui respectent les contraintes du réseau, préservent la satisfaction des utilisateurs et réduisent les coûts d'exploitation. Pour ce faire, elle s'appuie à la fois sur la planification en avance (day-ahead) et sur la prise de décision en temps réel (real-time), afin de proposer des cadres de gestion efficaces et pragmatiques, capables de s'adapter à la variabilité temporelle et comportementale.

La première partie de cette thèse est consacrée à une coordination équitable, en temps réel, fondée sur une approche d'apprentissage par renforcement profond multi-agent (MADRL). Dans ce cadre, chaque Agrégateurs de VE (EVA) est modélisé comme un agent d'apprentissage par renforcement utilisant un réseau Double Deep Q-Network (DDQN) combinant des taux d'apprentissage adaptatifs et une mémoire d'expériences priorisée, afin d'accélérer la convergence. Parallèlement, le GRD calcule la puissance maximale autorisée à chaque nœud via une optimisation de flux de puissance en courant alternatif, et la répartit en s'appuyant sur un modèle de compromis entre efficacité et équité de Jain (EJT). Au niveau des stations, un contrôleur intelligent de répartition en temps réel priorise la recharge de VE en fonction de leur facteur d'urgence, lequel combine l'heure de départ, la puissance maximale de charge, la demande énergétique et l'état de santé de la batterie. Des études de cas réalisées sur le

réseau transmission IEEE à 118 nœuds montrent que ce cadre permet de réduire la demande de pointe, de diminuer les coûts de recharge, de respecter les limites de tension et d'améliorer significativement l'équité par rapport aux approches de type premier arrivé–premier servi et recharge non contrôlée. Par ailleurs, les résultats indiquent que l'intégration de systèmes photovoltaïques (PV) dans ce cadre permet d'améliorer la flexibilité locale du réseau et de réduire la dépendance énergétique vis-à-vis du réseau principal.

La deuxième partie introduit une architecture prédictive fondée sur le regroupement en clusters, visant à améliorer la coordination de la recharge des VE à l'échelle de la planification anticipée et du temps réel. Une méthode novatrice de regroupement spatio-temporel est proposée pour former des aggrégateurs de VE. Contrairement à un regroupement purement géographique, cette méthode prend en compte la fréquence de recharge, le taux d'utilisation et les plages horaires d'usage. Au sein de chaque cluster, un modèle de type Temporal Fusion Transformer (TFT) est utilisé pour prédire les principaux paramètres comportementaux tels que l'heure d'arrivée, l'heure de départ et la demande énergétique, en exploitant les données historiques de transactions, les calendriers et les prévisions météorologiques. Ces prédictions alimentent un cadre d'enchères en deux étapes, qui équilibre les engagements pris lors de la planification day-ahead avec les ajustements en temps réel, tout en respectant les contraintes du marché. La stratégie proposée permet de réduire les coûts quotidiens et la puissance de pointe par rapport à une recharge non contrôlée, tout en minimisant les écarts entre les profils d'énergie planifiés et réels.

La troisième partie de la thèse propose un cadre de coordination hiérarchique à trois niveaux, dans lequel le contrôle de la recharge des VE est réparti entre les clusters, les aggrégateurs de VE et le GRD, selon une structure de décomposition basée sur la méthode des multiplicateurs alternés (ADMM). Au niveau des clusters, un nouvel algorithme appelé répartiteur proportionnel sensible à l'urgence (UAPA) remplace l'optimisation individuelle par VE par une seule variable décisionnelle agrégée par groupe, ce qui réduit considérablement la complexité computationnelle tout en maintenant une forte concordance avec les méthodes classiques d'optimisation. Au niveau EVA et GRD, un cadre ADMM enrichi par apprentissage automatique (ML-ADMM) utilise des réseaux de neurones profonds pour prédire des conditions initiales (warm-start) des variables primales et duales, réduisant ainsi significativement le nombre d'itérations nécessaires. Le système global démontre sa scalabilité, sa capacité à préserver la confidentialité des données, et son efficacité à respecter les contraintes du réseau, à travers des simulations sur les réseaux électriques IEEE 33 bus et IEEE 118 bus utilisant des données réelles de sessions de recharge.

Dans l'ensemble, cette thèse propose des méthodes de coordination évolutives et respectueuses

de la vie privée, unifiant la prévision, le contrôle fondé sur l'apprentissage et l'optimisation hiérarchique pour de larges populations de VE. Les cadres proposés s'appliquent aux réseaux publics de recharge, aux dépôts de flottes et aux programmes de réponse à la demande pilotés par les services publics. En réduisant la charge de communication et en améliorant l'équité, la stabilité et l'efficacité computationnelle, ils répondent aux principaux obstacles à une intégration massive des véhicules électriques.

ABSTRACT

Electric vehicle (EV) fleets are planned to play a central role in decarbonizing urban transportation systems. However, large-scale integration of EVs presents significant challenges to grid stability and communication systems due to uncertainties in driver behavior, increasing peak demands, and the computational complexity of coordinating millions of charging sessions. Centralized control mechanisms are becoming less practical because of concerns related to user data privacy (consumption profiles, travel habits, etc.), as well as the communication overhead that increases latency and undermines system responsiveness.

On the one hand, EV owners are often unwilling to share detailed personal data, and on the other hand, and the Distribution System Operator (DSO) is prohibited from disclosing confidential grid topology or internal operating constraints. As a result, the development of scalable, distributed, and hierarchical EV charging management frameworks that preserve privacy and reduce information exchange overhead becomes necessary.

This thesis aims to design robust, scalable, and interpretable strategies for EV charging coordination that respect grid constraints, preserve user satisfaction, and reduce operational costs. It achieves this by considering both Day-Ahead (DA) planning and Real-Time (RT) decision-making to deliver practical and efficient EV charging management frameworks that are responsive to temporal, behavioral, and infrastructural variability.

The first part of this thesis focuses on RT, fair, and privacy-preserving EV charging coordination through a Multi-Agent Deep Reinforcement Learning (MADRL) approach. Each EV Aggregator (EVA) is modeled as a Reinforcement Learning (RL) agent in the charging framework and utilizes a Double Deep Q-Network (DDQN) that combines adaptive learning rates and prioritized experience replay to accelerate convergence. Meanwhile, the DSO computes the maximum allowable power at each bus through an AC power flow optimization and allocates it using an Efficiency–Jain Fairness Tradeoff (EJT) model. At the station level, an RT Smart Dispatch (RSD) controller prioritizes EVs based on their urgency factor, which consists of time of departure, maximum rate of charge, energy needed, and battery health. Case studies on the IEEE 118-bus transmission system show that this framework reduces peak demand, decreases charging costs, ensures voltage limits, and significantly improves fairness compared to first-come-first-served and uncontrolled charging. Furthermore, the results indicate that integrating photovoltaic (PV) systems within this framework can enhance local grid flexibility and reduce energy dependency on the main grid.

The second part introduces a predictive cluster-based architecture that enhances DA and

RT EV charging coordination. A novel spatiotemporal clustering method is proposed to form EVAs from public charging ports. Unlike geographic-based grouping, clustering here contains charging frequency, utilization ratio, and time-of-day usage. Within each cluster, a Temporal Fusion Transformer (TFT) model forecasts key behavioral attributes such as arrival time, departure time, and energy demand by leveraging historical transaction data, calendar, and meteorological inputs. These predictions are then utilized as the inputs in a two-stage bidding framework that balances DA commitments with RT corrections under market constraints. The proposed strategy demonstrates daily cost and peak power reduction compared to uncontrolled charging, while also minimizing penalties between DA and RT energy profiles.

The third part of the thesis proposes a tri-level hierarchical coordination framework that decomposes EV charging control into clusters, EVAs, and the DSO using an Alternating Direction Method of Multipliers (ADMM)-based structure. At the cluster level, a novel Urgency-Aware Proportional Allocator (UAPA) eliminates the need for per-EV optimization by introducing an aggregated single decision variable per group, which dramatically reduces computational complexity while preserving high alignment with per-EV optimization-based methods. At the EVA and DSO levels, a machine learning-augmented ADMM (ML-ADMM) framework utilizes deep neural networks to predict warm-start values for primal and dual variables, thereby significantly reducing the number of ADMM iterations. The combined system demonstrates scalability, privacy preservation, and grid-constrained coordination across IEEE 33 bus and IEEE 118 bus electrical networks using real EV transaction datasets.

Overall, this thesis provides scalable and privacy-preserving coordination methods that unify forecasting, learning-based control, and hierarchical optimization for large EV populations. The proposed frameworks apply to public charging networks, fleet depots, and utility-led demand response programs. By reducing communication overhead and improving fairness, stability, and computational efficiency, they address key barriers to massive EV integration.

TABLE OF CONTENTS

LIST OF TABLES

LIST OF FIGURES

LIST OF SYMBOLS AND ACRONYMS

ADMM	Alternating Direction Method of Multipliers
CAISO	California Independent System Operator
DA	Day-Ahead
DDPG	Deep Deterministic Policy Gradient
DDQN	Double Deep Q-Network
DSO	Distribution System Operator
EJT	Efficiency-Jain Tradeoff
EV	Electric Vehicle
EVA	Electric Vehicle Aggregator
EVCS	Electric Vehicle Charging Station
FCFS	First Come First Serve
GAN	Generative Adversarial Network
GHG	Greenhouse Gas Emissions
GLU	Gated Linear Unit
GRN	Gated Residual Network
GRU	Gated Recurrent Unit
HDBSCAN	Hierarchical Density-Based Spatial Clustering of Applications with Noise
HVAC	Heating, Ventilation, and Air Conditioning
JFI	Jain's fairness index
LP	Linear Programming
LSTM	Long Short-Term Memory
MADRL	Multi-Agent Deep Reinforcement Learning
MARL	Multi-Agent Reinforcement Learning
MAE	Mean Absolute Error
MAPE	Mean Absolute Percentage Error
MCRs	Mobile Charging Robots
MDP	Markov Decision Process
MILP	Mixed-Integer Linear Programming
MINLP	Mixed-Integer Nonlinear Programming
ML-ADMM	Machine Learning-augmented Alternating Direction Method of Multipliers
MPC	Model Predictive Control
MPPT	Maximum Power Point Tracking

MSE	Mean Squared Error
NLP	Nonlinear Programming
NN	Neural Networks
OPF	Optimal Power Flow
PILCO	Probabilistic Inference for Learning Control
PV	Photovoltaic
RES	Renewable Energy Sources
RL	Reinforcement Learning
RMSE	Root Mean Square Error
RNN	Recurrent Neural Network
RSD	Real-time Smart Dispatch
RT	Real-Time
SC	Scenario
SoC	State of Charge
SOCP	Second-Order Cone Programming
TD	Temporal Difference
TFT	Temporal Fusion Transformer
ToU	Time of Use
UAPA	Urgency-Aware Proportional Allocator
V2G	Vehicle to Grid
VGs	Virtual Groups
VSN	Variable Selection Network

LIST OF APPENDICES

CHAPTER 1 INTRODUCTION

1.1 Motivation

The transport sector accounts for approximately 15% of global greenhouse gas emissions, with road transport alone contributing around 10% due to its strong reliance on fossil fuels [1]. For example, Canada has a goal of reducing its Greenhouse Gas (GHG) emissions by 30% below 2005 levels by 2030 under the Paris Agreement [2]. As we move toward a cleaner and more sustainable future, Electric Vehicles (EVs) are emerging as a key solution in controlling climate change. With the worldwide goal of reaching net-zero emissions by 2050, transitioning away from fossil-fueled transportation to electric transportation is undeniable. EVs offer a practical and immediate way to reduce GHG, especially when powered by Renewable Energy Sources (RES) as aprimary source of charging [3].

EV charging infrastructure involves several key stakeholders, including the Distribution System Operator (DSO), EV Aggregator (EVA), EV Charging Station (EVCS), and EV owners [4]. To motivate the stakeholders to participate in the smart charging program and guarantee its practical application, it is essential to consider the benefits they will obtain from the proposed framework. From the DSO's perspective, the primary concern is grid stability, power peak management and minimization of periodical maintenance costs [5]. EVAs act as an intermediate level between DSO and EVCSs in the charging management structure. Generally, EVAs aim to minimize charging costs for large fleets while also participating in energy markets [6]. EVCS operators aim to maximize charger utilization time and minimize peak tariffs or penalties, while EV owners seek a timely and fair charging process that satisfies their charging needs without compromising comfort or accelerating battery degradation [7]. A successful smart charging framework must therefore balance these objectives through transparent pricing and fair coordination mechanisms.

While the growth of EVs can reduce GHG emissions, their integration into the distribution system may cause challenges for the grid. The main issue is in the uncertainty surrounding EV users' behavior, which includes arrival and departure times, charging durations, and energy demands [8]. Without suitable coordination mechanisms, uncontrolled charging can cause voltage drops, transformer overloading, and increased operational costs for the DSO [9]. As a result, EV charging management must consider both accurate forecasting and control strategies to satisfy grid stability.

The behavior of EV owners, a primary uncertainty factor in the smart charging management of

EVs, can be modeled and predicted in various ways. While prior works have used a Gaussian distribution to model uncertainties [10], recent studies have focused on learning-based models to predict these uncertainties [11]. These data-driven approaches utilize historical charging data, time-of-use patterns, and contextual features, such as day of the week, weather, and location, to forecast EV arrival times, departure times, and energy demands with high accuracy [12]. High prediction accuracy is essential since these prediction results will be fed into the smart charging algorithms.

Smart charging refers to intelligent scheduling of EV loads. The aim is to control the EV charging power according to grid conditions, electricity prices, and EV users' travel and charging schedules to achieve predefined goals [13]. Smart charging provides advantages of reducing the EV charging cost, minimizing load peak shaving, and providing grid support services in addition to mitigating the negative impacts of uncontrolled charging [14]. Further more, smart charging can enhance battery longevity by controlling the rate of charge or deep cycling. Also, it can facilitate the integration of renewable energy sources by aligning charging demand with generation patterns, and ensure user satisfaction, which is essential for large-scale EV adoption [15].

Based on the available information and the time horizon, smart EV charging strategies can generally be categorized into two main types: Day-ahead (DA) planning and Real-time (RT) control. DA methods rely on forecasted uncertainty parameter data to optimize charging schedules in advance. These approaches are often used for scheduling charging loads, reducing peak demand, and participating in energy markets. In contrast, RT techniques operate on short timescales for an immediate system response to new states, such as unexpected EV arrivals or RT price signals. While model-based mathematical approaches are used for DA planning, Reinforcement Learning (RL) has become popular in solving RT EV smart charging [16]. Both categories play complementary roles in enabling efficient and reliable EV comprehensive charging management.

A comprehensive system knowledge and an efficient communication system are needed to implement smart charging, as was done in previous works, in a centralized fashion [17]. Centralized frameworks are built on the assumption that the whole system can be perfectly known and that all necessary information is available ahead of time. However, privacy issues and solving large and complex problem while keeping the optimality were the two main factors that led to the shift to distributed frameworks [18]. Hence, hierarchical structures have gained popularity as a practical approach to achieving both privacy and scalability simultaneously. By organizing decision-making across different layers, distributed frameworks allow each actor to make independent decisions based on local information, while still contributing to a

coordinated global objective.

In summary, the fast growth of EV utilization, particularly in countries like Canada, is changing how power systems are managed and operated today. While EVs offer benefits in terms of reducing carbon footprint, their integration into power systems creates significant operational challenges due to the uncertain nature of users' behavior. Smart charging as a key strategy to address these challenges is introduced by allowing coordinated and flexible energy management. Successful smart charging depends on the ability to accurately anticipate EV user behavior and to coordinate decisions across both DA and RT horizons. Achieving this while protecting user privacy and managing computational complexity requires transitioning from centralized architectures to distributed, hierarchical frameworks. These are the fundamental motivations and needs of this thesis, which aims to design advanced prediction and control strategies for smart charging management of EVs.

1.2 Description of the Problem

The rapid integration of EVs into power systems creates both opportunities and challenges. While uncoordinated charging risks demand peaks and grid instabilities, smart charging provides a pathway to mitigate these issues and benefit all stakeholders. A key requirement for efficient smart charging is the accurate modeling of EV owner behavior, which is uncertain and influenced by factors such as location, time of year, day of the week, and incentive programs. Clustering techniques and data-driven prediction methods can improve behavior forecasting and make the charging demand more predictable. Furthermore, due to scalability and privacy concerns, centralized frameworks are impractical, whereas distributed and hierarchical approaches offer viable solutions by decomposing the problem into smaller sub-problems with reduced data-sharing requirements.

In this thesis, we adopt hierarchical frameworks consisting of different layers (DSO, EVA, charging stations), with each layer having its own responsibilities and minimal communication with neighboring layers, while preserving the optimality of the total system.

While DA and RT EV charging coordination strategies have individually received significant attention in the literature, their coupling remains a major challenge in optimizing EV charging. This is primarily due to the lack of a complete dataset in this domain, uncertainties, and different control objectives involved in each stage. Moreover, RT-based approaches, generally executed every few minutes, have relied on rule-based algorithms because they are fast and straightforward. However, these approaches are mostly reactive and fail to anticipate system states and user behaviors. RL, as a strong solution, offers a data-driven alternative that does

not require knowing the exact model of the system and can find a suboptimal policy based solely on receiving states, while its inference step is fast enough to be executed in real time.

Decomposition techniques such as Alternating Direction Method of Multipliers (ADMM), although known as an alternative to centralized approaches, still suffer from their iterative convergence behavior, which can be slow, especially when applied to large systems with tight coupling constraints or high-dimensional variable spaces. This concern can be addressed from two distinct perspectives. One can reduce the computational complexity of the main problem to make the convergence time faster. The next solution is to use learning augmented methods to warm start distributed optimization and reduce the number of convergence iterations.

1.3 Objectives

There is an urgent need for EV smart charging coordination across different time scales. Most existing works treat DA planning, RT control, and multi-stakeholder coordination as separate problems, with few attempts to integrate them into a unified and scalable work.

The main objective of this thesis is to develop hierarchical, distributed, and interpretable frameworks, meaning approaches whose decision mechanisms are transparent and understandable, for intelligent EV charging coordination across different time horizons. These frameworks combine machine learning, distributed optimization, and RL to manage charging at the level of EVCS, EVA, and the DSO, while ensuring distribution network constraints, privacy of stakeholders, and behavioral diversity. We specify the key aspects of the objective through the following definitions:

- **Artificial intelligence for behavior modeling:** The frameworks utilize clustering to form EV groups with similar charging behavior and machine learning techniques to model and predict EV owner behavior based on historical data and contextual information. This integration of clustering and prediction improves the reliability of DA planning.
- **Multi-stakeholder compatibility:** The frameworks take into account the objectives of all different stakeholders, including EV users, EVCSs, EVAs, and DSO. Fair energy dispatch, cost minimization, and safe grid operation are considered while respecting the autonomy and privacy constraints of each actor.
- **Hierarchical and distributed coordination:** To address computational burden and preserve user privacy, the proposed frameworks are structured in a hierarchical structure

(EVCSs, EVAs, DSO). Each layer solves its subproblem locally, reducing information sharing and computational burden.

- **DA and RT operation:** DA planning and RT control have been considered in the proposed frameworks. DA optimization studies plan scenarios based on predicted behavior and expected conditions, whereas RT optimization adjust real-world deviations. Considering different time horizons enhances both reliability and adaptability of EV charging management in real-world applications.

In the following Chapter, we outline the structure of this thesis and demonstrate how each part contributes to achieving the stated objectives.

CHAPTER 2 ORGANIZATION OF THE THESIS

2.1 Structure of the Thesis

The primary goal of this thesis is to decompose EV charging management into smaller subproblems handled by the main stakeholders: the DSO, the EVAs, and the EV owners. Hierarchical and distributed frameworks allow each stakeholder to solve local problems with limited information exchange with the possibility of reaching global optimality and convergence when specific conditions are met.

Smart charging must also consider different time horizons. In the DA stage, EV uncertainties can be predicted using machine learning methods. The prediction accuracy can be enhanced by clustering to group EVs with similar charging patterns. In RT, however, the emphasis is on adaptiveness, since the framework must respond dynamically to uncertainties without prior knowledge.

We explore this idea in depth in three different parts.

- **Part I – RT RL Control (Article 1):** The first part focuses on RT hierarchical charging management of EVs using a Multi-Agent Deep Reinforcement Learning (MADRL) framework. At the top level, the DSO determines the maximum power each EVA can receive by solving an optimization problem subject to grid power flow and fairness. At the middle level, each EVA is modeled as a learning agent that decides the amount of energy to purchase based on aggregated EV data using a prioritized Q-learning method. Finally, at the lower level, the real-time Smart Dispatch (RSD) controller dispatches the purchased energy between EVs based on their emergency.
- **Part II – Two-Stage Optimization (Article 2):** This part introduces a spatiotemporal clustering method to group public EV charging ports on Montreal Island by similar usage behavior and create EVAs. After forming the EVAs, Temporal Fusion Transformer (TFT) models are used to forecast the arrival, departure, and energy demand of EVs related to each EVA. Using these forecasts, a two-stage coordination strategy is proposed. In the DA stage, EVAs determine charging schedules that minimize energy costs and peak power consumption. In the RT stage, the framework adapts to deviations from DA scheduled power by adjusting charging decisions to reduce discrepancies between planned and actual demand profiles.
- **Part III – Distributed EV Charging Optimization with ML-ADMM (Ar-**

ticle 3): The final part presents a tri-level coordination framework for EV charging management using ADMM through DSO, EVAs, and EV clusters. First, a dynamic clustering method for forming EVs inside EVAs is proposed. Next, a novel Urgency-Aware Proportional Allocator (UAPA) is introduced, which significantly reduces the number of decision variables at the cluster level. Moreover, A Machine Learning-augmented ADMM (ML-ADMM) predicts warm starts for EVA, and DSO is implemented to reduce the number of iterations required for convergence in the ADMM structure.

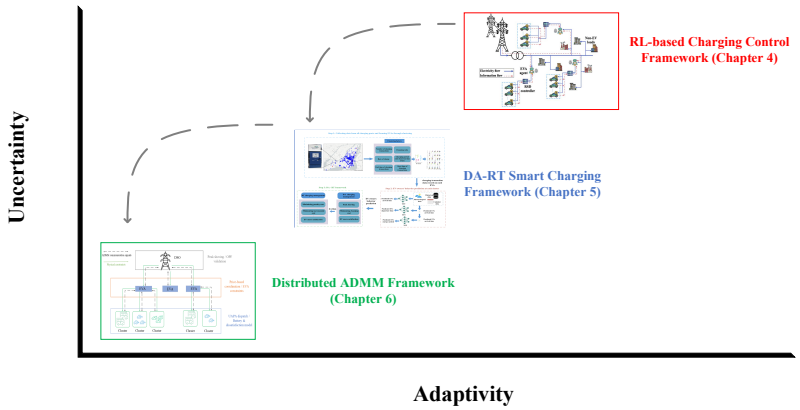

Figure 2.1 Link between each part of the thesis in terms of uncertainty and adaptivity.

The relationship between these parts and the main coordination objectives is illustrated in Fig 2.1. Along the adaptivity axis, "more adaptive" methods react quickly to changing conditions, while "less adaptive" ones provide greater stability and predictability. At the top right, the RL-based charging control framework introduces an RT learning-based strategy that handles dynamic grid environments and user behavior under high uncertainty. Moving along the adaptivity axis, the DA-RT Smart Charging Framework utilizes behavioral forecasting and two-stage planning to align offline commitments with online operations. The bottom-left corner represents the distributed ADMM framework, which focuses on hierarchical optimization while having a low uncertainty level.

2.2 Main Research Contributions

The overall contribution of this thesis is the development of three complementary frameworks for DA and RT EV smart charging that address the challenges of EV owners' behavioral

uncertainty, privacy concerns, and scalability under a multi-stakeholder coordination mechanism. Real charging transactions of Montreal are used to validate the superiority of these frameworks over uncontrolled charging.

The first contribution is an RT EV charging framework based on MADRL. In this framework, DSO first determines the maximum allowable power it can allocate to each EVA based on grid constraints and a fair mechanism. Within this framework, each EVA is modeled as an independent RL agent that decides the optimal power purchasing amount at each time using a DDQN enhanced with prioritized experience replay and adaptive learning rates. A RSD controller then prioritizes EVs based on an urgency metric that includes departure time, remaining demand, charging rate, and battery health. The main contribution of this work is the introduction of an RL-based framework that can find a suboptimal charging policy without knowing the complete system model, while ensuring fairness and efficiency at the same time.

The second contribution presents a two-stage predictive framework for coordinating DA and RT EV charging. This approach introduces a spatiotemporal clustering algorithm of charging ports to form EVAs based on public charging records. A TFT model is then trained to forecast key parameters of charging management, such as arrival and departure times to and from charging ports, and the energy required for all EVs within each EVA. These forecasts are used in a two-stage optimization procedure that first schedules energy bids in the DA market and then adjusts allocations in RT to correct for deviations. The main contribution of this work is the integration of charging port clustering with the TFT forecasting mechanism to achieve an accurate prediction result for use in the two-stage DA-RT framework.

The third contribution is a hierarchical distributed optimization framework based on the ADMM, enriched with learning-based acceleration. At the cluster level, a convex surrogate allocator named UAPA replaces detailed per-EV optimization by directly assigning energy based on aggregated urgency scores. At the EVA and DSO levels, an ML-ADMM is developed to predict warm-start values for primal and dual variables, significantly reducing the number of iterations required for convergence. The main contribution of this part lies in the integration of convex approximations and deep learning into a scalable ADMM framework, enabling near real-time coordination over IEEE 33- and 118-bus systems using real EV transaction data.

CHAPTER 3 LITERATURE REVIEW

In this chapter, some of the key general concepts are reviewed to help readers understand the following chapters. The introduction of each part provides a specific literature review.

3.1 Large-Scale Integration of EVs into Power Systems

As EV penetration increases, understanding its impact on the electrical grid becomes critical. A variety of approaches to model and mitigate the challenges arising from EV loads, particularly at the distribution level, are presented here.

3.1.1 Impact on generation, transmission, and distribution

The integration of EVs reveals different challenges across the power system structure. The charging demand of EV fleets is highly variable both temporally and spatially, which makes the planning for power generation and transmission systems complicated. At the generation level, increased EV demand shifts traditional load profiles and requires more flexible generation dispatch [19]. RESs are highly used in charging EVs, as they are distributed energy sources and can provide energy with low pollution for EVs [20]. Moreover, PVs can be installed on EVCSs' rooftops and can be used directly for charging without any loss in the distribution network during the daytime. EVs are flexible and controllable loads, which means they should be charged through a specific time window, but their charging can be done in a reasonable way. Hence, smart charging of EVs can give more flexibility to the DSO and avoid grid congestion [21]. From a transmission perspective, uncoordinated EV charging may cause stress during peak hours, which brings extra cost by infrastructure reinforcement or reserve activation. However, the most severe effects happen at the distribution level, where degradation of transformers, voltage instability, and power flow issues are common concerns [9]. As EV adoption continues to rise, coupling charging coordination frameworks with models that consider grid becomes increasingly essential.

3.1.2 Challenges in grid stability and reliability

At the distribution level, uncontrolled EV charging strategies can cause challenges related to the grid, such as voltage instability on buses, local transformer overloading [22], and increased peak demand during critical hours [23]. Each of these challenges can result in high-cost consequences. Transformer aging may necessitate replacement, increased peak demand may

require new power plants to be started and brought online, and voltage instability may cause load flow constraints to fail, leading to uncontrolled outages.

Load flow analysis (power flow calculation) is a fundamental process in electrical power systems to determine the system's steady-state in terms of voltage and power flow under a specific operating condition [24]. Load flow calculation determines all buses' voltages, active and reactive power consumption, and also indicates every line's power flow at each time step. When EV fleets charge simultaneously in an uncoordinated way, they introduce additional loads that can increase the existing peak power consumption or lead to new peaks on some buses and have a negative impact on the load flow solution and sometimes make it infeasible [25]. As a result, smart charging of EVs is essential to make sure that system constraints are satisfied, voltage levels remain within an acceptable range, and distribution network infrastructure stress is minimized.

RES are also a primary cause of grid instability, as the power generation of PV panels and wind turbines is weather-dependent and unpredictable. Rooftop PV panels and battery energy sources cause reverse traditional flow patterns, which complicate the protection and control schemes. Moreover, high RES penetration can drive negative prices, ancillary service issues, curtailment, and stress reliability-based market design [26].

3.1.3 Existing studies on EV grid interaction

Recent works regarding EV integration have been investigated in this section. In [27], a multilayer multiorder adaptive control for PV-assisted EV charging is introduced that enhances power quality, reduces harmonics, and maintains stability under grid abnormalities. In this work, a fuzzy logic controller dynamically tunes the step size of the Maximum Power Point Tracking (MPPT) algorithm to find the optimal power extraction from the PV system. Authors in [28] present a centralized three-stage control framework using Model Predictive Control (MPC). The objective of this work is to maintain grid voltage stability and EV batteries' State of Charge (SoC) within the acceptable range. In [29], a bi-level planning and scheduling framework that considers the uncertainty in EV behavior and residential demand is introduced. In the first level, the optimal placement of EVCSs is taken into account, while in the second level, the optimal charging/discharging strategy of EVs is investigated, which significantly reduces peak load, thermal overloading, voltage deviations, and network losses in distribution networks. Authors in [30] propose a two-layer optimal dispatch strategy for coordinating EV charging across the distribution network. The strategy performs peak shaving and minimizes distribution network losses at the upper level, while at the lower level, EVCSs guarantee user satisfaction and economic efficiency. In [31], a smart charging strategy

for enhancing the grid efficiency and sustainability is introduced, which takes into account both Time of Use (ToU) electricity pricing and marginal emission factors. An improved local search genetic algorithm is used in this work to reduce both charging cost and carbon emission while addressing the grid stress caused by the EV charging peak period. Authors in [32] propose an incentive mechanism based on location with integration of EV charging to reduce renewable energy curtailment and maintain the grid stability. This method improves energy utilization and prevents local congestion by considering distribution system constraints and dynamic EV behavior. Finally, in [33], the impact of charging stations on the stability of radial distribution systems are examined. This work proposes optimal placement and sizing of distributed generation and distribution static compensators in two scenarios, with and without charging station influence, under the load uncertainty. A metaheuristic optimization algorithm, the bald eagle search algorithm, is employed to minimize real power losses and improve voltage profiles on 34- and 118-bus test systems.

3.2 Smart Charging and Load Flexibility

EV smart charging highly depends on pricing signals. By adjusting charging schedules in response to electricity prices, EV owners can reduce charging costs and stress on the grid, whether it is related to peak power consumption or load flow constraints.

The first type of smart charging pricing signal is ToU, where electricity prices are determined based on predefined periods such as peak, mid-peak, and off-peak. The ToU signal can be used as an incentive for EV owners to shift their consumption and reduce their charging cost as mentioned in [34–36]. This approach is simple to implement and widely adopted by utilities, but it does not respond to RT system conditions.

The second type of smart charging is RT, or dynamic pricing. In this approach, prices reflect the current state of the power system. Generation costs, demand levels, and congestion can all affect the RT pricing, and this approach has been widely used in EV charging as in [37,38].

A more advanced smart charging strategy is Vehicle to Grid (V2G). In this mode, EVs are modeled as bidirectional energy exchange units that can inject power into the grid when needed. With the advantages of V2G mode, EVs can participate in ancillary services such as frequency regulation, voltage support, and peak shaving when implemented properly [39,40]. Despite its technical advantages, V2G can create several challenges, including battery degradation, communication requirements, and EV users' acceptance.

Hybrid strategies that combine pricing signals and V2G have also been explored [41,42]. In these works, the goal is to maximize both user benefits, such as lower costs and incentives, as

well as grid services, including peak shaving.

In a larger aspect, smart charging is a practical implementation of Demand Side Management (DSM). DSM refers to the modification of consumer demand profiles through mechanisms such as pricing, direct load control, or incentives. Traditionally, only fixed loads were taken into account for DSM, such as Heating, Ventilation, and Air Conditioning (HVAC) systems or industrial motors. However, with the growing number of EVs, they now play a key role in this domain.

3.3 Data-Driven Analysis of EV Charging Behavior

To develop smart charging frameworks, it is essential to predict the behavior of EV owners. Data-driven techniques such as clustering and machine learning forecasting have been used repeatedly for predicting charging patterns and characteristics. This is mainly because the availability of charging session data increases.

3.3.1 EV Charging Data Sources and Features

EV charging behavior is typically recorded by public or private charging stations. The ElaadNL dataset from the Netherlands and the Caltech ACN-Data from the United States are famous public datasets that have been used in the literature repeatedly [43, 44]. However, due to privacy concerns, there is limited publicly available data, and the available data does not provide a comprehensive record of EVs and charging stations.

In this study, we are utilizing Hydro-Québec charging transaction data that includes detailled session-level information, such as EV arrival and departure times, energy consumption, session duration, and anonymized user ID. Additional station-based features are also available, including geographic location, number of charging ports inside EVCS, and charging infrastructure level.

To implement clustering or forecasting tasks, these raw session logs are processed into structured feature vectors. Typical features include:

- Arrival/departure time, weekday/weekend flag, and session duration, which are mostly temporal features.
- Average energy demand per session and usage frequency, which are user-related data.
- Utilization rate, voltage level, and geographical latitude and longitude that are station-based data.

3.3.2 Clustering of EVs

EV users may exhibit different charging patterns based on geographic locations and time periods. Charging coordination for EV users individually is costly, but clustering offers grouping EVs or EV stations with similar characteristics, enhancing the scalability of their charging, as explored in [45, 46].

Clustering in an EV charging scheme can be implemented in two ways. The first approach, as mentioned in [11, 47], involves clustering EVs based on their characteristics such as arrival/departure times, and energy demand. The result of the EVs clustering can then be fed into the smart charging process, which increases the scalability and predictability of the charging process. The second approach, as mentioned in [48], is clustering EVCSs based on their geographical location, rate of charge, and utilization rate, and it can be further used to predict EVCSs' DA charging profiles.

The objective of clustering is to group similar items together as closely as possible within each group, while keeping different groups as distinct as possible. A common clustering problem can be formulated as:

$$\min_{\{z_{i,q},\mu_q\}} \sum_{q=1}^{K} \sum_{i=1}^{N} z_{i,q}\, \mathcal{D}(x_i, \mu_q), \tag{3.1}$$

subject to

$$\sum_{q=1}^{K} z_{i,q} = 1, \quad z_{i,q} \in \{0,1\}, \quad \forall i = 1, \ldots, N, \tag{3.2}$$

where $z_{i,q}$ is a binary assignment variable indicating if data point i belongs to cluster q, μ_q is the centroid of cluster q, and $\mathcal{D}(\cdot,\cdot)$ is a distance function such as the Euclidean norm. Different clustering methods have been used in the EV charging management, such as K-mean [49] and Hierarchical Density-Based Spatial Clustering of Applications with Noise (HDBSCAN) [50].

The performance of clustering is commonly evaluated by metrics such as Silhouette Score, Davies–Bouldin index, or the elbow method. A good clustering method balances compactness within clusters and separation between clusters [51].

3.3.3 Prediction of EV charging demand

Prediction plays a key role in the smart charging management of EVs. There are three main time horizons used for prediction; the appropriate time horizon depends on the application context. Short-term forecasts, such as 15 or 30 minutes ahead prediction, are useful for RT scheduling, while mid-term forecasts, such as DA or week-ahead, are suitable for charging planning and energy procurement. Finally, long-term forecasts are mainly used for expansion

planning and providing sufficient infrastructure for EVs charging management. Choosing the appropriate horizon depends on the use case, available data, and system structure.

Charging prediction of EVs highly depends on external factors such as temperature, day of the week, holiday schedules, or local traffic conditions [52]. People may show different charging behaviour during weekdays and weekends, as well as during summer and winter. Considering these external factors in the prediction can highly improve the accuracy of the prediction.

When prediction is combined with clustering, it can enhance prediction accuracy, as we expect to see more similar behavior from EVs within the same clusters. Prediction of EV charging demand can be implemented in multiple ways. In some works, such as [53, 54], the main idea is to predict key smart charging features, including the arrival/departure times of EVs at EVCSs and the energy required for their charging. These predicted results can then be used as the inputs in the smart charging management process. However, this approach needs a complete dataset regarding EV charging transactions. Another approach, as illustrated in [55, 56], is to predict EVs' daily charging profiles directly; in this approach, the predicted result can be used as a benchmark for further charging management. Finally, some other approaches indirectly predict the EV charging profile pattern, such as [57], which predicts EVs' waiting time at EVCSs for long road trip scheduling, or as in [58] that predicts EVs' driving range, which can be indirectly used for charging management of EVs.

Recently, novel approaches have been utilized in EV domain prediction. In [59], a spatial–temporal graph convolutional model enhanced with dynamic time warping is introduced to find the correlations among geographically distributed charging stations and to improve prediction accuracy. Authors in [60] proposed a multi-output deep learning model for energy demand and port availability forecasting in EV charging infrastructure, which efficiently functions under unexpected conditions like the COVID-19 pandemic. Finally, Authors in [61] propose a DA EV charging demand forecasting model that combines quadratic decomposition with dual attention mechanisms to better capture nonlinear patterns and contextual dependencies in EVs charging pattern.

Evaluation of the prediction accuracy is based on metrics such as Mean Absolute Percentage Error (MAPE), Root Mean Square Error (RMSE), R^2 score, and Mean Absolute Error (MAE) [62].

3.4 Coordination and Optimization in EV Charging Networks

The growth of EVs and their integration into power systems introduces challenges for different stakeholders. EV owners are looking for the final desired SoC, while EVCSs and EVAs aim

for profit maximization, and DSOs need to maintain grid conditions. Moreover, all these stakeholders are unwilling to share their privacy-related data, such as customer data or grid topology, as privacy must be completely taken into account. This section reviews key optimization frameworks and control strategies proposed for managing EV charging across centralized, distributed, and hierarchical architectures, with a focus on their applicability in operations.

3.4.1 Centralized, decentralized, and distributed coordination

In centralized coordination, a central operator or controller receives all relevant data from all EVs, EVCSs, and distribution system components. All this data will then be used to solve a global optimization problem. Since a central controller exists in this framework, the system has a high level of observability and can achieve the optimal charging or control strategy. However, this optimality comes with a cost. First, all the computational burden is on a single controller, which can increase the risk of failure. Second, all data from stakeholders should be shared with the central controller, which can put the privacy issue at high risk [63]. Moreover, due to the delays in data aggregation or the scalability issue, a centralized architecture may not be suitable for RT control.

Decentralized architectures are easy to expand, and the addition of many agents to the system is possible without significantly impacting the charging management frameworks. Moreover, this type of coordination is robust as there is no risk of a point of failure, and it also fully preserves the privacy of the agents. On the other hand, without having sufficient communication with other agents, each agent may act selfishly, and the system's global constraints may not be fully satisfied. Moreover, without pricing or policy signals, agents might not behave in a socially optimal way [64].

In contrast, distributed coordination frameworks decompose the global problem into smaller subproblems. Based on the decomposition, each EV, EVCS, or EVA can be considered as an agent, and each agent's decisions are made locally with minimum communication with other agents. This locally based optimization can reduce the need for a communication structure and computational burden. Moreover, the risk of a point of failure decreases because there is no single central controller in this structure, and if one agent controller stops working, the system can still function. However, distributed coordination frameworks pose new challenges, including the slow convergence issue and synchronization requirement [65]. Table 3.1 shows a comparison of centralized, decentralized, and distributed coordination across key aspects.

Table 3.1 Comparison of Coordination Architectures

Aspect	**Centralized**	**Decentralized**	**Distributed**
Control	Central unit	Independent agents	Local agents + coordination
Scalability	Low	High	Medium–High
Computation	Centralized	Fully local	Shared among agents
Privacy	Low	High	Medium–High
Failure Risk	High	Low	Low
Optimality	High	Low	Medium–High
Communication	High	None	Moderate
Real-time Use	Poor	Good	Depends on speed
Challenges	Privacy, bottlenecks	No coordination, selfish agents	Convergence, synchronization

3.4.2 Optimization Algorithms

An optimization problem generally means minimizing or maximizing an objective function $f : \mathbb{R}^n \to \mathbb{R}$. The optimization problem comes with a set of decision variables $x \in \mathbb{R}^n$ and constraints. A standard form of optimization problem can be expressed as:

$$\begin{aligned} \min_{x \in \mathbb{R}^n} \quad & f(x) \\ \text{subject to} \quad & g_i(x) \leq 0, \quad i = 1, \ldots, m \\ & h_j(x) = 0, \quad j = 1, \ldots, p, \end{aligned} \tag{3.3}$$

where $f(x)$ is the objective function, and $g_i(x)$ and $h_j(x)$ are inequality and equality constraints, respectively.

Generally, optimization problems without constraints are the simplest type of optimization and can be solved using the gradient descent method. In this method, the decision variables are iteratively updated in the direction of the negative gradient of the objective function:

$$x^{(k+1)} = x^{(k)} - \alpha \nabla f(x^{(k)}), \tag{3.4}$$

where $\alpha \in (0, 1]$ is the step size. More advanced techniques, such as Newton's method, use second-order information to accelerate convergence speed.

In many real-word optimization problems, some decision variables are required to take integer values. For example, in EV smart charging management, charging rates are often modeled as discrete or integer values in [66]. Conversely, in charging station allocation within the power grid, the problem formulation involves integer variables since the decision consists of selecting the optimal locations of stations at specific buses in the network [67]. These problems are considered as Mixed-Integer Linear Programming (MILP) or Mixed-Integer Nonlinear Programming (MINLP) and can be solved using branch-and-bound or cutting-plane methods.

Heuristic algorithms are often employed when exact methods become infeasible, for example in large-scale EV coordination with thousands of vehicles or when non-convex AC power flow constraints are included [68, 69]. Algorithms such as genetic algorithms, simulated annealing, and particle swarm optimization are widely used in EV smart charging [70, 71]. These algorithms are mainly useful when the problem is non-convex and large-scale, while these methods can not guarantee convergence, they often provide satisfactory solutions within acceptable time frames. The choice of optimization algorithm depends on the nature of the problem and the available computational resources. A strong understanding can help us find the most suitable technique in real-world applications.

3.4.3 Distributed optimization techniques

As mentioned earlier, the scalability issue and privacy concerns were the primary reasons for shifting from centralized optimization to distributed optimization.

In hierarchical frameworks, an upper-level controller oversees global decisions and monitors the objectives. It may also give some limited decision-making authority to lower-level agents, such as EVAs and EVCSs, to control their local constraints and objectives. In contrast, in distributed frameworks, there is no need for a central controller, as peer-to-peer local information exchange is available. A general form of a distributed optimization problem is:

$$\begin{aligned} \min_{x \in \mathbb{R}^n} \quad & f(x) \\ \text{subject to} \quad & Ax = b. \end{aligned} \tag{3.5}$$

The Lagrangian associated with this problem can be written as:

$$\mathcal{L}(x, \lambda) = f(x) + \lambda^\top (Ax - b), \tag{3.6}$$

where λ is the vector of Lagrange multipliers. Dual ascent methods can be used by alternating between minimizing the Lagrangian with respect to x and updating λ when the objective

function $f(x)$ is convex.

When the objective function is separable, it can be shown as follows:

$$f(x) = \sum_{i=1}^{N} f_i(x_i), \quad \text{with} \quad Ax = \sum_{i=1}^{N} A_i x_i = b, \tag{3.7}$$

Dual decomposition methods allow each agent i to solve its local problem:

$$x_i^{(k+1)} = \arg\min_{x_i} \mathcal{L}_i(x_i, \lambda^{(k)}), \tag{3.8}$$

here, the dual update can be illustrated as:

$$\lambda^{(k+1)} = \lambda^{(k)} + \alpha^{(k)} \left(\sum_{i=1}^{N} A_i x_i^{(k+1)} - b \right), \tag{3.9}$$

where $\alpha^{(k)}$ is a step size. Here, convergence may be slow, particularly if the problem is not strictly convex.

As a result, the method of multipliers augments the Lagrangian with a penalty term to increase the robustness:

$$\mathcal{L}_\rho(x, \lambda) = f(x) + \lambda^\top (Ax - b) + \frac{\rho}{2} \|Ax - b\|^2. \tag{3.10}$$

The ADMM can improve scalability by breaking the problem into alternating primal updates. When the objective is expressed as $f(x) + g(z)$, subject to $Ax + Bz = c$, the augmented Lagrangian is minimized as follows:

$$x^{(k+1)} = \arg\min_{x} \mathcal{L}_\rho(x, z^{(k)}, \lambda^{(k)}) \tag{3.11}$$

$$z^{(k+1)} = \arg\min_{z} \mathcal{L}_\rho(x^{(k+1)}, z, \lambda^{(k)}) \tag{3.12}$$

$$\lambda^{(k+1)} = \lambda^{(k)} + \rho(Ax^{(k+1)} + Bz^{(k+1)} - c). \tag{3.13}$$

The alternating approach makes ADMM suitable and attractive for EV distributed charging, as each update can be done locally with minimal information exchange. Moreover, ADMM's convergence is guaranteed under the convexity assumption [72].

Convergence of ADMM is typically monitored using two residuals:

- **Primal residual:**

$$r^{(k+1)} = Ax^{(k+1)} + Bz^{(k+1)} - c, \tag{3.14}$$

which measures the violation of the constraint $Ax + Bz = c$.

- **Dual residual:**

$$s^{(k+1)} = \rho A^\top B \left(z^{(k+1)} - z^{(k)} \right), \tag{3.15}$$

which measures the change in the dual variable and reflects convergence in the dual space.

ADMM is considered to have converged when both the primal and dual residuals fall below predefined tolerances:

$$\|r^{(k+1)}\|_2 \leq \varepsilon^{\text{pri}}, \quad \|s^{(k+1)}\|_2 \leq \varepsilon^{\text{dual}}, \tag{3.16}$$

3.4.4 Machine learning approaches

In recent years, the application of machine learning in charging management of EVs is undeniable. Neural networks (NNs) are considered the foundational class of machine learning models and have been repeatedly utilized to predict EVs' charging patterns and behavior. A NN consists of connected layers of neurons. In its simplest form, there are only three layers: input, hidden, and output. In the NN structure, each neuron calculates a weighted sum of its inputs, which will be fed to a nonlinear activation function. When a vector $\mathbf{x} \in \mathbb{R}^n$ is used as an input, simple NN computes:

$$\mathbf{h} = \phi(W_1 \mathbf{x} + \mathbf{b}_1), \tag{3.17}$$

followed by an output prediction:

$$\mathbf{y} = \psi(W_2 \mathbf{h} + \mathbf{b}_2), \tag{3.18}$$

where W_1 and W_2 are weight matrices, $\mathbf{b}_1$ and $\mathbf{b}_2$ are bias vectors, and $\phi(\cdot)$ is an activation function such as ReLU or sigmoid.

NNs are trained based on historical data, and the parameters $W, \mathbf{b}$ are adjusted in the training phase based on backpropagation to minimize the loss function. Finally, the model should be evaluated on unseen new data, and its accuracy will be determined based on this unseen data.

Some studies, such as [73, 74], have used recurrent neural networks and Long Short-Term Memory (LSTM) to predict EV charging behaviour. Recurrent architectures are well-suited for modeling temporal dependencies in sequential data, such as daily or weekly patterns in EV arrivals and energy demands. These types of networks can retain the memory of

past experiences, which are useful in forecasting load profiles. Finally, NNs are used as decision-making controllers for different purposes such as navigation strategy to find the shortest path or to find optimal charging policy in charging strategy frameworks [75, 76].

3.4.5 Reinforcement learning for real-time control

RL has gained popularity in recent years as a decision-making control tool in environments with high levels of uncertainty. The basic concept of RL is the interaction between an agent and the environment, where the agent learns through experience.

An RL framework is commonly modeled as a Markov Decision Process (MDP), defined as:

$$\mathcal{M} = (\mathcal{S}, \mathcal{A}, p, r, \gamma),$$

where $\mathcal{S}$ shows the set of states. States are the environmental conditions at each time step. The set of possible actions for an agent is shown as $\mathcal{A}$. Actions have consequences that move the agent toward the next state. The function $p(s'|s, a)$ represents the transition probability of agents' moving from state s to a new state s' when action a is taken. The reward function $r(s, a)$ illustrate the benefit that the agent receive from taking action a in state s, and $\gamma \in (0, 1]$ is the discount factor that give priority to immediate rewards while considering the upcoming possible rewards.

In the RL, the objective is to learn a policy $\pi : \mathcal{S} \rightarrow \mathcal{A}$ that maximizes the expected reward:

$$J(\pi) = \mathbb{E}_\pi \left[\sum_{t=0}^{T} \gamma^t r(s_t, a_t) \right], \tag{3.19}$$

RL can be divided into two main categories: model-free and model-based RL. In model-free RL, the agent does not need to know the environment model; it directly learns a value function or policy. A famous example of a model-free RL algorithm is Q-learning, which estimates the Q-value:

$$Q^\pi(s, a) = \mathbb{E}_\pi \left[\sum_{t=0}^{\infty} \gamma^t r(s_t, a_t) \mid s_0 = s, a_0 = a \right], \tag{3.20}$$

$$\pi(s) = \arg\max_a Q^\pi(s, a). \tag{3.21}$$

In contrast, in model-based RL, an environment model $\hat{p}(s'|s, a)$ is needed to simulate interactions. One well-known model-based RL is Probabilistic Inference for Learning Control

(PILCO). In the EV charging context, RL has been widely adopted, while various agents, including DSO, EVAs, EVCSs, and EVs, have been considered [7, 77, 78]. At the distribution level, the RL agent can find the best grid's configuration based on information received from EVCSs and EVAs to minimize grid losses or maintain voltage stability. At the EVA and EVCS levels, the RL controller can be utilized to find the optimal charging policy for EV fleets. Finally, at the EV level, the RL agent can navigate EVs to the nearest available charging station based on their needs.

In recent years, the RL topic in EV charging management has advanced in various ways. Multi-agent RL has been introduced where two or more agents collaborate in the same environment, which can address the privacy issue in the EV charging domain [79]. Safe RL has been introduced to ensure operational aspects of the grid by considering the acceptable range of action for the agent at each time step [80]. And finally, transfer learning has also been used to transfer knowledge from one region to train a policy for another [81]. Nevertheless, several gaps remain. Many RL methods still require large amounts of training data and interactions with the environment; as a result, their sample efficiency with large networks is limited. Moreover, existing safe RL approaches often reduce to simple actions such as power clipping, without explicitly considering voltage limits, thermal constraints, or battery degradation. Furthermore, fairness among heterogeneous EV owners is rarely considered, as most approaches optimize only global cost or grid objectives [82, 83].

CHAPTER 4 ARTICLE 1: MULTI-AGENT DEEP REINFORCEMENT LEARNING WITH ONLINE AND FAIR OPTIMAL DISPATCH OF EV AGGREGATORS

Authors: Arian Shah Kamrani, Anoosh Dini, Hanane Dagdougui, Keyhan Sheshyekani

Submitted on November 21st, 2024 and accepted on January 3rd, 2025 at *Machine Learning with Applications*[1]

Contributions: Conception of the work's idea, literature review, design of experiments, development of the training environment, conduct of part the experiments, analysis of the results, and writing.

4.1 Introduction

4.1.1 Motivation

In recent years, electric vehicles (EVs) have attracted attention for their environmentally friendly nature and higher efficiency compared to fossil-fueled vehicles [85]. The growing number of EVs, however, may pose challenges such as voltage fluctuations, transformer overloading, and power outages [86]. Additional challenges in the charging process of EVs arise from uncertainties associated with EV users' behavior, non-EV load demand, renewable energy sources (RESs), and fluctuations in electricity prices [87]. On the other hand, EVs provide flexibility, allowing them to participate in energy markets [88], demand response programs [89], and ancillary services [90] facilitated by aggregators. Consequently, the efficient management of EV charging is of significant importance for both DSO and aggregators.

EVs online charging management has consistently presented challenges for DSO and aggregators due to the uncertain nature of this problem. Traditional EV charging strategies, based on optimization, require substantial computational resources, so their performance is heavily reliant on prior knowledge of the system [91]. In contrast to the traditional approaches, reinforcement learning (RL) enables learning optimal control strategies through the interaction between agents and the environment, without the need for an accurate system model and uncertainties [92]. Moreover, unlike offline and prediction-based optimization methods which are computationally intensive, learning-based strategies offer a balance between online implementation and achieving optimal solutions [93]. Hence, RL is proficient at efficiently

[1] Available at [84].

solving sequential decision problems in complex and uncertain environments, including EVs real-time charging optimization.

4.1.2 Related works

In previous years, EV fleet charging management utilizing RL algorithms has increased attention [94]. [95] proposed an RL-based smart charging algorithm to reduce the charging cost while considering peak load shaving under uncertainties related to EV owners. Moreover, an enhanced customized actor-critic learning algorithm is introduced to reduce the state dimension and thus improve the computational efficiency. [96] employed a multiagent deep deterministic policy gradient approach to acquire the optimal energy purchasing strategy for charging stations. Additionally, an online heuristic dispatching scheme is proposed to formulate an energy distribution strategy among EVs. [97] initially introduced the EV charging scheduling problem and the NP-hardness of the problem is demonstrated. Subsequently, the scheduling problem of EV charging is formalized as a Markov decision process (MDP), and deep RL algorithms are suggested for its resolution. The algorithms proposed aim to minimize the total charging time of EVs and achieve a maximal reduction in the origin-destination distance. While this paragraph discusses existing research in the domain of RL-based EV fleet charging, notable shortcomings persist in the field. The mentioned works can be broadly categorized into two groups: the first focuses on centralized management with a single controller entity utilizing single-agent RL, while the second employs multi-agent reinforcement learning (MARL) for decentralized optimization, treating each EV as an agent. Notably, to the best of the authors' knowledge, only few studies consider the EV aggregator (EVA) as an agent in a MARL environment for maximizing its benefit by managing the purchasing and distribution strategy of energy among EVs simultaneously. Additionally, in the domain of RL-based charging management of EVs, there is a lack of work addressing the acceleration of RL algorithm convergence speed for real-time purposes.

As modern society continues to advance, the demand for electricity is steadily rising, leading to an increase in the scale and complexity of power systems [98]. Allocating resources among users is a common challenge in any distributed system. In power distribution systems, a *fair* allocation ensures each consumer receives an equitable share of power. However, an *efficient* allocation is achieved when the DSO sells the maximum allowable power to each consumer. While DSO's goal is to maximize efficiency, consumers are more inclined to maximize their benefits, often resulting in conflicts of interest [99]. Fairness can be incorporated into any resource allocation problem, regardless of its application. However, it is often overlooked in power system studies, with only a few research investigating it. [100] developed a structure

to exchange energy within a low voltage community whose goal is to minimize the overall community cost. The structure exploits the resilience offered by surplus storage and generation capacity, and then it uses the Nash equilibrium to fairly share the overall cost among members. However, the approach is purely economic-centered, failing to consider equitable access to energy resources among members. On the other hand, [101] focuses on fair energy allocation during power contingencies. It utilizes Jain's fairness index (JFI) to evaluate and enhance fairness in energy allocation among EVs during outages. However, the study focuses on just one charging station and uses simulations that update every hour, which isn't practical for real-time use. Other studies on fairness within power systems scope focus on PV curtailment during off-peaks to avoid reverse power flow and overvoltage issues [102]. The mentioned research considers fairness from the perspective of load balancing, not from the standpoint of equitable resource allocation.

Unlike fairness, the literature on hierarchical frameworks on EV charging scheduling is rich. At the EV level, the main goal of these frameworks is to fulfill the charging demands of EV users. However, at the DSO and aggregator levels, these frameworks aim to tackle goals, such as peak shaving [103], reducing demand charges [104], minimizing EV charging costs [105], and privacy preservation [106]. In this context, [103] proposed a two-level hierarchical framework to involve EVs in peak shaving while meeting users' demands. However, the paper primarily focuses on demand management and grid services facilitation without considering the power flow constraints to ensure the safe operation of the grid. Additionally, a distributed model predictive control-based strategy for multiple EV charging stations is proposed by [107]. While the proposed strategy is online and capable of ensuring the grid's safe operation, it depends on the charging station operator having access to the grid's parameters. However, this may not always be feasible due to concerns over data privacy and the varying economic interests of different charging stations. Furthermore, [104] formulated the EV charging scheduling problem as a multi-agent based optimization in a distributed and privacy-preserved manner. Although the grid's security constraints are satisfied in the proposed scheme, it initially sets a fixed charging schedule for EVs upon their arrival without reassessing the charging plans based on subsequent changes in the grid's load.

4.1.3 Contributions

To address the previously mentioned issues, an online safe multi-agent deep reinforcement learning (MADRL) framework for energy purchasing and distribution of EVAs has been introduced. This framework ensures data privacy for all entities while simultaneously considering their respective benefits. Moreover, in the proposed MADRL framework, a double deep

Q-network (DDQN) featuring adaptive learning rates and a prioritized experience replay is employed to enhance the convergence of the agent towards optimality and make it particularly effective for online applications. Last but not least, at the level of DSO, energy dispatch among EVAs has been done based on optimal efficiency-jain tradeoff (EJT) and constraint of the distribution network to ensure fairness and reliability of the framework.

Overall, the key contributions of this study can be summarized as follows:

- Presenting an online safe MADRL framework aimed at minimizing the purchasing and distribution costs of EVAs while accounting for distribution network constraints, which incorporates a DDQN algorithm featuring adaptive learning rates and prioritized experience replay for accelerated convergence compared to traditional RL techniques.
- Ensuring the safe operation of the grid by calculating the maximum allowable power based on real-time grid conditions, and leveraging these calculations to determine the optimal EJT point. This approach guarantees fair power allocation among EVAs while enabling the DSO to sell the maximum amount of power at each time step.
- Preserving the privacy of EV owners, EVAs, and DSO, eliminating the need for them to share their respective data in the proposed hierarchical structure. Furthermore, the structure prioritizes the mutual benefits of all stakeholders involved simultaneously.

The remainder of this paper is structured as follows: Section 4.2 provides an overview of the proposed framework. In Section 4.3, we provide a detailed explanation of the proposed MADRL model, including the method for determining the maximum allowable power and the integration of fairness into our work. Section 4.4 discusses the case study, followed by an analysis of simulation experiments in Section 4.5. Finally, conclusion and future work are summarized in Section 4.6.

4.2 Proposed framework

4.2.1 Developed model

The top-down approach of our proposed hierarchical framework is shown in Fig. 4.1. At the upper level, the responsibility of assuring the reliability of the distribution network and fair energy allocation to EVAs is held by the DSO. In this framework, the DSO initiates the calculation of the maximum allowable power allocated (i.e., safe margin) to each EVA at each time step. This computation is based on non-EV loads, the location of each EVA on the distribution network, and load flow constraints. Moreover, at the level of DSO, optimal

EJT strategy is employed to assure fairness in energy allocation among EVAs. Ultimately, a signal set point indicating the maximum power available for purchase is transmitted from the DSO to each EVA at every time step. At the lower level, which is comprised of two sub-levels, first, EVAs act as agents within the proposed MADRL structure, determining the optimal amount of energy to purchase from DSO at each time step. They make decisions based on data provided by the DSO and RSD controller, which includes electricity price, the average state of charge (SoC) of their associated EVs, and the number of EVs involved. The amount of energy purchased should be carefully calibrated to meet the needs of EVs without being too low, as well as avoiding excess that could result in wastage. Afterward, the RSD controller conducts EV prioritization for energy dispatch at each time step by sorting the EVs based on their departure time, SoC, and maximum charging rate. This process involves considering the energy acquired by EVAs and subsequently dispatching it among the EVs. In this framework, when it comes to preserving the privacy of stakeholders, the DSO is not required to share any sensitive data regarding the distribution network topology with the EVAs. Furthermore, EVAs avoid sharing consumer data with both each other and the DSO. The only data that each EVA receives is generalized cumulative information about its associated EVs from RSD controller. From the perspective of stakeholders' benefits, the DSO ensures distribution system reliability and scalability, EVAs receive a fair energy allocation to maximize their profits, and EV owners obtain an energy dispatch service from RSD that considers the lifespan of EV batteries and the desired final SoC.

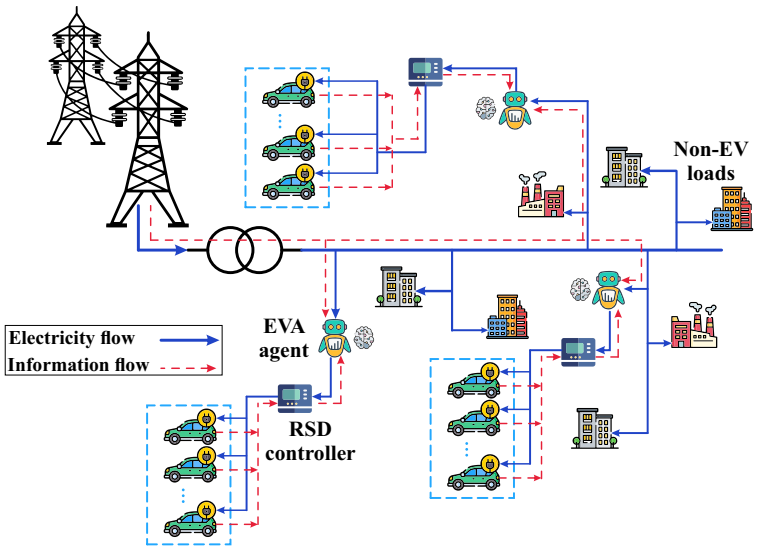

Figure 4.1 Proposed Framework.

4.2.2 Application of MADRL

Traditional optimization methods struggle to handle the dynamic and multi-dimensional nature of real-time decision-making, such as the charging management of EVs. These methods often fail when faced with a high degree of uncertainty related to EV owners' behavior and fluctuating real-time electricity prices [108]. However, MADRL is highly effective in these environments because it continuously learns and adapts to changes, handles complex interactions between agents, and is well-suited for managing real-time energy distribution and EV charging challenges [109]. Moreover, MADRL supports scalability by enabling a large number of EVAs to operate and learn in parallel without the need for centralized control, thereby reducing computational overhead. Finally, in terms of privacy, since each EVA (agent) only needs generalized cumulative information and does not require access to detailed consumer data and the entire network topology, privacy is preserved for all stakeholders.

4.3 Problem Formulation

4.3.1 Safe Margin Power

The safe margin power is a parameter obtained by DSO which guarantees the safe operation of the grid. This parameter indicates the maximum power that each EVA is allowed to draw at each time step. Inspired by [104], we propose an optimization problem to calculate this value. In this regard, let N denotes the total number of buses in the grid. For each bus n, if an EVA is present, its associated safe margin power is represented as $P_n^{agg}(t)$; otherwise, the value is set to 0. Therefore, the vector of safe margin power at time step t, $\mathbf{P}^{SM}(t)$, can be defined as a vector of length N, where each element corresponds to a bus in the grid. This vector will be obtained such that the sum of its elements is maximized. DSO calculates $\mathbf{P}^{SM}(t)\,|_{t\in T}$ online and dispatches equitably adjusted values of the vector to their respective EVAs. To achieve the first goal, DSO solves the following optimization problem at each time step:

$$\mathbf{P}^{SM}(t) = \arg \max_{\substack{V_n,\varphi_n,\\(n,b)\in\mathcal{B}}} \left\{ \sum_{n=1}^{N} \mathbf{1}_{\{n\in\mathcal{A}\}} \cdot P_n^{agg}(t) \right\} \tag{4.1a}$$

$$\text{s.t.} \quad P_{nb} = y_{nb}\left(V_n^2 \cos(\phi_{nb}) - V_n V_b \cos(\varphi_n - \varphi_b - \phi_{nb})\right), \tag{4.1b}$$

$$Q_{nb} = y_{nb}\left(V_n^2 \sin(\phi_{nb}) - V_n V_b \sin(\varphi_n - \varphi_b - \phi_{nb})\right), \tag{4.1c}$$

$$\sum_{b:y_{nb}\neq 0} P_{nb} = \frac{P_n^g(t) - \left(P_n^d(t) + P_n^{agg}(t)\right)}{S_{base}}, \tag{4.1d}$$

$$\sum_{b:y_{nb}\neq 0} Q_{nb} = \frac{Q_n^g(t) - Q_n^d(t)}{S_{base}}, \tag{4.1e}$$

$$\underline{V_n} \leq V_n \leq \overline{V_n}, \tag{4.1f}$$

$$\underline{\varphi_n} \leq \varphi_n \leq \overline{\varphi_n}, \tag{4.1g}$$

$$\sqrt{P_{nb}^2 + Q_{nb}^2} \leq \frac{\overline{S_{nb}}}{S_{base}}, \tag{4.1h}$$

where $\mathcal{A}$ and $\mathcal{B}$ represent the set of buses with EVAs and all the buses in the distribution system, respectively. Accordingly, the pair $(n, b) \in \mathcal{B}$ specifies the connections between buses, where n and b are indices of the connected buses. Additionally, $\mathbf{1}_{\{n\in\mathcal{A}\}}$ is an indicator function that equals 1 if bus n has an EVA (i.e., $n \in \mathcal{A}$), and 0 otherwise. This function ensures that $P_n^{agg}(t)$ contributes to the sum only if an EVA is present at bus n.

Furthermore, $V_n\angle\varphi_n$ denotes the per-unit voltage at bus n, and $y_{nb}\angle\phi_{nb}$ indicates the series admittance between buses n and b. The active and reactive power flows on the branch from bus n to bus b are represented by P_{nb} and Q_{nb}, respectively. The problem also considers active and reactive power generated ($P_n^g(t)$ and $Q_n^g(t)$) and consumed ($P_n^d(t)$ and $Q_n^d(t)$) at each bus n, along with the power consumption of EVAs ($P_n^{agg}(t)$) where applicable. Constraints (4.1f) to (4.1h) indicate voltage magnitude, voltage angle, and apparent power flow limits, respectively, which are operational constraints and ensure the system's safety and reliability. In this context, the overline and underline symbols indicate the upper and lower limits for parameters, respectively. Moreover, S_{base} represents the base power used for per-unit calculations.

As outlined in (4.1), the safe margin power indicates the maximum allowable power that can be drawn from each bus while respecting the grid's operational constraints. This question then arises: how much of this power should be allocated to the EVA connected to that bus? Allocating the entire amount to the corresponding EVA is one strategy. Nevertheless, this might not be equitable for other EVAs and loads. The fairness issue arises because an EVA's location in the grid and the loads on that branch mainly determine the safe margin value, making it unlikely for all EVAs to have equal safe margin values. Furthermore, assigning the entire safe margin to an EVA allows it to increase its power to this limit, possibly leading to

line congestion or voltage drop. This is particularly problematic if other loads on the same branch also wish to increase their consumption, leading the DSO to restrict such increases to ensure grid stability. In the next section, we present a strategy to achieve the optimal EJT point that takes into account the DSO benefit and ensures fair assignment of the maximum power to each EVA.

4.3.2 Fair Resource Allocation

To effectively meet the demands of EV owners while maintaining the safe operation of the grid, it is essential to allocate a fair maximum power limit for each EVA. The fairness indicator used in this study (i.e., JFI) is originally used in communication networks but also applies to other fields [110].

Let $\mathbf{P}$ be a vector whose elements indicate the benefits, i.e., the allocated power, determined by DSO for I EVAs. Consider $\mathbf{P} \in \mathcal{S} \subseteq \mathbb{R}_+^I$, where $\mathcal{S}$ contains all the possible benefit vectors bounded by the safety margins. The space $\mathbb{R}_+^I$ contains all vectors with dimensions I that have non-negative components. Each element of $\mathbf{P}$ (i.e., P_i) corresponds to the allocated power of the i-th EVA.

Definition 1 (JFI [110] and Efficiency)**.** *For $\mathbf{P} \in \mathbb{R}_+^I$, Jain's fairness index $J : \mathbb{R}_+^I \to \mathbb{I}_+$ and efficiency $\psi : \mathbb{R}_+^I \to \mathbb{R}_+$ are respectively obtained by*

$$J(\mathbf{P}) = \left(\sum_{i=1}^{I} P_i\right)^2 \Big/ I \sum_{i=1}^{I} P_i^2 \,, \tag{4.2}$$

$$\psi(\mathbf{P}) = \sum_{i=1}^{I} P_i, \tag{4.3}$$

where I represents the total number of EVAs. The fairness of this allocation is quantified by $J(\mathbf{P})$. It is a continuous function with a range from $\frac{1}{I}$ to 1. A value of $J(\cdot) = \frac{1}{I}$ corresponds to least fair allocation, where only one EVA receives a non-zero values. Conversely, $J(\cdot) = 1$ indicates the most fair distribution, with every EVA receiving an identical value as the allocated power.

There is often a trade-off between resource efficiency and JFI [99]. Our goal is to find the optimal balance between the two, maximizing efficiency while keeping JFI close to 1.

Definition 2 (Optimal EJT [99])**.** *Let $\mathcal{S}$ be a set of vectors, and $\mathbf{P}^*$ be an element of $\mathcal{S}$. The element $\mathbf{P}^*$ is considered to be the optimal EJT if no $\mathbf{P} \neq \mathbf{P}^*$, satisfies either: 1) $\psi(\mathbf{P}) > \psi(\mathbf{P}^*)$, and at the same time, $J(\mathbf{P}) \geq J(\mathbf{P}^*)$, or 2) $\psi(\mathbf{P}) \geq \psi(\mathbf{P}^*)$, and at the same time, $J(\mathbf{P}) > J(\mathbf{P}^*)$.*

The concept described in the above definition is similar to the situation in multi-objective optimization problems. Having both efficiency and JFI as objectives, an optimal point is reached when any attempt to improve one objective worsens the other. A technique to obtain the optimal EJT is presented by [99]. In order to effectively represent the proposed technique, we first need to introduce some key terms. Let τ indicates the minimum efficiency. Additionally, we can define the set of benefit vectors that meet two criteria: they exceed the value of τ, while at the same time having the highest possible JFI. We refer to this set as:

$$\mathcal{P}_\tau \triangleq \left\{ \mathbf{P} | \mathbf{P} = \arg \max_{\psi(\mathbf{P}) \geq \tau,\ \mathbf{P} \in \mathcal{S}} J(\mathbf{P}) \right\}. \tag{4.4}$$

The goal is to identify the benefit vectors that provide the optimal EJT, so those that maximize the $\psi(\mathbf{P})$ are favorable. In this regard, we consider $\mathbf{P}^*_\tau$ to be the chosen benefit vector that fulfills this condition of optimal EJT in relation to τ, as expressed by:

$$\mathbf{P}^*_\tau \in \arg \max_{\mathbf{P} \in \mathcal{P}_\tau} \psi(\mathbf{P}). \tag{4.5}$$

Equations (4.4) and (4.5) satisfy the condition in Definition 2. Therefore, the set of benefit vectors that possess the optimal EJT can be obtained in a procedure that iteratively adjusts the value of τ from its maximum ($\tau_{\max}$) to its minimum ($\tau_{\min}$) in decrements of a step size ε. Given the non-concave nature of $J(\mathbf{P})$ [99], using this method for real-time applications is not practical, especially when the set $\mathcal{S}$ contains a large number of possible benefit vectors. Therefore, finding an alternative solution for such applications is of great importance. In this respect, [99] prove the existence of an alternative equivalent function to obtain $\mathbf{P}^*_\tau$ for any convex set $\mathcal{S}$:

$$\mathbf{P}^*_\tau = \arg \min_{\psi(\mathbf{P}) = \tau,\ \mathbf{P} \in \mathcal{S}} \|\mathbf{P}\|^2. \tag{4.6}$$

Since each element of benefit vectors in $\mathcal{S}$ is bounded by its corresponding safety margin value, $\mathcal{S}$ is considered a hyperrectangle, which makes it a convex set [111]. Utilizing (4.6) in Algorithm 1 enables us to compute the optimal EJT, which, in the scope of this paper, means an efficient fair maximum allocated power for each EVA.

Algorithm 1 Obtaining optimal EJT

Input: Distribution system model, operational constraints (4.1f) to (4.1h), non-EV loads, time step number T, and step $\varepsilon > 0$

Output: $\mathbf{P}_{\tau}^{*}$

```
Initialize grid parameters
for t = 0 to T do
    Formulate and solve (4.1)
    Form the set S using P^{SM}
    Compute τ_min = min_{P∈S} ψ(P), τ_max = max_{P∈S} ψ(P), and L = ⌊(τ_max − τ_min)/ε⌋
    for l = 0 to L do
        τ = τ_max − εl
        Compute P*_τ using (4.6)
        if J(P*_τ) = J(P*_{τ+ε}) then
            break
        end if
    end for
end for
return P*_τ
```

4.3.3 MDP Formulation of EVAs Energy Purchasing Problem

MDP formulation of EVAs purchasing and distribution of energy within this framework has been inspired by [96]. Accordingly, here are essential notations and definitions for the MDP outlined in this work.

Agents i: in this framework, each EVA is considered as an agent. Here the number of agents is denoted as I.

State Space $\{S_i\}_{i\in I}$: the state space of the environment is denoted as $s_{it} = \{SoC_{i,t}^{av}, N_{i,t}^{EV}, e_{i,t}^{g}\}$ for each EVA i at a time step t where $SoC_{i,t}^{av}$ is the average SoC of all EVs; $N_{i,t}^{EV}$ is the number of available EVs during charging process; and $e_{i,t}^{g}$ is the electricity purchasing price for the EVAs which is determined by DSO.

Observation Space $\{O_i\}_{i\in I}$: this work adopts the common assumption that the state of the environment is partially observable for an agent. Each agent i can gain only the observation $o_{it} = \{SoC_{i,t}^{av}, N_{i,t}^{EV}, e_{i,t}^{g}\}$.

Action Space $\{A_i\}_{i\in I}$: the agent i's discrete action space is specified as $a_{it} = P_{i,t}^{g}$, with $P_{i,t}^{g}$ representing the amount of power purchased by agent i from the main grid at time step t.

$$0 \leq P_{i,t}^{g} \leq P_{i,t}^{\max}. \tag{4.7}$$

$P_{i,t}^{\max} \in \mathbf{P}_{\tau}^{*}$ indicates the maximum power that DSO can dedicate to agent i at time step t.

Transition Dynamic $f(s_{i,t}, a_{i,t}^{1}, a_{i,t}^{2}, \ldots, a_{i,t}^{n}) \rightarrow s_{i,t+1}$ depict the probability of the environment transitioning from state $s_{i,t}$ to $s_{i,t+1}$ when agent i undertake actions $a_{i,t}^{1}, a_{i,t}^{2}, \ldots, a_{i,t}^{n}$.

Reward Function: the reward function in this study takes into account both the profit gained from selling power to the EVs and the cost of purchasing energy from the main grid simultaneously. Hence, in this paper, the reward function for an agent i is defined as follows:

$$r_{it} = (\sum_{z=1}^{Z} P_{z,t}^{s} \cdot e_{i,t}^{s} - P_{t,i}^{g} \cdot e_{i,t}^{g}) \times \Delta T, \tag{4.8}$$

where Z is the index of EVs set, $P_{z,t}^{s}$ denotes the volume of power that an EV z buys from EVA and receives from RSD controller in time step t, $P_{t,i}^{g}$ is the volume of power that the EVA i purchased from the main grid. Additionally, $e_{i,t}^{s}$ represents the unit price of power sold by an EVA to EVs, $e_{i,t}^{g}$ is the unit price of power purchased by an EVA from the main grid, and ΔT represents the duration of each time step.

4.3.4 Enhanced DDQN

The DDQN represents a reinforcement learning algorithm designed to tackle challenges in sequential decision-making. Unlike the standard DQN, DDQN incorporates two Q-networks to mitigate Q-value overestimation issues [112]. Compared to actor-critic methods like deep deterministic policy gradient (DDPG), which require training both an actor network for policy and a critic network for value estimation, DDQN is computationally less intensive and easier to tune because it only needs to train two similar Q-networks, simplifying the implementation. Furthermore, a prior study by [113] on RL for EV management highlighted that the DDPG algorithm is highly sensitive to hyperparameter selection, where even a single incorrect parameter can significantly disrupt the learning process. DDQN works well in environments where actions are discrete and the dimensionality of the state space is not excessively high [114].

The two networks in DQQN serve distinct purposes: one for action selection and the other for Q-value estimation. The choice of actions is determined by the online network based on greedy algorithms, while the estimation of Q-values for the selected actions is carried out by the target network. The target Q value for each agent can be calculated as follows:

$$\begin{aligned} Y_{i,t} = r_{it} + \gamma_i Q_{i,t}\big(& s_{i,t+1}, \\ & \operatorname{argmax}_a Q_{i,t}\left(s_{i,t+1}, a_{i,t+1}; \theta_{i,t}\right); \theta_{i,t}^{-}\big). \end{aligned} \tag{4.9}$$

where, for agent i at time step t, the online network's parameters are denoted as $\theta_{i,t}$ while the target network's parameters are denoted as $\theta^{-}_{i,t}$ and γ_i is the discount factor. Correcting for potential overestimation, the $Q_{i,t}$ value of the primary network is adjusted using $\theta^{-}_{i,t}$. Following is an expression for the mean square error loss function between the online and target network's Q-value.

$$L\left(\theta_{i,t}\right) = E\left[\left(Y_{i,t} - Q_{i,t}\left(s_{i,t}, a_{i,t}; \theta_{i,t}\right)\right)^2\right]. \tag{4.10}$$

Last, the parameters of the online network are gradually transferred to the parameters of the target network through a slow averaging process with a rate of $\zeta \in (0,\, 1]$.

$$\theta^{-}_{i,t} = \zeta\theta_{i,t} + (1-\zeta)\theta^{-}_{i,t}. \tag{4.11}$$

Prioritized experience replay is a methodology that emphasizes the replay of particular experiences within the training process by utilizing a replay buffer [115]. The prioritization is determined by the magnitude of the temporal difference (TD) error δ, which measures the difference between the anticipated Q-value and the actual reward obtained. The representation of the TD error at each time step for each agent is as follows:

$$\begin{aligned}\delta_{i,t} = r_{it} + \gamma Q^{\text{target}}_{i,t}\left(s_{i,t+1},\right. \\ \left.\text{argmax}_a\left(Q\left(s_{i,t}, a_{i,t}\right)\right)\right) - Q\left(s_{i,t}, a_{i,t}\right).\end{aligned} \tag{4.12}$$

The agent's learning efficiency improves when instances characterized by notably large TD errors are replayed more frequently. Experiences become more valuable for learning when a considerable TD error exists indicating a significant difference between the agent's prediction and the actual outcome [116]. During training, experiences are chosen from the replay buffer based on probabilities linked to their priority values. Events with higher priority values have an elevated likelihood of being sampled and replayed. This process enhances the agent's ability to learn more effectively from its most informative experiences. The probability of sampling the experience tuple d is defined as follows:

$$Z_i(d) = \frac{Pr_{i,d}}{\sum_l Pr_{i,L}}, \tag{4.13}$$

where $Pr_{i,d}$ represents the priority of experience d for agent i and can be calculated as follows:

$$Pr_{i,d} = |\delta_{i,d}| + \epsilon, \tag{4.14}$$

where ϵ represents a small positive constant that guarantees that every experience has a chance, however small, of being selected for replay.

Adaptive learning rate refers to a technique in optimization algorithms where the learning rate is adjusted during the training process. The difficulty in selecting an appropriate fixed learning rate can lead to slow optimization, getting stuck in local minima with a too-small rate, or experiencing oscillations and convergence issues with a too-large rate [117]. The adaptive learning rate enables the algorithm to take larger steps when the optimization is progressing well and smaller steps when it is not. This adaptability can lead to faster convergence [118]. The following equation indicates the updating process of the learning rate:

$$\alpha_{i,t} = \alpha_i^0 \cdot \frac{\sqrt{1-\beta_{i,t}^2}}{1-\beta_{i,t}^1}, \tag{4.15}$$

where $(\alpha_{i,t})$ is the adaptive learning rate at time step t for agent i in terms of the initial learning rate (α_i^0), and the hyperparameters $\beta_{i,t}^1$ and $\beta_{i,t}^2$ used in the Adam optimizer.

4.3.5 Real-Time Smart Dispatch

The objective of the RSD controller is to efficiently distribute the maximum purchased energy among EVs coordinated by EVAs. It begins by sorting EVs based on their charging urgency, and assigning charging priority accordingly. The aim is to prioritize the charging of EVs in a manner that maximizes the energy available for sale to all EVs in the system.

$$\alpha_{i,z,t} = \beta_{\mathrm{SOC}_{i,z,t}} \cdot \frac{d_{z,i}}{(t_{z,i}^{de} - t) \cdot p_{z,i}^{max}}, \tag{4.16}$$

where at time step t, at EVA i, $\alpha_{i,z,t}$ represent the charging urgency factor of EV z, $d_{i,z,t}$ represents the volume of the electricity demand of EV z, $t_{z,i}^{de} - t$ represents the time interval between the departure time of EV z and the current time, and $p_{z,i}^{max}$ denotes the maximum charging power dedicated to Each EV specifically according to the model of EV z, and finally, $\beta_{\mathrm{SOC}_{i,z,t}}$ represents the SOC-dependent factor which takes into account the lifespan of EV batteries.

$$\beta_{\mathrm{SOC}_{i,z,t}} = e^{-k \cdot \mathrm{SOC}_{i,z,t}}, \tag{4.17}$$

where $k \in [0, 1]$. The exponential decay function indicates that as the SOC increases, the factor $\beta_{\mathrm{SOC}_{i,z,t}}$ decreases exponentially. This implies that there is a diminishing urgency to charge the EV as its SOC increases, resulting in an extended battery lifespan.

In the RSD scheme, a higher urgency in EV charging demand, especially as it approaches departure time or requires more electricity, increases the likelihood of receiving priority in electricity distribution. On the other hand, when EVs reach to an acceptable SoC, the charging rate decreases to prevent any potential harm to the lifespan of the EV batteries. Finally, the SoC of EVs will be updated based on the following formula:

$$\mathrm{SoC}_{i,z,t+1} = \mathrm{SoC}_{i,z,t} + \frac{\Delta t}{C_{i,z}} \cdot P^{s}_{i,z,t}, \tag{4.18}$$

where at EVA i, $\mathrm{SoC}_{i,z,t}$ is the state of charge of EV z at time t, Δt is the time step, $C_{i,z}$ is the capacity of the battery of EV z, and $P^{s}_{i,z,t}$ is the power consumption of EV z at time t.

Algorithm 2 Enhanced DDQN and RSD scheme Algorithm

Input: Episode number E, time step number T, EVA number I
Output: Energy purchasing and distribution strategy for EVAs

1: Initialize prioritized experience replay R
2: **for** $e = 1$ to E **do**
3: **for** $t = 1$ to T **do**
4: **for** $i = 1$ to I **do**
5: Obtain the observation of agent o_{it}
6: Obtain $P^{\max}_{t,i}$ from **Algorithm 1**
7: Agent executes action based on ϵ-greedy (4.7)
8: RSD controller dispatch the energy among EVs using (4.16), (4.17) and report total profit to the agent
9: Update the SoC of EVs using (4.18)
10: Calculate the reward using (4.8)
11: Store transition $(s_{i,t}, A_{i,t}, r_{i,t}, s_{i,t+1})$ in R
12: Sample a mini batch from the replay buffer by taking (4.13) into account
13: Compute the expected Q-values using (4.9)
14: Compute the loss $(L(\theta_{i,t}))$ using (4.10)
15: Update target network parameters using (4.11)
16: **end for**
17: Update the learning rate using (4.15)
18: **end for**
19: **end for**
20: **return** The energy purchasing strategy for EVAs

Algorithm 2 indicates the enhanced DDQN and RSD scheme. At each episode, during the learning process, agents observe the environment, and actions are executed based on the DDQN network. Following the interaction between agents and RSD controllers, the energy will be dispatched among EVs, the reward will be calculated, and transition tuples will be stored in the replay memory, detailed in lines 8–11. Finally, updates are applied to the enhanced DDQN network and learning rate as depicted in lines 12–15.

4.4 Case Study

4.4.1 Power System Model

In this study, the 118-bus distribution test feeder by [119] is used for the case studies. The system includes six EVAs, strategically positioned at the end of branches. As illustrated in Fig. 4.2, positioning the EVAs at these specific locations is a deliberate choice, influenced by the fact that buses located at the end of branches encounter more significant challenges related to voltage drops and power losses within the distribution grid. As the framework is

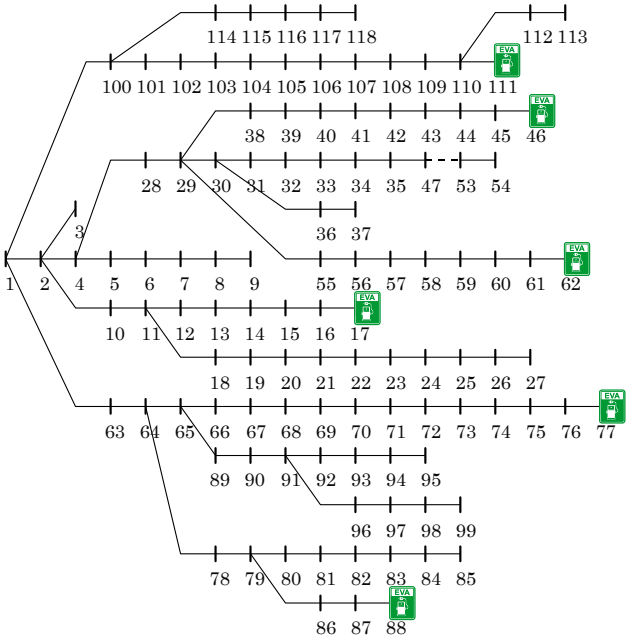

Figure 4.2 Distribution network and the location of EVAs.

designed for online applications, the study considers each time step a 15-minute interval within 24 hours. Table 4.1 presents essential information on the daily inflow of EVs to each EVA, including their arrival and departure times determined by the Gaussian distribution factor. Furthermore, real distribution grids typically accommodate different types of consumers (i.e., residential, commercial, and industrial). To accurately model the grid, demand curve data for different types of consumers is obtained from [120] and [121] representing non-EV loads. These load profiles are then randomly assigned to different buses in the network..

Moreover, to calculate the reward function on (4.8), a real time pricing scheme has been taken into account as $e^g_{i,t}$ which implies the rate of the electricity purchasing price of EVAs from DSO while $e^s_{i,t}$ implies a fix rate of 0.5 \$/kWh selling energy to EVs. Finally, EVs type and their market share have been extracted from [96].

Table 4.1 EVA Information. μ and σ values indicating the mean and standard deviation of arrival/departure times in 15-minute time intervals, respectively

EVA	**EV Number**	**Arrival** μ_{arrival}, σ_{arrival}	**Departure** $\mu_{\text{departure}}$, $\sigma_{\text{departure}}$
1	100	32, 20	64, 16
2	140	30, 16	55, 12
3	150	50, 16	75, 8
4	60	24, 20	50, 8
5	110	36, 12	64, 16
6	80	55, 16	75, 4

4.4.2 Simulation Environments and MADRL Parameters

By linking MATLAB and Python, this work takes advantage of both environments. Problem (4.1) is formulated in MATLAB and solved by *fmincon* using MATPOWER [122] package. In addition, the MADRL framework is implemented in Python and MATLAB API is used to obtain safe margin and optimal EJT. Using MATLAB API in Python environment renders a real-time simulated framework. The simulation results are obtained on a PC with an Intel Core i7-12700H CPU 2.30 GHz and 40 GB of RAM.

In the context of DDQN parameters, the discount rate γ is set to 0.95, the exploration-exploitation trade-off parameter ϵ in ϵ-greedy is set to 0.95, the mini-batch size is set to 32, the experience replay buffer size is set to 1000, the learning rate is set to 0.001, and the target network update frequency is set to 1000.

4.5 Experimental Results

This section presents the results of three distinct scenarios (SC): 1) the proposed safe MADRL framework (SC1) , 2) Uncontrolled charging (SC2) and 3) First come first serve (FCFS) (SC3). A comparative analysis between these three scenarios is then carried out.

4.5.1 The proposed safe MADRL framework charging (SC1)

In this framework, as explained in Section 4.2.1, there is an online interaction between the DSO and each EVA at each time step. The maximum allowable power set points are calculated and signal set points are sent to EVAs separately. Accordingly, each EVA (agent) based on its observation determines its energy purchased. In Fig. 4.3, the daily charging profiles of all EVAs in SC1 are displayed. All EVAs prefer to purchase power during periods of relatively

lower electricity prices from the DSO.

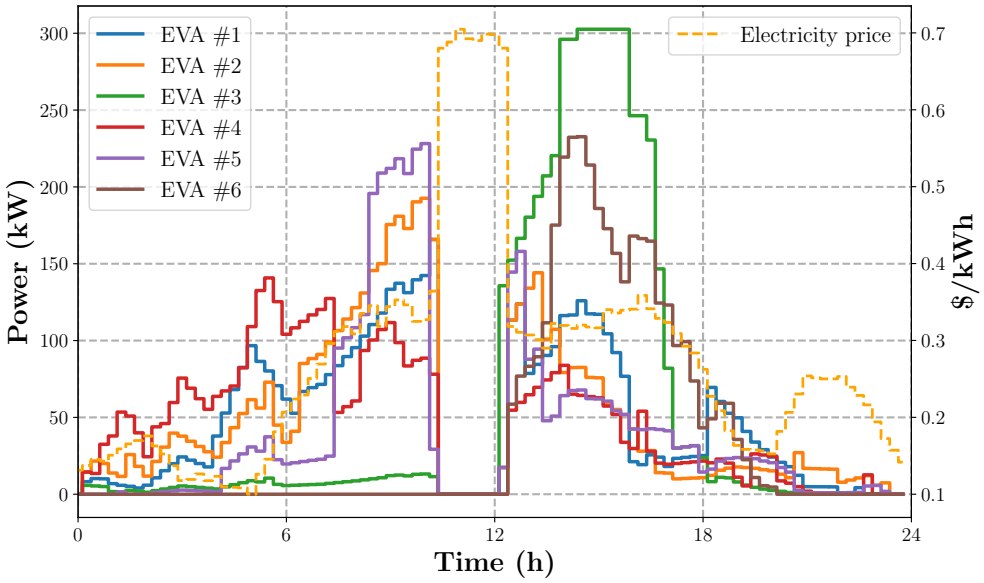

Figure 4.3 EVAs daily consumption - SC1.

Fig. 4.4 illustrates the charging strategy for EVs associated with EVA 4. The RSD controller allocates energy to each EV based on the urgency of their charging needs at each time step. Initially, upon their arrival, EVs tend to charge at a higher rate with respect to their maximum charging rate, to quickly reach a satisfactory SoC. Once a suitable SoC is achieved, the charging rate decreases to extend the battery's lifespan, gradually leading to the desired SoC.

Fig. 4.5 displays the initial and final SoC of EVs of each EVA in SC1. The initial SoC distribution for EVs follows a Gaussian pattern specific to each EVA. The average initial SoC for EVs across all EVAs is 0.45. Fig. 4.5 also illustrates the final SoC of EVs in SC1, demonstrating the effective performance of RSD in dispatching energy among EVs, given that a significant proportion of the EVs have achieved the desired final SoC.

To indicate the superiority of enhanced DDQN, its performance has been compared with DDQN [123], DDPG [124] and proximal policy optimization (PPO) [125] as illustrated in Fig. 4.6. The solid and its respected shadow show the mean and standard deviation of the cumulative rewards of all EVAs over 10 runs, respectively. Evidently, enhanced DDQN achieves a near-optimal solution in a significantly reduced number of episodes. A prioritized experience replay helps DDQN focus on more important experiences, enhancing learning efficiency and speeding up convergence to an optimal policy. Additionally, an adaptive learning rate allows for quicker exploration initially and finer adjustments later, improving stability

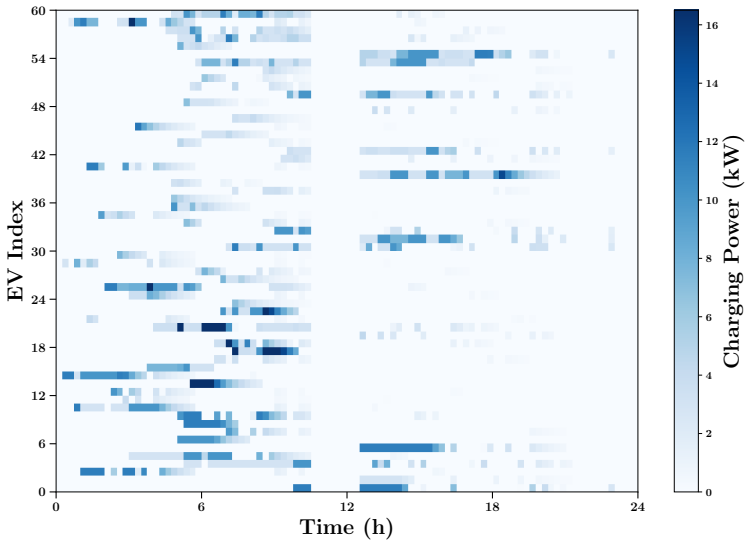

Figure 4.4 Charging plan of EVs of EVA #4 - SC1.

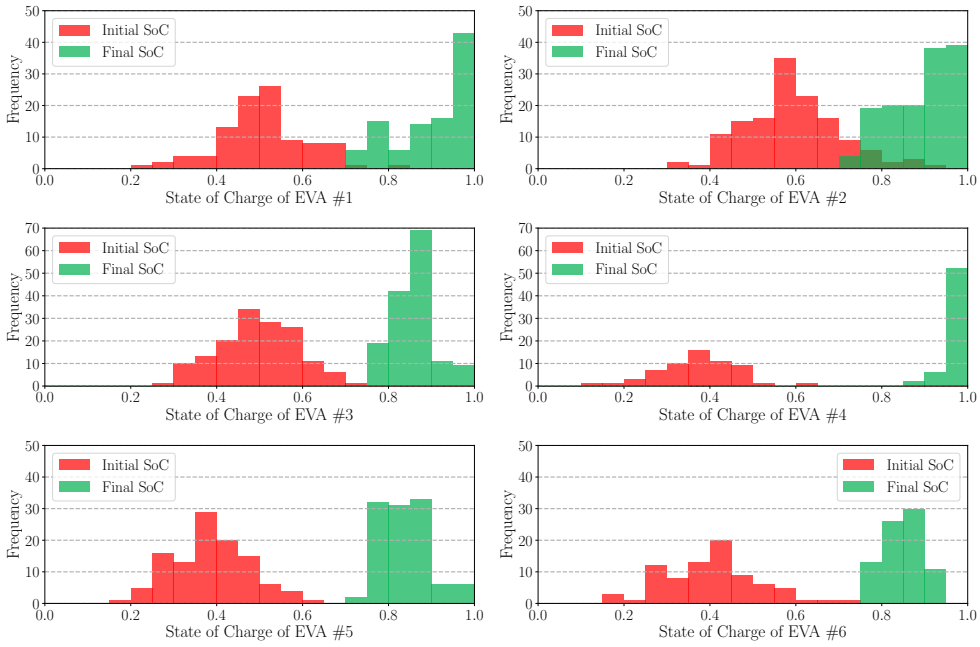

Figure 4.5 Initial and final SoC distribution - SC1.

and avoiding suboptimal solutions. These methods combined result in better performance and higher cumulative rewards than standard DDQN, DDPG and PPO. Finally, the computational training times of these four methods are illustrated in Table 4.2. The enhanced DDQN method took 3134 seconds, showing a slight increase in time over standard DDQN, which completed in 2569 seconds. In contrast, DDPG required 4431 seconds, reflecting the added complexity of its actor-critic architecture. PPO, being a policy gradient method with stability-enhancing features, exhibited the highest training time at 5934 seconds, significantly surpassing the other methods.

Table 4.2 Computational training times for different methods in 1000 episodes.

Methods	**Enhanced DDQN**	**DDQN**	**DDPG**	**PPO**
Computational Training Time (seconds)	3134	2569	4431	5934

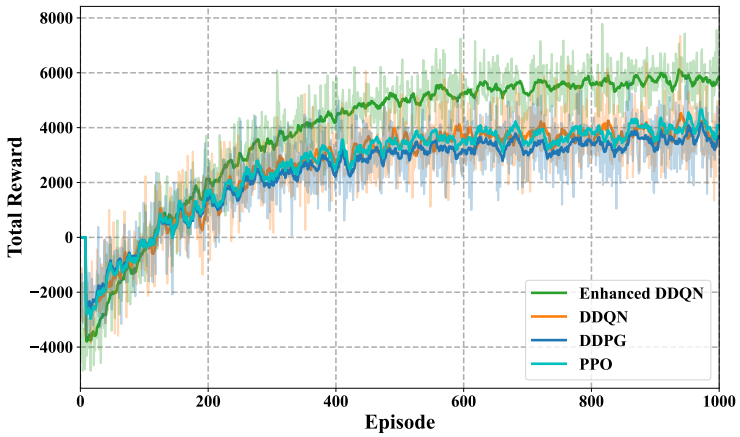

Figure 4.6 Comparison of different RL methods over 10 runs - SC1.

4.5.2 Uncontrolled charging (SC2)

In SC2, the assumption is made that all EVs will be charged at their maximum rate upon reaching charging stations. Additionally, it is presumed that there are no restrictions for EVAs regarding purchasing energy from the DSO, allowing them to purchase as much energy as needed according to their demand. As illustrated in Fig. 4.7, in SC2, the collective charging of a significant number of EVs at their maximum charging rates leads to a higher peak power consumption for EVAs in comparison with SC1 which may cause operational challenges for the DSO. As an example, as shown in Table 4.3, in SC2, the daily peak power consumption of EVAs 3 and 6 is 498.12 kW and 299.44 kW, respectively. This signifies a 62.22% increase

for EVA 3 and a 27.67% increase for EVA 6 when compared to the 307.05 kW and 234.54 kW observed in SC1, respectively.

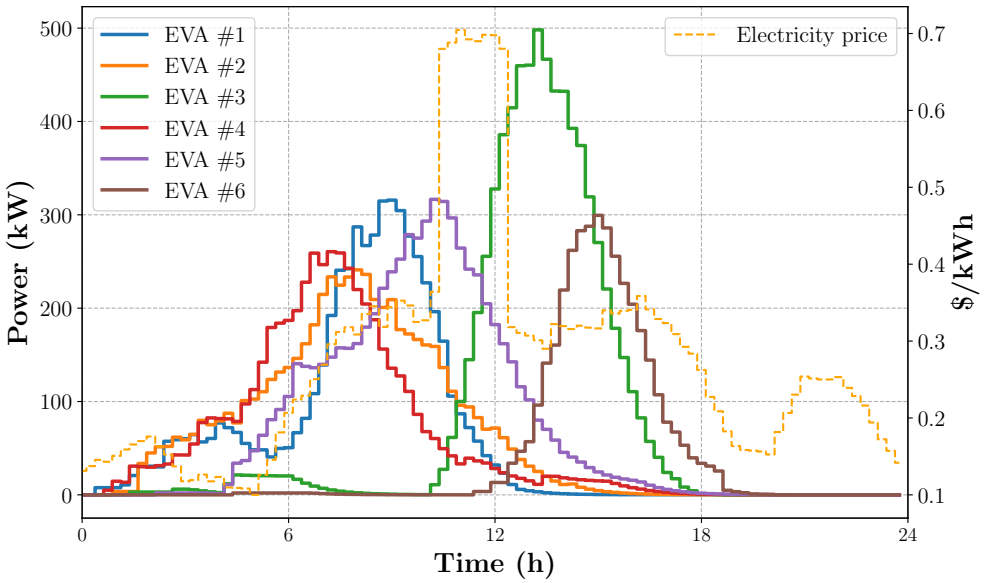

Figure 4.7 EVAs daily consumption - SC2.

Due to the fact that in SC2 EVs are charged with their maximum rate of charge, it is undeniable that the final SoC distribution is in better condition than that is in SC1. However, this achievement is obtained at the cost of higher energy purchasing prices for EVAs compared to SC1 as EVAs charge a considerable number of associated EVs during times of on-peak electricity prices as shown in Table 4.3.

4.5.3 FCFS (SC3)

In SC3, the assumptions remain identical to those in SC2, with the only difference being the maximum number of EVs allowed for charging per time step, set to 50 per EV aggregator. Additionally, EVs are prioritized based on their arrival times. As illustrated in Fig. 4.8, the charging profiles of EV aggregators with a larger number of daily EVs are more impacted, as seen with EVAs 3, 5, and 6, where the charging duration is longer compared to SC2. This increase in charging time is due to the prioritization of EVs based on their arrival sequence. Moreover, some EVs may not receive sufficient energy by their departure time since they have waited in the queue for a significant period, which could lead to a decrease in the EV aggregators' profit from charging and cause dissatisfaction among EV owners. Ultimately, for instance, the electricity purchasing costs in SC3 for EVAs 1, 3, and 5 are 1670.11, 2653.54, and 2431.53 $, respectively, representing increases of 9.01%, 19.29%, and 25.66% compared

to their corresponding costs in SC1. Additionally, their daily peak power consumptions are 255.82, 346.25, and 271.50 kW, respectively, which are 75.65%, 12.76%, and 19.47% higher than the corresponding daily peak powers in SC1, as depicted in Table 4.3.

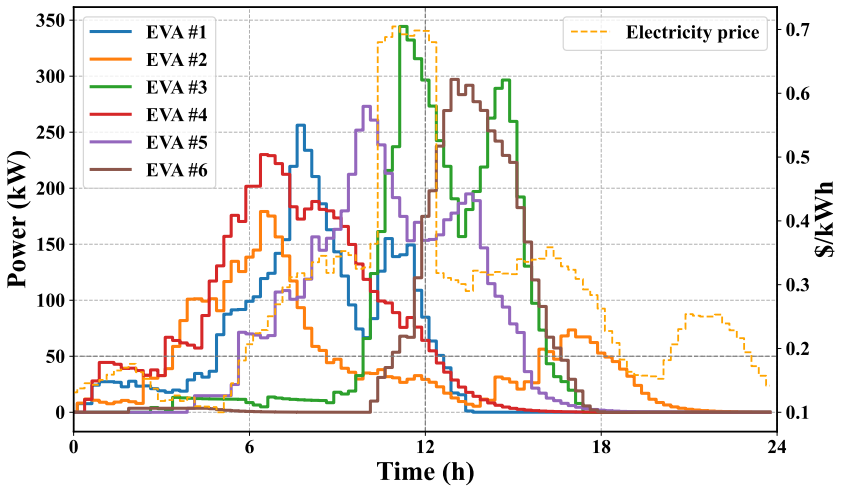

Figure 4.8 EVAs daily consumption - SC3.

Table 4.3 Electricity Purchasing Costs and Peak Power for EVA

EVA	Peak Power in SC1 (kW)	Electricity Purchasing Cost in SC1 ($)	Peak Power in SC2 (kW)	Electricity Purchasing Cost in SC2 ($)	Peak Power in SC3 (kW)	Electricity Purchasing Cost in SC3 ($)
EVA #1	145.64	1532.10	315.73	2127.44	255.82	1670.11
EVA #2	188.28	1701.76	241.05	1805.48	178.15	1203.67
EVA #3	307.05	2224.48	498.12	2559.07	346.25	2653.54
EVA #4	142.11	1172.06	260.50	1345.69	230.19	1678.92
EVA #5	227.25	1935.02	316.55	3129.68	271.50	2431.53
EVA #6	234.54	1935.02	299.44	1663.02	297.45	1688.13

Fig. 4.9 illustrates power allocation and consumption patterns for EVAs over the 24-hour simulation period. It presents a comparative demonstration of non-EV loads, safe margin values, optimal EJT, SC1, and SC2. The results highlight the effectiveness of the proposed framework in maintaining power consumption within the optimal EJT. This assures the grid's safe operation while considering both efficiency and fairness in power allocation to EVAs, as opposed to uncontrolled charging in SC2. For instance, Fig. 4.9(a) shows the success of the proposed framework in shifting the EV consumption to avoid peak and distributing the

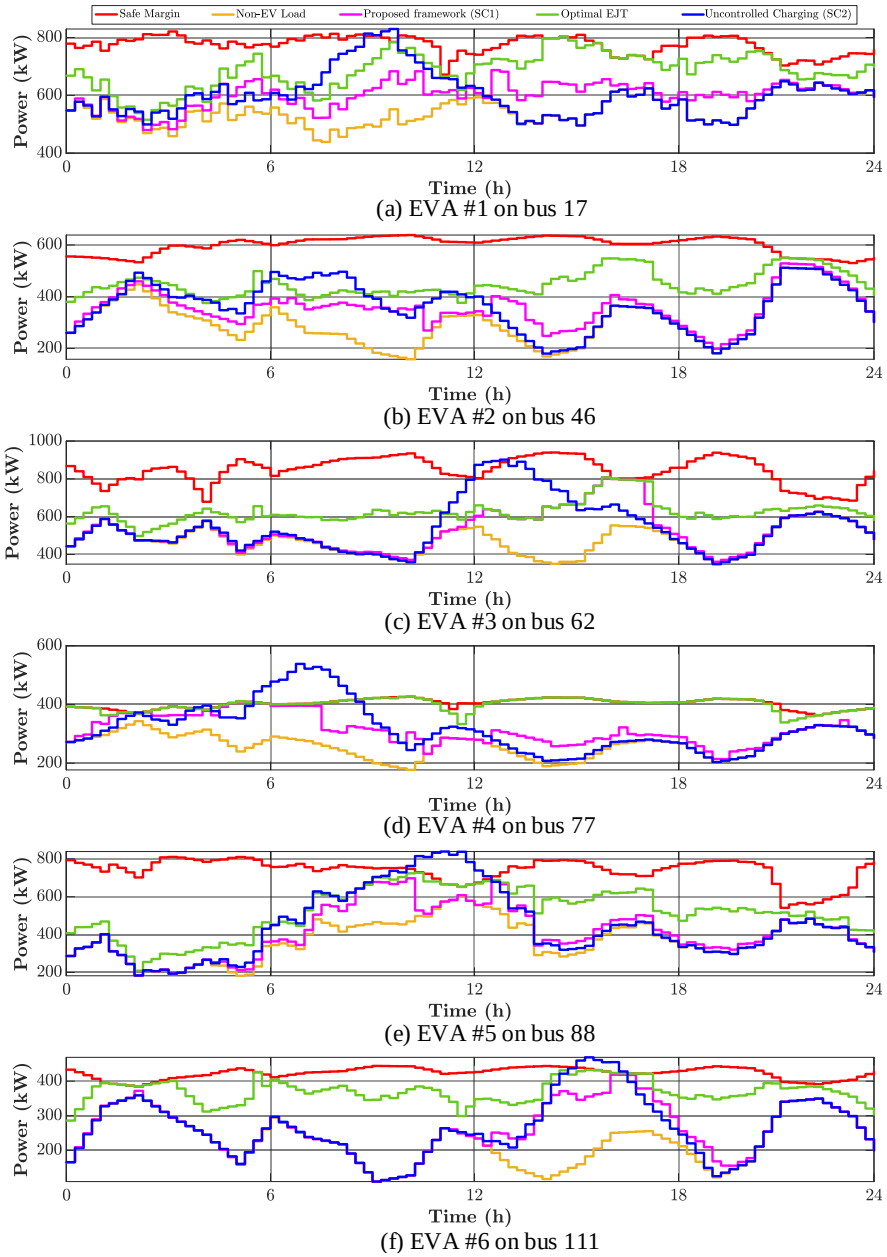

Figure 4.9 Power allocation and consumption of EVAs in SC1 and SC2.

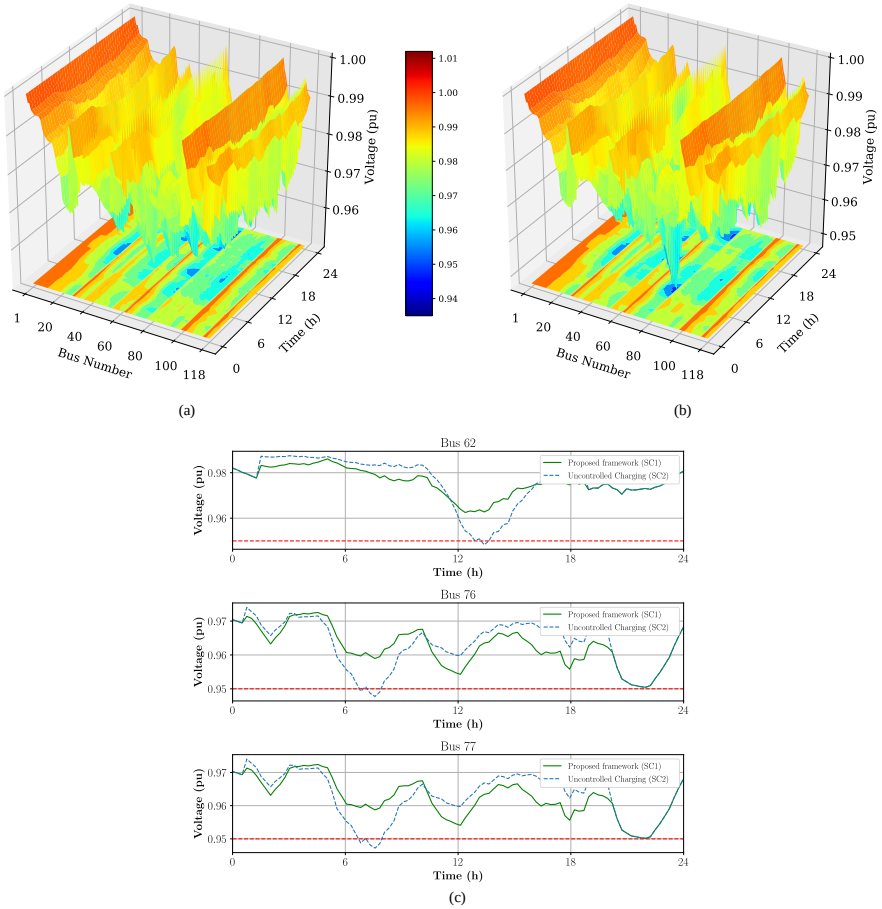

Figure 4.10 Voltage magnitude. (a) Voltage under proposed framework (SC1). (b) Voltage under uncontrolled charging (SC2). (c) Buses with voltage violation.

EV demand more evenly across the simulation time. Although SC2 does not violate the safe margin in Fig. 4.9(b), during some intervals, it exceeds the optimal EJT, suggesting that fairness is not adequately maintained, especially compared to the result observed in SC1. Moreover, despite EVA 3 short window for charging EVs, as per Table 4.1, Fig. 4.9(c) indicates its successful performance in using the available time, as indicated by the power consumption closely following the optimal EJT. The correlation between safe margin and optimal EJT for EVA 4, as seen in Fig. 4.9(d), suggests that the grid constraints are tight at bus 77. Therefore, considering the fairness concept enables EVA 4 to potentially be allowed to draw maximum power (i.e., safe margin) over many intervals. Lastly, Fig. 4.9(e) and Fig. 4.9(f) display the effectiveness of the proposed framework in charging EVs in a shiftable manner without overloading the grid even with a late average arrival time for EVs, as indicated in Table 4.1. Moving from analyzing EVAs' power consumption patterns, Fig. 4.10 presents an examination of voltage profiles under two scenarios. In this study, the acceptable voltage magnitude for buses is defined with a lower bound of 0.95 pu and an upper bound of 1.05 pu. As depicted in Fig. 4.10(a), voltage of buses in SC1 is within the acceptable range. Yet, in SC2, violations of this constraint are observed at buses 62, 76, and 77, as shown in Fig. 4.10(b) and Fig. 4.10(c). At bus 62, SC1 successfully maintains the voltage level within the safe operational limits. This, in fact, is obtained by allocating a value below safe margin power (i.e., optimal EJT) to the EVA. Conversely, under SC2, a deviation in voltage is observed, which matches the EVA 3 peak charging period in Fig. 4.9(c). Furthermore, the results at buses 76 and 77 highlight the benefit of using the MADRL approach to manage EV charging through EVA. Given that no EVA is connected to bus 76, the results suggest that uncontrolled charging may lead to unsafe grid operation. It is also observed that among the buses with EVAs, only buses 62 and 77 experience a voltage drop under SC2. While EVA 2 in SC2 stays within the safe margin, the EVAs associated with buses 17, 88, and 111 distinctly exceed their respective safe margins. This indicates that another critical operational threshold of the grid, line capacity or thermal limit, is at risk.

Fig. 4.11 illustrates the allocated power to each EVA during the 24-hour period obtained by optimal EJT calculation. As it is demonstrated in Fig. 4.9(d), allocated power to EVA 4 is mostly equal to the safe margin. This means that at certain times during the day, EVA 4 has a lower allocated power compared to other EVAs.

4.5.4 Integration of RESs

In this section, we investigate the performance of the proposed framework in the presence of RESs, focusing on PV systems. The location of these systems in the grid affects the allocated

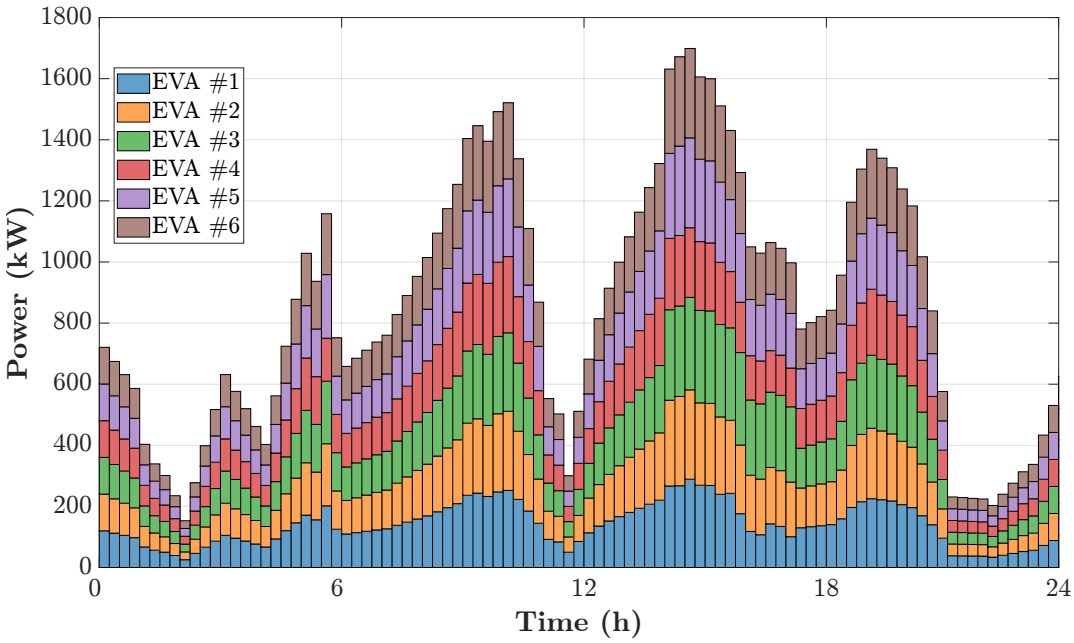

Figure 4.11 Allocated power to each EVA by DSO through optimal EJT calculation.

power to each EVA and potentially the safe margin. We first demonstrate how PV integration into buses with existing EVAs mainly alters the allocated power to those EVAs. Second, we show that installing PV systems on other buses can potentially enhance the safe margin value.

PV Placement on EVA Buses

In this subsection, we analyze the effects of placing PV systems on buses with EVAs. In this scenario, it is assumed that PV systems are installed on all six buses hosting EVAs. A sensitivity analysis is then performed based on the percentage of total energy consumed by each EVA throughout the day. Specifically, we evaluate cases where the PV systems can supply up to 35 percent of the total energy required by an EVA over a 24-hour period. The safe margin is tied to the constraints of the grid and may not be significantly changed by the placement of PV systems under typical operating conditions. However, using PV allows the bus to satisfy part of its demand locally. As all EVAs benefit from this opportunity, we should expect an increase in the power allocated to EVAs derived from optimal EJT during the daytime when solar radiation is available, as shown in Fig. 4.12. This increase makes the grid more reliable and helps EVAs potentially earn more money by relying less on costly grid electricity.

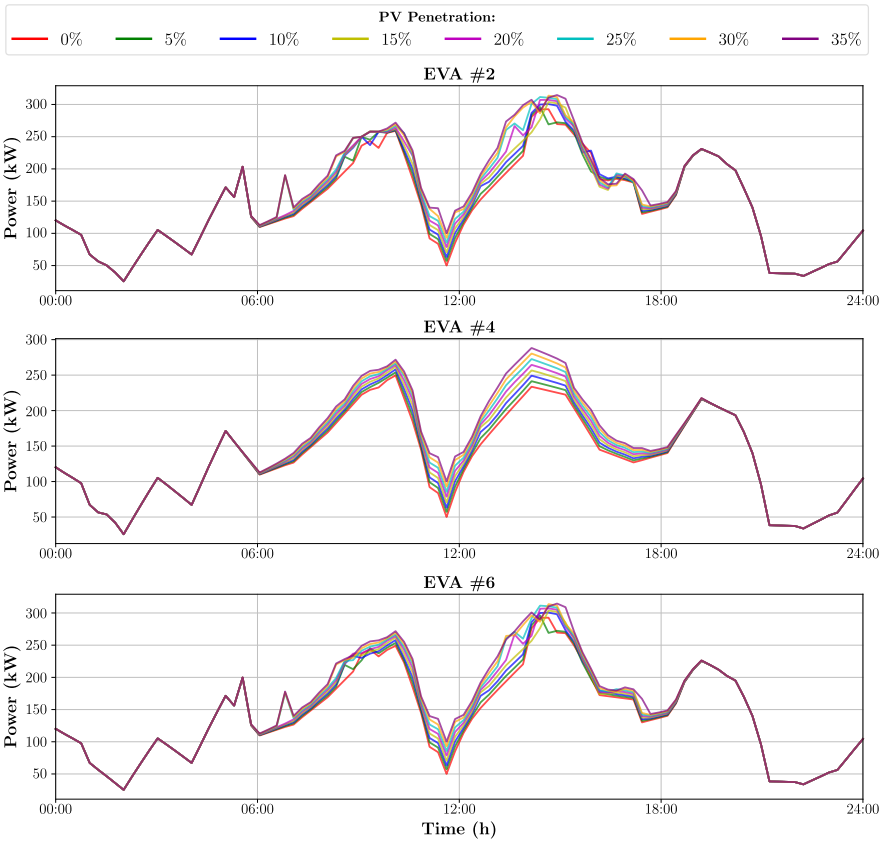

Figure 4.12 Allocated power to each EVA by DSO through optimal EJT calculation under different PV penetration.

PV Placement on Other Buses

In this scenario, PVs are installed at buses 41, 69, and 105. These locations are chosen because they are positioned near the middle of the branches, with EVAs located at the branch ends. This placement can potentially help mitigate voltage drops and reduce loading on the lines. To investigate the impact of PV penetration levels on the safe margin values, a sensitivity analysis is performed by changing the percentage of the bus's total energy demand that is supplied by PV during the day. As the results demonstrate in Fig. 4.13, regardless of the level of PV penetration at bus 41, the safe margin values of EVA in the same branch do not change. The ongoing congestion in the branch connecting buses 41 and 46 is causing this issue. This also indicates the need for corrective actions, such as enhancing lines' capacity. On the other hand, PV penetration on buses 69 and 104 effectively increase the safe margin values at the EVAs at the end of their respective branches.

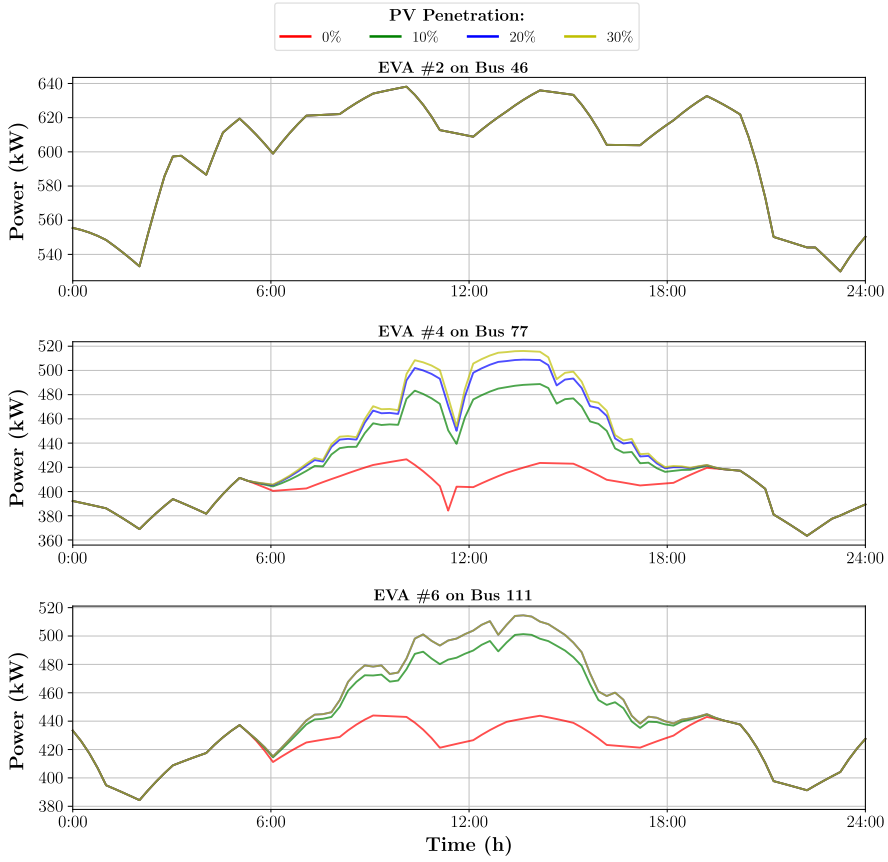

Figure 4.13 PSafe margin variations for different PV penetration levels with installations located at the midpoints of branches.

4.6 Conclusion

This research introduced a MADRL framework for managing energy purchasing and distribution for EVAs while considering distribution network constraints. The framework operates hierarchically, allocating maximum allowable power to each EVA to ensure grid safety, while also achieving equitable energy distribution among EVAs. At the top level, it identifies the optimal EJT point, balancing the maximum total energy the DSO can sell with equitable power allocation among the EVAs.

At the lower level, each EVA functions as an autonomous agent, adopting a DDQN with adaptive learning rates and prioritized experience replay. Through this method, EVAs are able to refine their energy purchasing strategies, increasing their profits. Additionally, at this level, an RSD controller manages the energy distribution among EVs based on their requirements. The proposed framework, including scenarios with PV systems integrated at various buses, is implemented on the 118-bus distribution test feeder, and its performance is compared with uncontrolled and FCFS charging scenarios. The results suggest that the proposed framework significantly enhances grid stability and energy distribution, outperforming the two other mentioned scenarios in terms of both energy purchasing price and peak demand reduction for EVAs.

As a next step in this research, the integration of uncertainty in energy demand and EV behavior should be explored, along with the application of robustness techniques to ensure reliable system performance during grid faults or price fluctuations. Subsequent works can also explore MARL approaches that consider interactions between EV aggregators and other grid elements such as energy markets.

CHAPTER 5 ARTICLE 2: TEMPORAL FUSION TRANSFORMER-BASED PREDICTIVE STRATEGY FOR EFFICIENT CLUSTERED ELECTRIC VEHICLES CHARGING MANAGEMENT

Authors: Arian Shah Kamrani, Hanane Dagdougui, Dalal Asber

Submitted on March 25st, 2025 at *Engineering Applications of Artificial Intelligence*, under review.

Contributions: Conception of the work's idea, literature review, design of experiments, implementation of the code, conducting the experiments, analysis of the results, and writing.

5.1 Introduction

5.1.1 Motivation

Nowadays, electric vehicle (EV) fleets have emerged as a main component of transportation systems, playing a significant role in mitigating greenhouse gas emissions (GHG) [126]. For example, in Canada, the transport sector, which was the second-largest contributor to GHG emissions, accounting for over 22% of emissions in 2020, has become a prime focus of numerous policy initiatives [127]. Since July 2024, there have been nearly 30,000 public charging stations in Canada [128], with more than a third of them located in the province of Quebec. However, as the number of charging stations grows, the uncertainty of charging behaviors also increases, making managing their operations problematic. Therefore, EV aggregators (EVAs) are essential in the EV charging management framework as they facilitate the management of EV charging infrastructure across various locations, participate in demand response programs and energy markets, and provide grid support services such as peak load shaving and frequency regulation.

Aggregating EV ports only based on their geographical locations fails to capture temporal dynamics, making it difficult to predict behavior of their associated EVs and manage their demand effectively, as such aggregation overlooks variations in usage patterns. In contrast, clustering charging ports using spatiotemporal features has been shown to better capture trends in charging behaviour, improving the forecasting accuracy of charging patterns and providing better management of data diversity EVs [129].

In recent years, machine learning-based models have played a vital role in handling the increasing complexity of EV charging behaviors, especially for their smart charging management.

One promising approach to enhance the prediction accuracy of EV charging patterns is to predict the uncertainties in EV owners' behavior [130]. Alternatively, instead of focusing on individual EV owners' behavior, which can be resource-intensive and complex due to various changes in driving habits, another way is to predict EV port usage which allow the aggregation of these behavior into manageable patterns and capture the dynamics of charging demand patterns across locations. Such aggregation mode can also help decision makers to develop dynamic pricing strategies, encouraging off-peak charging and balancing demand across various ports. Even though Models like recurrent neural networks (RNNs) or long short-term memory (LSTM) networks can effectively capture immediate temporal dynamics for short-term fluctuations, more advanced models, such as temporal fusion transformers (TFTs), are well-suited for long-term dependencies as they employ attention mechanism for their prediction. These models improve the accuracy of EV charging predictions, leading to more reliable and efficient management of EV fleet operations in both day-ahead (DA) and real-time (RT) scenarios.

Due to privacy concerns and limited access to real EV charging transaction data, most studies have focused only on EV charging management in DA or RT markets. However, considering both DA and RT aspects in the charging management of EVs is necessary for efficient distribution network operation. As a result, there is a gap in addressing the complexities of accurately predicting EV owners' behavior in each port which this paper addresses to reduce the operational costs of EVAs across both DA and RT operations.

5.1.2 Related works

EVAs are essential components of the grid, as they coordinate the charging of multiple EVs into the grid by considering efficient energy use and minimizing charging costs. The aggregation of EVs can be done in various ways depending on their application. For instance, [131] proposed a heterogeneous aggregation model for EVs. Here, the term "heterogeneous" refers to the EVs' physical characteristics and charging behaviors, such as battery capacity and power consumption, which are considered in their control and coordination strategies. Another method of aggregation of EVs can be related to the type of energy sector. As an example, residential EVs are considered by [132], which proposes a non-intrusive load extraction algorithm or [133] that investigate various smart charging strategies for a commercial EV fleet in Germany, taking into account RT pricing tariffs linked to DA market prices and the integration of renewable energy sources. Clustering based on the characteristics of EV owners is another way of aggregation of EVs. [134] proposed EVs clustering based on their battery capacity and efficiency (measured in Wh/km) as part of a two-stage optimization

approach to reduce computational complexity. [135] introduced a novel methodology that begins by clustering historical charging sessions based on key user characteristics, such as arrival time, charging duration, and average power consumption. The approach then predicts individual charging sessions using these parameters, eventually forecasting the cumulative energy demand of the charging infrastructure.

The EV owners' behavior prediction for DA charging management with machine learning algorithms is another topic that should be investigated. [87] presented a data-driven generative adversarial network (GAN) to address uncertainties in EV users' behavior and presented a DA smart charging method that minimizes costs related to distribution systems, EV battery degradation, and emissions while optimizing power scheduling in EV parking lots with photovoltaic systems. [136] used LSTM networks for individual EV charging behavior prediction for the upcoming day, which focused on the main charging parameters such as duration, frequency of charging, and the likelihood of occurrence of charging. [137] introduced a novel deep neural network framework that predicts EV user behavior, including charging duration and energy consumption, by jointly training the model for both tasks. [138] employed a neural network-based charging demand forecasting method to manage charging tasks. An optimization model was introduced that accounts for charging costs, battery degradation, and user dissatisfaction.

EVs DA and RT charging management has recently become an important topic. [95] proposed RT smart charging management of EVs based on reinforcement learning, which aimed at minimizing charging costs while addressing peak load shaving under uncertainties related to EV owners. Moreover, to improve computational efficiency, they introduced an advanced actor-critic learning algorithm to reduce state dimensionality. [139] initially formulated a stochastic bi-level optimization model to integrate bidding and pricing strategies. Then, a semi-dynamic traffic assignment model is developed to forecast EV charging behaviors under various pricing schemes. [105], proposed a three-layer hierarchical framework for DA optimal EV charging scheduling containing distribution system operator, EVAs, and EV charging stations. This framework employs an alternating direction method of multipliers-based single-loop iterative algorithm for faster convergence, addressing charging cost minimization, peak load shaving, and voltage regulation. [140] presented a DA and RT optimization for EVs charging management. This work addresses uncertainties in charging demand through a deep learning-based approach that combines clustering historical travel data to analyze EVs demand and employing LSTM networks for prediction. [141] proposed a DA-RT centralized framework that aims to minimize the total charging cost for the EVs, formulated as mixed-integer programming. While the model during DA assumes full knowledge of EV demand and energy generation, during RT, an online algorithm is proposed, which iteratively calls the

offline model and addresses unknown uncertainties. [142] proposed an RT deep-Q network-based reinforcement learning demand management strategy for EV charging stations, which reduces the grid load during peak hours. The deep reinforcement schedules the charging and discharging of EVs to minimize the cost and manage the charging station load.

5.1.3 Contribution and paper organization

According to the literature review:

- Most existing works, such as [129, 134, 135], have focused on clustering individual EVs rather than EV charging ports. However, the spatiotemporal patterns exhibited by charging ports are more consistent than those exhibited by individual EVs. Therefore, considering public charging ports for clustering can improve predictability and provide more stable forecasting models [143].

- Several works, such as [87,136,137], have considered uncertainties in EV owners' behaviors and proposed different prediction methods to address this challenge. However, most approaches mainly consider individual EV owners and do not take into account the benefits of aggregating EV charging ports. Here, aggregating EV charging ports means grouping chargers at a common location into a single EVA whose demand is managed collectively rather than per EV. One main benefit of spatiotemporal clustering is that it helps the predictive models identify the overall charging patterns more effectively. This can yield improved accuracy and provide a better understanding of EV charging demand.

- Previous studies have mainly utilized RNN-based models, particularly LSTM, for the prediction of EV charging behavior [129, 136, 140]. Although these methods capture short-term dependencies efficiently, they cannot often model long-range temporal relationships in time-series data. On the other hand, transformer-based models address these challenges by utilizing attention mechanisms to identify key temporal patterns and overcome uncertainties.

- To the best of the authors' knowledge, a study that simultaneously considers the clustering of charging ports, the prediction of EV behavior based on this clustering, and the integration of these predictions into DA and RT charging frameworks remains lacking. This gap in the literature is highlighted in Table 5.1. Such an integrated approach is critical for optimizing charging strategies and improving system efficiency and reliability.

In this work, a novel cluster-based aggregation method for EV charging ports is introduced, which utilizes spatiotemporal factors to form EVAs. Next, a TFT model is employed to predict key parameters for EVs within each cluster, ensuring accurate forecasting of EV charging behavior. Based on these predictions, a two-stage DA and RT charging bidding

Table 5.1 Comparison of the proposed scheme with the state-of-the-art

Reference	**Clustering**	**Prediction**	**Smart Charging**	**DA or RT optimization**	**Method Used**
[136]	No	Yes	No	-	LSTM
[87]	No	Yes	Yes	DA	GAN & Interior point method
[129]	Yes	No	Yes	DA	K-means & grey wolf optimization
[134]	Yes	No	Yes	DA	K-means & CPLEX Optimizer
[137]	No	Yes	No	-	JETPANN
[105]	No	No	Yes	DA	ADMM
[135]	Yes	Yes	No	-	OPTICS & LSTM
[141]	No	No	Yes	DA & RT	Mixed-integer programming & Online scheduling
Proposed Scheme	**Yes**	**Yes**	**Yes**	**DA & RT**	**TFT & K-means & CVXPY**

strategy is developed, aimed at minimizing charging costs, performing peak shaving, and reducing the charging pattern difference between DA and RT. The DA strategy optimizes energy procurement based on predicted charging demand, while the RT strategy adjusts to actual demand. Both strategies align with electricity market dynamics, ensuring compliance with California Independent System Operator (CAISO) rules. The approach minimizes discrepancies between DA commitments and RT adjustments, helping avoid penalties and improving market efficiency. Discrepancies are minimized because DA schedules are based on TFT forecasts, and the RT step continuously corrects deviations using updated arrival and demand information. The specific contributions of this work are as follows:

- A new approach for spatiotemporal clustering of EV ports is presented, which results in the formation of EVAs. The clustering is done based on popularity, utilization, charging level, and average time of use of the EV ports. These factors provide valuable insights into understanding and predicting the behavior of EV owners.
- A TFT model is utilized to predict key parameters of EVs inside each cluster for charging, including arrival times, departure times, and energy consumption. Due to the fusion and attention-based mechanisms of the TFT, it can successfully learn temporal patterns and uncertainties, which makes it a highly accurate model for time series predictions.
- An effective bidding strategy for DA and RT EV energy management has been designed

to minimize EVAs' charging costs, daily peak power consumption, and the discrepancy in charging profiles between DA and RT.

The rest of this paper is organized as follows. In Section 5.2, the proposed scheme is presented. Section 5.3 describes the problem formulation. The case study is introduced in Section 5.4. Section 5.5 provides the simulation results and analysis. Finally, the conclusions are presented in Section 5.6.

5.2 Proposed Scheme Overview

The proposed scheme's main objective is to develop an efficient charging strategy for EVA that addresses both DA and RT operations. As shown in Fig 5.1, the proposed EV port aggregation and charging management scheme is organized into three steps. In the first step, historical charging transaction data for each public charging port is collected, analyzed, and prepared for clustering. Popularity and utilization (spatial factors), along with charging level and time-related aspects (temporal factors), are used to cluster EV ports and hence form EVAs based on clustering results. This spatiotemporal clustering process enhances the predictability of EV user behavior, and in the subsequent step, the behavior of EV owners in each EVA will be predicted. To implement a smart charging program, EVAs must predict key parameters such as EVs' arrival times, departure times, and energy requirements. Three TFT models are used to predict these parameters in each cluster, as illustrated in Fig 5.1. Three TFTs are used because arrival time, departure time, and energy demand have different distributions and correlations, and predicting them separately yields higher accuracy. First, arrival times are predicted, and then they will be used as the inputs for the following two TFT models to predict both departure times and energy requirements, as there is a strong correlation between these parameters in EV charging behavior. In the final step of this scheme, a two-stage DA and RT charging bidding strategy for EVs is implemented to perform peak shaving, reducing overall costs and minimizing the difference between DA and RT costs. This step implements DA smart charging using EV owner behavior predictions from TFT. The EVA set its bid and minimizes charging costs by leveraging demand flexibility and securing the required charging demand through the DA and RT markets. Under CAISO rules, DA bids are binding and must be fulfilled the next day. Participants may adjust their DA bids incrementally in the RT market, but non-compliance with DA commitments incurs payment reductions and penalties, as detailed by [144].

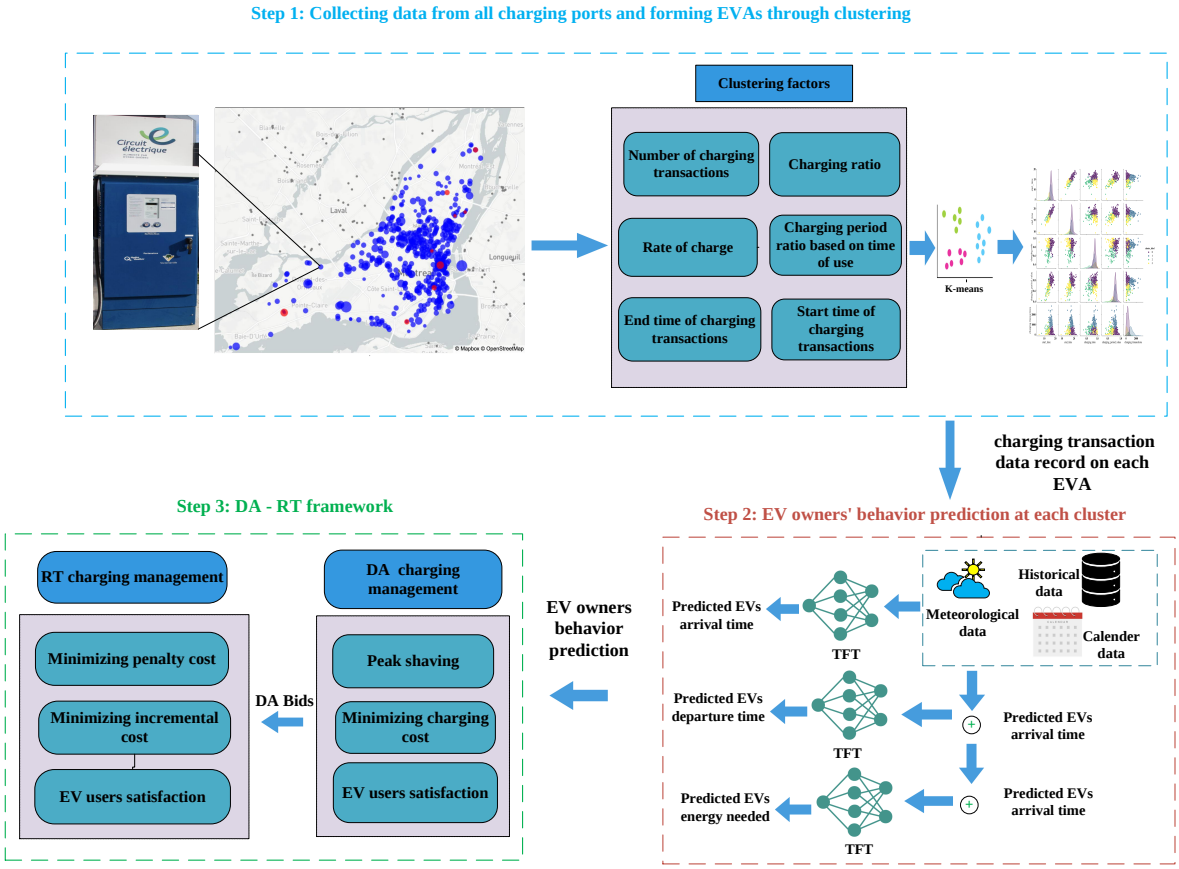

Figure 5.1 Proposed scheme

5.3 Problem formulation

This section provides a detailed introduction to the problem formulation for each step of this work.

As shown in Fig. 5.1, clustering and prediction processes constitute this study's first and second steps. In this regard, the K-means technique has been employed for clustering, followed by the TFT-based method for prediction.

Cluster-based prediction improves accuracy by identifying patterns and correlations among similar data points within each cluster.

5.3.1 K-means-based clustering of charging ports forming EVAs

There are some factors that affect EV charging port usage, such as location popularity, station utilization, required charging levels, and charging times. Clustering techniques can be used to group charging ports with similar characteristics into EVAs to manage this variability. In this framework, each EVA corresponds to one cluster. One such technique is K-means clustering, an unsupervised learning algorithm that partitions data into K-distinct clusters based on feature similarity. K-means is used due to its simplicity, scalability, and stable performance on usage-pattern data, although other clustering methods could also be applied.

K-means clustering is an unsupervised learning algorithm that MacQueen J. first introduced in 1967 [145]. Objects are grouped closely together in each cluster while being kept as distant as possible from data points in other clusters. This is achieved through the use of the Euclidean distance function. In this algorithm, n data points are clustered into k clusters to minimize each cluster's squared error objective function outlined in Eq 5.1.

$$J_k = \sum_{i=1}^{k} \sum_{j=1}^{c_i} (|X_j - V_i|)^2 \tag{5.1}$$

where X = $\{X_1, X_2, ...X_n\}$ is the set of data points and V = $\{V_1, V_2, ...V_k\}$ is the set containing the mean of data points in each cluster. $\{X_j - V_i\}$ is the Euclidean distance between X_j and V_i, k is the number of clusters and c_i is the number of data points in the *ith* cluster. This study will be formed based on factors mentioned in step 1 of Fig. 5.1 and using the K-means technique EVAs.

Why K-means?

Although several recent clustering algorithms, such as hierarchical density-based spatial clustering of applications with noise (HDBSCAN) [146] and ordering points to identify the clustering structure (OPTICS) [147] , have been extensively used in high-dimensional or density-varying datasets, they are not well-suited for the specific characteristics of EV charging port features used in this work.

First, our dataset contains continuous and low-dimensional features such as utilization, rate of charge, and start/end time. These features form approximately spherical cluster tendencies when normalized, and therefore, distance-based partitioning is sufficient and computationally superior.

Second, the spatio-temporal distribution of EV ports in our dataset does not show irregular structures. Algorithms such as HDBSCAN and OPTICS are designed for clusters with irregular densities and noise points [148]. In contrast, charging ports in a cluster contribute meaningfully in terms of usage statistics and can not be considered as noise. Density-based methods would incorrectly classify low-utilization stations as noise or form overly fragmented clusters, which undermines the goal of forming stable EVAs.

Third, spectral clustering has significantly higher computational complexity $O(n^3)$, which becomes prohibitive for datasets with more than 2000 ports and millions of transaction records. K-means scales linearly with the number of ports and therefore provides the necessary computational efficiency for a large-scale, real-system deployment.

For these reasons, K-means provides the best trade-off between interpretability, computational efficiency, and suitability to the structure of EV charging port features.

5.3.2 TFT-based EV owners behavior forecasting

Our research utilizes a TFT-based model, as shown in Fig 5.2, to predict EV owners' behavior for DA charging management. TFT is designed to handle multivariate multi-series data and evaluate the significance of static covariates, exogenous variables, and temporal features using interpretable multi-head attention mechanisms and variable selection networks. This capability allows the TFT model to outperform simple time-series methods like LSTM and gated recurrent unit (GRU), particularly in capturing static data [149].

In our work, TFT is used to predict the arrival times, departure times, and energy needed for charging EVs at each cluster. The model employs three TFT networks within each cluster: the first predicts EV arrival times, which are then used as inputs for subsequent networks to forecast departure times and energy requirements. Also, TFT utilizes inputs such as calendar

and meteorological information, station characteristics such as station ID and utilization level, and dynamic features like historical patterns of EV arrivals, departures, and energy requirements for prediction.

Compared to traditional black-box models like artificial neural networks or complex integrated approaches, the TFT model captures long-range dependencies in sequential data more accurately [150]. TFT benefits from multi-head attention mechanisms to effectively model relationships during different time horizons of a time series data. This provides a significant advantage in applications where understanding long-term temporal patterns is critical [151], such as predicting EV owners' behavior.

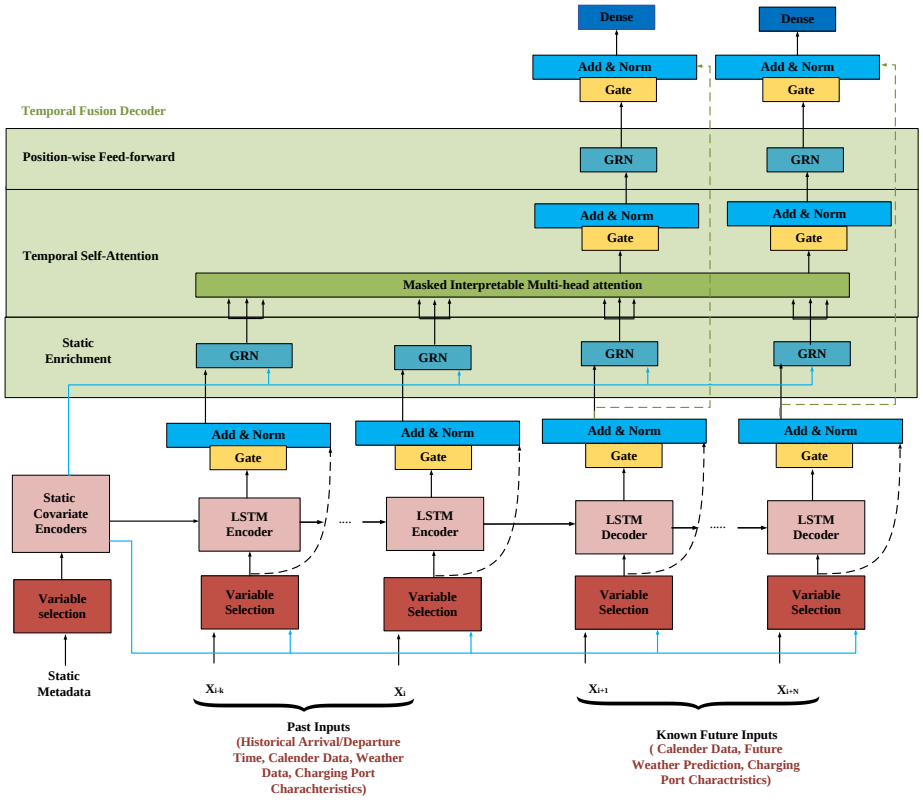

Figure 5.2 TFT structure

Gating mechanism

The TFT uses a gated residual network (GRN) to selectively apply nonlinear functions to input features. This allows the model to handle uncertainty in exogenous factors such as time-of-day effects, station utilization trends, and seasonal variations that exist in charging

transaction records. The GRN processes an input $\mathbf{a}$ and an optional context vector $\mathbf{c}$ as follows:

$$\mathrm{GRN}_{\omega}(\mathbf{a}, \mathbf{c}) = \mathrm{LayerNorm}(\mathbf{a} + \mathrm{GLU}_{\omega}(\eta_1)) \tag{5.2}$$

$$\eta_1 = W_{1,\omega}\eta_2 + \mathbf{b}_{1,\omega} \tag{5.3}$$

$$\eta_2 = \mathrm{ELU}(W_{2,\omega}\mathbf{a} + W_{3,\omega}\mathbf{c} + \mathbf{b}_{2,\omega}) \tag{5.4}$$

Where LayerNorm shows layer normalization, and ELU is the exponential linear unit activation. The gated linear unit (GLU) refines this process by controlling information flow, formulated as:

$$\mathrm{GLU}_{\omega}(\gamma) = \sigma(W_{4,\omega}\gamma + \mathbf{b}_{4,\omega}) \odot (W_{5,\omega}\gamma + \mathbf{b}_{5,\omega}) \tag{5.5}$$

Where $\sigma(\cdot)$ is the sigmoid activation, W are weight matrices, $\mathbf{b}$ are bias vectors learned during training, and $\odot$ represents the pointwise multiplication of corresponding elements.

Variable selection networks

The variable selection network (VSN) dynamically assigns importance weights to input features to prioritize the most relevant factors that influence EV charging behavior. The VSN improves interpretability while filtering out irrelevant information. Suppose that $\boldsymbol{\Xi}_t = [\xi_t^{(1)}, ..., \xi_t^{(m_\chi)}]$ is a flattened input vector, which includes features such as calendar data (day of the week, holidays), historical charging behavior, and meteorological conditions. The selection weights $\boldsymbol{\nu}_{\chi_t}$ are computed as:

$$\boldsymbol{\nu}_{\chi_t} = \mathrm{Softmax}(\mathrm{GRN}_{\nu_\chi}(\boldsymbol{\Xi}_t, \mathbf{c}_s)) \tag{5.6}$$

Each input feature $\xi_t^{(j)}$, representing key characteristics in EV owners' behavior prediction such as time-of-day, historical charging behavior, and station utilization rates, undergoes nonlinear transformation via a GRN:

$$\tilde{\xi}_t^{(j)} = \mathrm{GRN}_{\tilde{\xi}^{(j)}}(\xi_t^{(j)}) \tag{5.7}$$

The final processed features are combined using their selection weights:

$$\tilde{\boldsymbol{\xi}}_t = \sum_{j=1}^{m_\chi} \nu_{\chi_t}^{(j)} \tilde{\xi}_t^{(j)} \tag{5.8}$$

Where $\nu_{\chi_t}^{(j)}$ represents the importance of the j-th input feature.

Interpretable multi-head attention

In the structure of TFT, the LSTM encoder-decoder captures short-term temporal patterns in EV charging behavior, while multi-head attention handles long-term dependencies [152].

Attention mechanisms evaluate relationships between keys $\mathbf{K}$, queries $\mathbf{Q}$, and values $\mathbf{V}$, as shown in:

$$\text{Attention}(\mathbf{Q}, \mathbf{K}, \mathbf{V}) = A(\mathbf{Q}, \mathbf{K})\mathbf{V} \tag{5.9}$$

Where $A(\mathbf{Q}, \mathbf{K})$ is the attention score computed from the queries $\mathbf{Q}$ and keys $\mathbf{K}$.

The multi-head attention mechanism enhances learning by extracting different representations from input features such as historical charging trends, calendar-based variations, and weather influences. The scaled dot-product attention is applied to each head:

$$A(\mathbf{Q}, \mathbf{K}) = \text{Softmax}\left(\frac{\mathbf{Q}\mathbf{K}^T}{\sqrt{d_{\text{attn}}}}\right) \tag{5.10}$$

Where d_{attn} is the attention space dimension. The multi-head attention mechanism aggregates outputs from all heads:

$$\text{MultiHead}(\mathbf{Q}, \mathbf{K}, \mathbf{V}) = [\mathbf{H}_1, \ldots, \mathbf{H}_{m_H}]W_H \tag{5.11}$$

Where m_H is the number of attention heads, and W_H is the weight matrix combining all outputs. To improve interpretability, the value $\mathbf{V}$ is shared across heads, ensuring consistency in feature importance:

$$\text{InterpretableMultiHead}(\mathbf{Q}, \mathbf{K}, \mathbf{V}) = \tilde{\mathbf{H}}W_H \tag{5.12}$$

$$\tilde{\mathbf{H}} = \frac{1}{m_H} \sum_{h=1}^{m_H} \text{Attention}(\mathbf{Q}W_Q^{(h)}, \mathbf{K}W_K^{(h)}, \mathbf{V}W_V) \tag{5.13}$$

Where $W_Q^{(h)}$, $W_K^{(h)}$, and $W_V^{(h)}$ are head-specific weight matrices.

5.3.3 Two-stage EVA strategy

In this section, the proposed two-stage framework for EVs smart charging has been introduced.

DA energy management

During this phase, each EVA or cluster employs predicted EV key parameters using TFT to optimize its DA charging management. The model assumes that EVAs can purchase their forecasted energy needs in the DA market without supply limitations. The multiobjective optimization problem solved at the level of each EVA or cluster for determining DA energy bids can be expressed as follows:

$$\text{Minimize } Cost^{DA} = \alpha \cdot Cost^{DA}_{\text{Peak}} + \beta \cdot Cost^{DA}_{\text{Charge}} \tag{5.14}$$

$$Cost^{DA}_{\text{Peak}} = \max_{t} \sum_{i=1}^{I} P_i^{DA}(t) v_i(t) \tag{5.15}$$

$$Cost^{DA}_{\text{Charge}} = \sum_{t=1}^{T} \sum_{i=1}^{I} C^{DA}(t) P_i^{DA}(t) v_i(t) \tag{5.16}$$

$$SoC_i(t) = SoC_i(t-1) + P_i^{DA}(t)\eta_i \Delta t, \quad \forall t, \forall i \tag{5.17}$$

$$0 \leq P_i^{DA}(t) \leq \bar{\gamma}_i, \quad \forall t, \forall i \tag{5.18}$$

$$\underline{SoC}_i \leq SoC_i(t) \leq \overline{SoC}_i, \quad \forall t, \forall i \tag{5.19}$$

$$SoC_i^{\text{des}} \leqslant SoC_i^{dep}, \quad \forall i \tag{5.20}$$

$$v_i(t) = \begin{cases} 1, & \text{if vehicle is at charging station at time } t \\ 0, & \text{otherwise} \end{cases} \tag{5.21}$$

Introducing the notations in the DA energy management, α and β are scaling factors in the objective function. $P_i^{DA}(t)$ is the power consumption of EV number i, $C^{DA}(t)$ is the DA power purchasing price of electricity, $v_i(t)$ is a binary variable which indicates the existence of i_{th} EV at the EVA. $SoC_i^{DA}(t)$, $\bar{\gamma}_i^{DA}$ and η_i are the SoC, the upper bound for the rate of charge and charging efficiency of each EV. $\underline{SoC}_i^{DA}$ and $\overline{SoC}_i^{DA}$ are minimum and maximum acceptable SoC for EV i. Finally, SoC_i^{des} and SoC_i^{dep} are each EV's desired and departure

SoC at EVA, respectively.

Eq.(5.14) defines the total cost of each EVA at the DA level as the sum of two components: the peak demand cost and the charging cost. Eq.(5.15) computes the daily peak demand consumption as the maximum total power consumption across all EVs over all time intervals. Eq.(5.16) defines the charging cost as the sum of energy prices over all time intervals. Eq.(5.17) describes SoC dynamics, ensuring that the SoC of each EV is updated at every time interval. Eq.(5.18) ensures that the charging power assigned to each EV does not exceed its maximum charging rate at any time interval. Eq.(5.19) enforces the constraint that the SoC of each EV must remain within its minimum and maximum allowed values at all times. Eq.(5.20) guarantees user satisfaction by ensuring that each EV's SoC at departure time meets the desired level specified by the user.

RT energy balancing

In the RT part of our formulation, an optimization problem is introduced, inspired by CAISO RT market rules, to evaluate the EVA's performance on the day its bids are deployed. During this phase, the EVA faces real EV charging parameters and must adjust its energy bids to meet EV demand while honoring its awarded DA Market bids. The primary objective of this optimization problem is to evaluate the EVA's overall performance in the energy market and the impact of EV demand forecasts on its decisions.

$$\text{Minimize } Cost^{RT} = Cost^{\text{INC},RT} + Cost^{\text{PEN},RT} \tag{5.22}$$

$$Cost^{\text{INC},RT} = \sum_t P^{\text{INC},RT}(t) \cdot \rho_{\text{INC},RT}(t) \quad \forall t \tag{5.23}$$

$$Cost^{\text{PEN},RT} = \sum_t P^{\text{PEN},RT}(t) \cdot \rho_{\text{PEN},RT}(t) \quad \forall t \tag{5.24}$$

$$\sum_i P_i^{DA}(t) + P^{\text{PEN},RT}(t) - P^{\text{INC},RT}(t) = \sum_i P_i^{RT}(t) \quad \forall t, \forall i \tag{5.25}$$

$$0 \leq P^{\text{INC},RT}(t), \quad 0 \leq P^{\text{PEN},RT}(t) \leq \sum_i P_i^{DA}(t) \quad \forall t, \forall i \tag{5.26}$$

$$SoC_i(t) = SoC_i(t-1) + P_i^{RT}(t)\eta_i \Delta t, \quad \forall t, \forall i \tag{5.27}$$

$$0 \leq P_i^{RT}(t) \leq \bar{\gamma}_i, \quad \forall t, \forall i \tag{5.28}$$

$$\text{subject to constraints (5.19) and (5.20)} \tag{5.29}$$

The variable $Cost^{RT}$ represents the total cost in the RT market, combining the incremental cost $Cost^{\mathrm{INC},RT}$ for procuring additional energy and the penalty cost $Cost^{\mathrm{PEN},RT}$ for failing to fulfill the awarded DA market bids. The variable $P^{\mathrm{INC},RT}(t)$ denotes the incremental power demand, with $\rho_{\mathrm{RT}}(t)$ representing the corresponding price in the RT market, while $P^{\mathrm{PEN},RT}(t)$ is the penalty power demand, and $\rho_{\mathrm{PEN},RT}(t)$ corresponds to the penalty cost price, all at time step t. The variable $P_i^{RT}(t)$ represents the RT charging power EV i at time step t, with the condition that $P_i^{RT}(t)$ is bounded by the maximum allowable power limit $\bar{\gamma}_i$.

The power balance equation in (5.25) ensures that the sum of the DA power demand, the incremental power demand, and the penalty demand matches the RT power requirements for all time steps.

In summary, the three-step EV charging management algorithm is presented in Algorithm 3.

5.4 Case study

In this section, we present the details related to the case study including the data set used for the aggregation methods, and the input data used for prediction.

5.4.1 EVs Aggregation and prediction

As shown in Fig 5.1, the first and second steps of this work involve clustering-based aggregation of EV ports and predicting the DA EV owners' behavior at each cluster, which are explained in the following sections.

EV Data set

In this study, the public charging transactions data provided by Quebec's electricity provider is used. This data set includes more than 3 million transactions that took place between May 2020 and May 2024 in the Quebec province. These transactions contain information such as charging start time, charging end time, connector connection time, level of charging and EV type.

To account for a crucial temporal aspect in clustering analysis, the frequency of charging transactions occurring each hour of the day during the mentioned horizon is depicted in Fig 5.3. Utilizing this profile, hours of the day have been categorized into three labels: on-peak (red), mid-peak (yellow), and off-peak (green), facilitating their application in the subsequent

Algorithm 3 3 Steps EV Charging Management Algorithm

Step 1: Clustering of EV Charging Ports
Input: Charging port utilization data, Charging port level
Output: Number of clusters k, Assignment of each charging port to a cluster
Extract spatiotemporal features of ports from the historical charging transaction data
Use the Silhouette Method to determine the optimal number of clusters k
Apply K-means to group charging ports into EVAs, minimizing intra-cluster variance as shown in (5.1)
Step 2: EV Owners Behavior Prediction Using TFT
for each EVA **do**
    Input: Historical charging transaction, meteorological, and calendar data
    Output: Predicted EV arrival time, departure time, and energy required
    Refine input features by the gating mechanism using(5.2) to (5.5).
    Assign factor importance using VSN as outlined in equations (5.6) to (5.8).
    Enhance feature representation and capture temporal dependencies in EV charging. using multi-head attention as shown in equation (5.9) to (5.13).
end for
Step 3: DA and RT Charging Optimization
for each EVA **do**
    Input: TFT-based predicted EV owners' behavior.
    Output: DA and RT optimized charging profiles.
    Utilize the TFT-based predicted EV owners' behavior to perform DA EV charging management as formulated in equations (5.14) to (5.21).
    Submit DA bids based on the optimized charging schedule.
    In RT adjust charging schedules dynamically to minimize deviations from DA bids while ensuring feasibility, following the optimization framework in equations (5.22) to (5.29).
end for

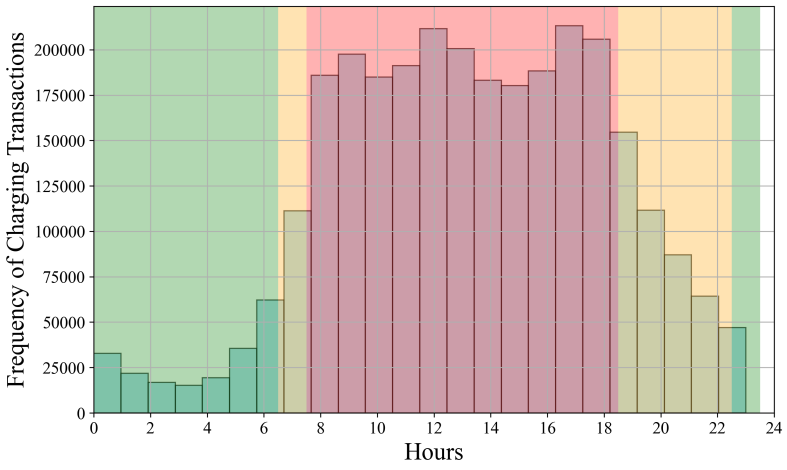

Figure 5.3 Frequency of charging transactions

clustering phase.

Clustering aggregation

In this section, charging port aggregation is performed by the $k-means$ clustering algorithm based on the following characteristics.

- Popularity: total number of charging transactions of each port.
- Utilization: charge time ratio, i.e., the mean value of the ratio between charge time and connection time calculated from all transactions taking place at the port.
- Time of use: a value called "charging period value" between 0 and 1 will be assigned to each charging port based on its daily usage hours record. As shown in Fig 5.3, ports primarily used during peak hours will have a value close to 1, while those used mainly during off-peak hours will have a value close to 0.
- Rate of charge: charging ports in our dataset contain Level 2 and Level 3 charging and have varying rates of charge, ranging from 7.5 kW to 200 kW.
- Temporal usage pattern consisting of two parts: charge start time and end time.

The silhouette method [153] is used in this study to determine the optimal number of clusters for EV charging stations. By plotting the silhouette score against the number of clusters, this approach identifies the optimal number of clusters with the highest silhouette score.

Based on Fig. 5.4 the silhouette method shows that the optimal number of clusters is 5. Moreover, Table 5.2 shows the number of charging ports and their proportion in each cluster (EVA).

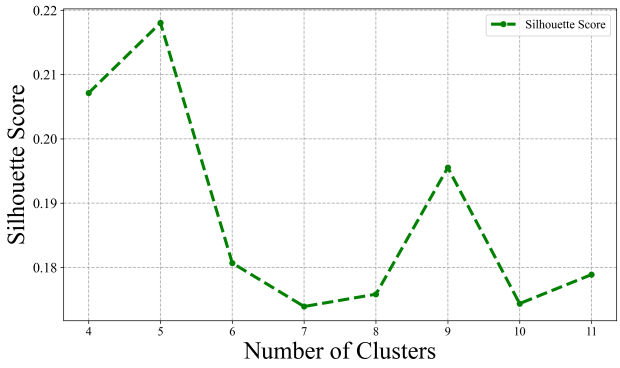

Figure 5.4 Silhouette score per cluster

Table 5.2 Number of ports in each cluster and their proportion

	Number of Ports	Proportion (%)
Cluster 1	97	4.83%
Cluster 2	518	25.79%
Cluster 3	235	11.71%
Cluster 4	418	20.81%
Cluster 5	740	36.86%

Prediction input factors

The prediction of the charging behavior of EV owners can be affected by many factors and can be classified into the following three categories:

- Date indicator (day, week, month ID): EV owners may behave differently during different days, weeks, and months of the year. For example, during holidays or weekends, EV owners may exhibit different charging habits or trip frequencies. Hence, this factor plays a crucial role in predicting EV owner behavior and understanding variations in charging behavior.
- Meteorological data: meteorological factors can highly influence the behavior of EV drivers. For example, fluctuations in outdoor temperature can make drivers using the air conditioning system more frequently, which, in turn, impacts the charging patterns of EVs. This includes changes in charging duration and the initial SoC.

- Historical data: the predictions in this study are based on 15-minute time intervals, utilizing historical data to capture detailed patterns of EV owner behavior, including arrival times, departure times, and the energy required for charging at each time step.

The proposed prediction method was implemented using three TFT models to predict EV arrival time, departure time, and energy required for charging for each EV at each aggregator (or cluster). Each model leverages historical data, including previous charging records, and shares the same hyperparameter configuration: 4 attention heads were used to capture temporal relationships effectively, with the LSTM encoder-decoder hidden layer size set to 128. Four heads allow the model to view temporal patterns from multiple perspectives, while a hidden size of 128 keeps the model expressive yet manageable in practice. The learning rate was initialized at 0.001 and optimized using the Adam optimizer. A batch size of 64 was used for efficient training, with a maximum of 50 epochs. The models incorporate static covariates such as day of the week, week ID, and month ID; observed covariates like previous charging records (e.g., historical arrival and departure times, and energy consumed; and known covariates, including outdoor temperature and humidity). This setup ensures accurate predictions of EV charging patterns by effectively modeling temporal dynamics and static features.

5.4.2 DA-RT framework

In the final step, we present a novel DA-RT framework incorporating a bidding strategy to effectively manage and optimize the operational cost of EVAs. In this section, we introduce a flexible range of charging rates, allowing for variations between 0 to 19 kW for level 2 and 0 to 100 kW for level 3. The charging price profile has been taken from [154]. Both $\rho_{\mathrm{INC},RT}$ and $\rho_{\mathrm{PEN},RT}$ are 1.5 times greater than the regular price profile. Although generator penalties in markets like CAISO can be much higher, such extreme values are not applied here because EVAs do not face generator-level imbalance charges. DA-RT framework is formulated in Python and solved by CVXPY. The simulation results are obtained on a laptop with an Intel Core i7-8565U CPU 1.8 GHz and 16 GB of RAM.

5.5 Simulation and results

In this section, the results which are obtained through the simulations of the proposed scheme are presented.

5.5.1 Clustering

In this section, according to the 6 characteristic factors described in section 5.4, the results of the clustering section are displayed. Here, kernel density estimation is used to approximate the probability density functions.

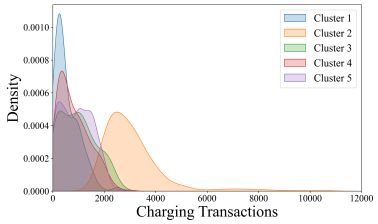

(a) Density graph of number of transactions

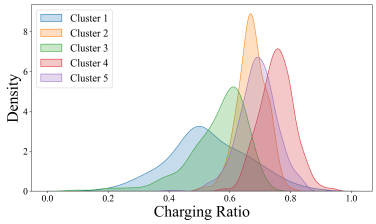

(b) Density graph of charging time ratio

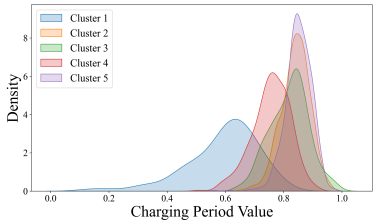

(c) Density graph of charge time period value

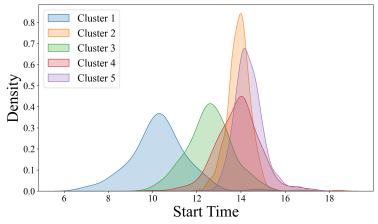

(d) Density graph of start time of transactions

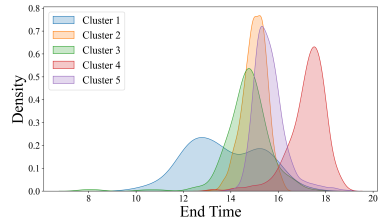

(e) Density graph of end time of transactions

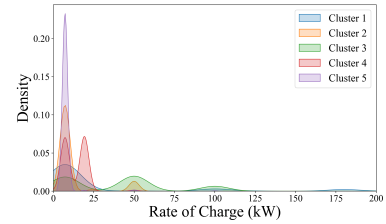

(f) Density graph of rate of charge of transactions

Figure 5.5 Six EV ports characteristic factors for clustering

Fig. 5.5a shows the density graph of the total number of transactions in the ports of each cluster. The charging ports in cluster 2 are more popular and have been used more than others. However, charging ports in cluster 1 are not frequently used, and the number of charging transactions in these ports is relatively low.

Fig. 5.5b shows the density graph of the charging ratio in the ports of each cluster. Clusters 1 and 3 consist of charging ports with high variation in charging ratio, mostly below 0.8. A low value for the charging port indicates that there is typically no queue for that port. This suggests that many EVs in these clusters remain connected even after reaching full charge. The charging ports in clusters 2, 4, and 5 have the same high charging ratio patterns, showing that users use ports in these clusters to the extent that they need to charge their EVs and no more. Fig. 5.5c illustrates the charging period value for each cluster. Charging period values close to "1" in clusters 2, 3, 4, and 5 indicate that these clusters consist of charging ports that are predominantly active during peak hours. Such clusters with high peak-hour

activity may have high concentration of EV owners with commuters behavior, may require for instance enhanced grid support and smart dynamic charging prices. Conversely, ports in cluster 1 are mostly used during mid-peak hours, with charging period values close to "0.5". Fig. 5.5d and Fig. 5.5e show the average start and end time of charging transactions in the ports of each cluster, respectively. Clusters 1 and 3 mainly consist of ports used in the morning and noon, while clusters 2, 4, and 5 are primarily used in the afternoon and evening. Finally, Fig. 5.5f illustrates the rate of charge for ports within each cluster. Except for cluster 5, which comprises only Level 2 charging ports, the other clusters include a mix of Level 2 and Level 3 charging ports. Notably, in clusters 1 and 3, some superchargers have a rate of charge exceeding 100 kW.

Fig. 5.6 illustrates comprehensive visualization of the daily charging profile records, along with the mean and median for all clusters. Each cluster is displayed in separate sub-figures, for a better interpretability of the clusters. The mean serves as a central tendency metric, reflecting an average behavior in each cluster, whereas the median reveals the central position of the distribution. For instance, Cluster 2 and 5 have higher mean daily peak values due to their high number of charging transactions (Fig. 5.5a) and charging port numbers (Table 5.2). On the other hand, in cluster 1, the mean daily peak value for EVs power consumption is low due to the low number of charging ports in this cluster. However, cluster 1 has only a single peak early in the morning, possibly indicating users' preparation for daily activities. Finally, in all clusters, the mean charging power is slightly higher than the median, which shows a small number of EVs consume a disproportionately high amount of power.

5.5.2 Prediction

This section presents the results of DA behavior prediction for EV owners using TFT in clusters 1 and 5 and compares these results with two well-known time series-based methods: LSTM and GRU. These two clusters are the clusters with the lowest and highest number of charging ports according to Table 5.2. The prediction results of arrival time, departure time, and energy needed for cluster 1 and cluster 5 using TFT are shown in Fig. 5.7 and Fig. 5.8.

In Table 5.3, results of the EV owners behavior prediction at the level of aggregators are shown. Three performance indicators, namely, RMSE, R2 score, and MAE are used for accuracy evaluation. The results show the superiority of TFT over LSTM and GRU across all metrics, particularly for energy needed prediction, with the lowest MAE (4.55), RMSE (5.91), and the highest R^2 (0.83). For arrival time and departure time prediction, TFT also demonstrates better accuracy, with lower MAE and RMSE values than LSTM and GRU. In general, GRU shows the weakest performance, especially for departure time, with the highest

Table 5.3 Performance indicators of prediction results in cluster 1

Method	Metric	Arrival time	Departure time	Energy Needed
LSTM	RMSE	9.75	8.60	7.04
	R^2	0.72	0.74	0.78
	MAE	5.20	5.78	5.10
GRU	RMSE	10.20	9.29	7.50
	R^2	0.73	0.71	0.74
	MAE	5.50	6.10	5.60
TFT	RMSE	8.92	7.65	5.91
	R^2	0.82	0.82	0.83
	MAE	4.52	5.31	4.55

Table 5.4 Performance indicators of prediction results in cluster 5

Method	Metric	Arrival Time	Departure Time	Energy Needed
LSTM	RMSE	5.43	8.72	9.58
	R^2	0.87	0.76	0.74
	MAE	2.31	6.29	6.68
GRU	RMSE	5.7	9.14	9.99
	R^2	0.8	0.73	0.71
	MAE	2.5	6.61	7.02
TFT	RMSE	4.14	7.10	7.85
	R^2	0.92	0.84	0.83
	MAE	1.14	5.46	5.66

errors and the lowest R^2 score (0.71).

Table 5.4 also indicates the preferable performance of TFT over LSTM and GRU in cluster 5 EV owners' behavior prediction. In this cluster, the results are more accurate than cluster 1, as cluster 5 has more ports, leading to more comprehensive historical records available for training. The superior predictive performance of TFT is consistent across all clusters; however, to avoid redundancy, results are only presented for two representative clusters.

Clustering charging ports with similar spatiotemporal features into the same aggregators helps achieve acceptable accuracy by making their charging behavior more predictable. The proposed DA-RT framework in the final step of this study requires a high level of prediction accuracy. This section shows that TFT can be a suitable prediction model for key parameters of EVs as it achieves the highest accuracy. Therefore, the TFT prediction results obtained at this step will be used for the DA charging management scenario for all clusters, while the real data of arrival time, departure time, and energy needed will be used in RT.

To further enhance the interpretability of the TFT model, Fig. 5.9 illustrates the normalized

contribution of each input feature across the three prediction tasks—arrival time, departure time, and energy needed—averaged over all clusters. These importance values are extracted from the VSNs embedded within the TFT architecture. As expected, historical behavior emerges as the dominant factor. In the arrival-time forecasting model, only historical arrival records are included and they receive the largest importance weight; historical departure or energy histories are not used as inputs. Similarly, the departure-time model relies solely on historical departure patterns, while the energy-required model exclusively incorporates past energy consumption data. Calendar-based covariates (weekday/weekend, week ID, month ID) contribute moderately and consistently across all tasks, reflecting weekly and seasonal charging regularities. Meteorological information, represented here by outdoor temperature, has a higher influence in the energy-needed model due to temperature-dependent auxiliary loads.

5.5.3 DA-RT charging management framework

In this section, a specific date has been considered for implementing the proposed charging management framework. First, based on Equations (14-21) and using the predicted data by TFT, the DA charging management will be done, and then in the following day, the real data will be used for RT charging management of EVs according to equations (22-29). The results section considers three scenarios (SC) to illustrate the application of the proposed framework. SC1 emphasizes charging cost minimization, where $\alpha = 0$ and $\beta = 1$ in Eq. (5.14). SC2 focuses on peak shaving, with $\alpha = 1$ and $\beta = 0$ in Eq. (5.14). SC3 aims to minimize both peak power and charging cost simultaneously, where $\alpha = 0.5$ and $\beta = 0.5$ in Eq. (5.14). In SC3, the normalized values of $Cost^{DA}_{\text{Peak}}$ and $Cost^{DA}_{\text{Charge}}$ are used.

SC1-Charging cost minimization

Fig. 5.10 illustrates the DA and RT charging profiles, along with the incremental and penalty charging profiles for all EVAs. In this SC, where EVAs aim to minimize their charging costs, most of the charging occurs during off-peak and mid-peak hours, resulting in higher peak consumption during those times. However, some EVs are required to charge during on-peak hours because their time of stay predominantly falls within these hours, and their desired departure SoC must be achieved. As indicated in Fig. 5.10, Cluster 1 exhibits lower consumption during on-peak hours, which can be attributed to its shorter charging period value, as shown in Fig. 5.5c. Incremental and penalty charging profiles, shown in Fig. 5.10, result from inaccuracies in predicting EV owners' behavior. However, these profiles represent only a small portion of the total charging profiles, demonstrating the effectiveness

and superiority of the proposed TFT-based prediction.

Table 5.5 SC1 cost comparisons over clusters

Cost Type	Cluster 1	Cluster 2	Cluster 3	Cluster 4	Cluster 5
DA Charging Cost ($)	1177.51	21704.73	4190.8	9017.23	12859.49
DA Daily Peak (kW)	270.69	2378.67	614.42	1000.11	1601.19
RT Incremental Cost ($)	92.46	1410.51	239.64	190.6	366.92
RT Penalty Cost ($)	196.53	4210.73	613.06	1097.81	1684.25

Table 5.5 provides a comprehensive comparison among all clusters regarding charging cost, daily power consumption peak, incremental cost, and penalty cost. Cluster 2 has the highest charging cost (21704.73 $) and peak demand (2378.67 kW); this was expected due to its large number of charging transactions and share of EV ports. In contrast, cluster 1 has the lowest charging costs (1177.51 $) and peak demand (270.69 kW), as it has the lowest number of charging ports among all clusters. Regarding RT costs, cluster 1 and cluster 2 have the highest portion of deviation costs (incremental and penalty costs) over the charging costs, which are 30.84 % and 25.9 %, respectively, while cluster 4 has the lowest portion, which is only 14.28 %.

SC2-Peak shaving

Fig. 5.11 illustrates the daily power profiles for all EVAs. In this SC, the objective is to minimize the peak power consumption of the daily load profile for EVs while ensuring the satisfaction of EV owners' departure SoC. As shown in Fig. 5.11, both DA and RT power profiles are almost flat from morning to evening. In all clusters, the RT profiles closely follow the DA profiles; hence, incremental and penalty costs are lower than SC1. This happens because, in SC2, for all EVs, a smooth charging rate is needed to keep the profiles flat, while in SC1, extreme charging rates were needed to charge EVs during mid-peak to minimize charging costs and avoid charging them during on-peak.

Table 5.6 SC2 cost comparisons over clusters

Cost Type	Cluster 1	Cluster 2	Cluster 3	Cluster 4	Cluster 5
DA Charging Cost ($)	1347.68	23128.12	4477.52	9582.04	13777.44
DA Daily Peak (kW)	116.73	1380.69	304.29	530.47	865.17
RT Incremental Cost ($)	90.34	588.18	42.08	103.39	130.66
RT Penalty Cost ($)	10.11	1869.37	202.2	702.84	856.50

Table 5.6 presents costs in SC2 and reveals notable differences in DA and RT costs compared

to SC1. All clusters experience a reduction in their peak daily power consumption, while cluster 1 exhibits the highest percentage decrease, dropping by 56.87% (from 270.69 kW to 116.73 kW). Moreover, Cluster 2 records a 998 kW drop in peak power consumption, corresponding to a 41.96% decrease in peak consumption. This peak shaving highlights a more balanced load distribution and reduced stress on the grid components. However, this improvement comes at a cost, as charging expenses rise across all clusters due to the need to charge EVs during on-peak to satisfy their desired departure SoC. For example, cluster 2 sees a 6.56% increase (from 21704.73 $ to 23128.12 $), and Cluster 5's charging cost climbs by 7.14% (from 12859.49 $ to 13777.44 $).

SC3-Peak shaving and charging cost minimization

Fig. 5.12 presents the profiles for all EVAs in SC3. In this SC, the goal is to minimize both the peak power consumption of the daily load profile and the EV charging costs, while ensuring the satisfaction of the EV owners' departure SoC. This SC represents a trade-off between SC1 and SC2. As observed, the peak power consumption in SC3 lies between the values of the previous two SCs, and the charging cost is also an intermediate value between SC1 and SC2.

Table 5.7 SC3 cost comparisons over clusters

Cost Type	Cluster 1	Cluster 2	Cluster 3	Cluster 4	Cluster 5
DA Charging Cost ($)	1238.72	21861.13	4258.19	9032.34	12878.49
DA Daily Peak (kW)	147.81	1845.74	369.20	687.34	1153.12
RT Incremental Cost ($)	57.16	392.08	114.41	166.89	123.95
RT Penalty Cost ($)	126.56	2932.85	451.40	999.72	1423.44

The specific cost values for SC3 are shown in Table 5.7. As an example, in cluster 3, the DA charging cost is lowest in SC1 (4190.8 $), increasing by 6.84% in SC2 and 1.61% in SC3, demonstrating SC1's cost efficiency for charging. However, SC1 has a significantly higher DA daily peak (614.42.42 kW), which is 101.92% higher than SC2 (304.29 kW) and 57.46% higher than SC3 (390.20 kW), indicating better load balancing in SC2 and SC3. Similarly, RT incremental cost is much higher in SC1 (239.64.06 $), with reductions ranging from 82.44% to 52.25% in SC2 (42.08 $) and SC3 (114.41 $). This highlights SC2 and SC3 as more effective in mitigating RT costs in this cluster despite slightly higher DA charging costs.

In Cluster 5, as expected, a similar trend is observed in Table 5.7. The DA charging cost is lowest in SC1 (12859.49 $), increasing by 7.13% in SC2 (13777.44 $) and 0.15% in SC3 (12878.49 $). Regarding daily peak and RT costs, SC1 is showing higher values. DA daily peak is 45.97% lower in SC2 (865.17 kW) and 27.98% lower in SC3 (1153.12 kW) in comparison

with SC1 (1601.19 kW), suggesting improved peak shaving in these scenarios. The overall RT incremental and RT penalty costs also drop considerably in SC2 (987.16 $) and SC3 (1547.39 $), with reductions between 51.87 % and 24.56 % in comparison with SC1 (2051.17 $). This indicates that while SC1 offers marginal savings in DA charging costs, SC2 and SC3 perform better in overall cost reduction by addressing peak loads and RT penalties effectively.

5.6 Conclusion and future work

In this paper, we presents a novel scheme to manage the uncertainties in EV charging management based on three main steps. The initial step involved the development of a cluster-based method for designing EV aggregators, with a specific focus on spatiotemporal features of charging ports. This approach aims to enhance the aggregation process by considering both the spatial distribution of ports and the temporal usage patterns of each ports. In the second step of the proposed scheme, three TFT-based models were utilized to predict EV owners' behavior inside each EVA for day-ahead charging management. TFT showed superior results in the accuracy of prediction over LSTM and GRU, which are conventional time series prediction methods. This superiority comes from a multi-head attention mechanism and the handling of multivariate data that exists in TFT. The prediction results obtained from the TFT models are subsequently integrated into a DA and RT bidding framework. Computational experiments using historical charging data from Quebec province in 3 scenarios demonstrate the effectiveness of the proposed approach in minimizing operational costs by reducing the deviation between DA and RT charging load profiles. While SC1 reduces daily charging costs and SC2 minimizes peak power consumption, the hybrid approach in SC3 achieves both objectives, lowering daily charging costs by 5.99% compared to SC2 and enhancing daily peak shaving by 29.13% compared to SC1. These results highlight the potential of this approach to optimize EV charging management in future transportation and energy systems.

For future work, it would be beneficial to consider how EVAs will interact with the distribution system operators. Furthermore, integrating real-time feedback mechanisms and adaptive learning models, such as reinforcement learning, would help reduce uncertainties in EV owners' behavior. These methods would allow more accurate and dynamic adjustments to charging management strategies, improving whole system reliability and user experience.

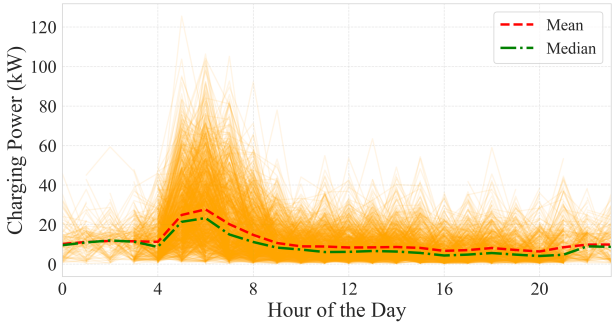

(a) Cluster 1

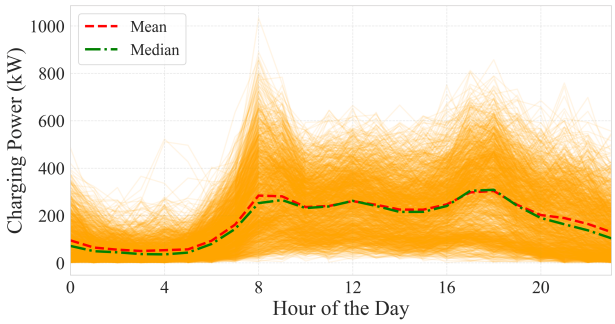

(b) Cluster 2

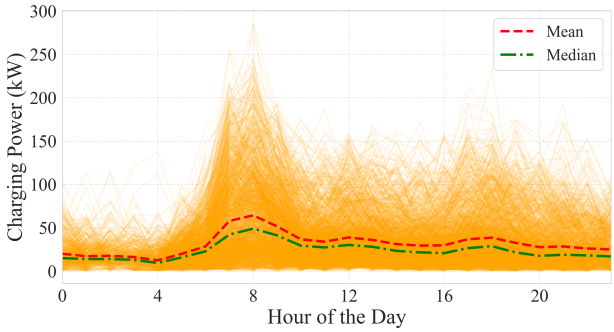

(c) Cluster 3

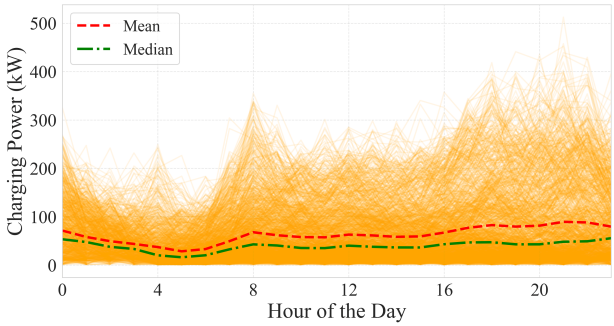

(d) Cluster 4

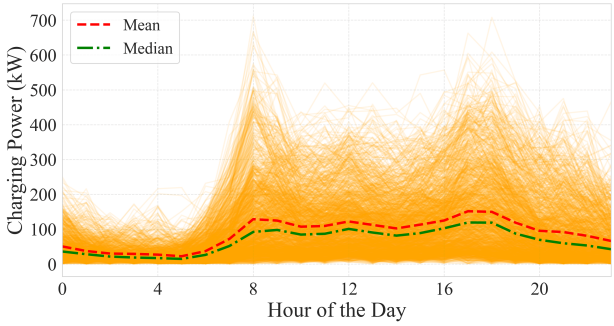

(e) Cluster 5

Figure 5.6 daily charging profile records for all clusters

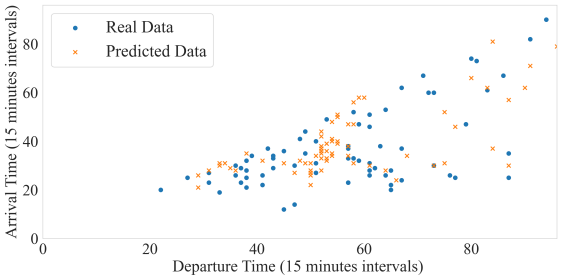

(a) Departure time based on arrival time

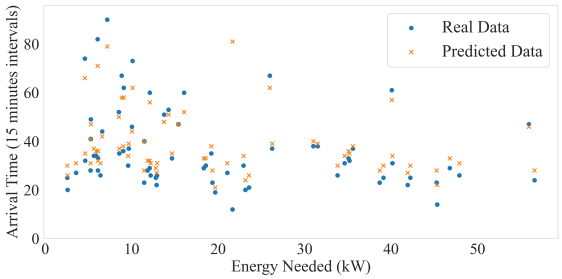

(b) Energy needed based on arrival time

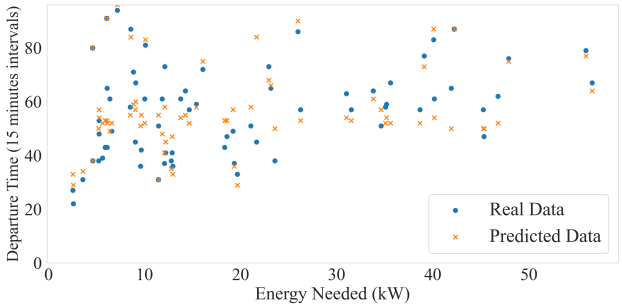

(c) Energy needed based on departure time

Figure 5.7 EVs behavior prediction in cluster 1 for a specific day

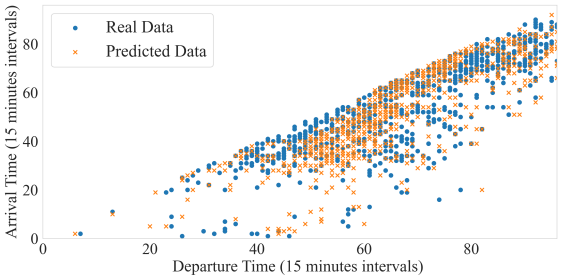

(a) Departure time based on arrival time

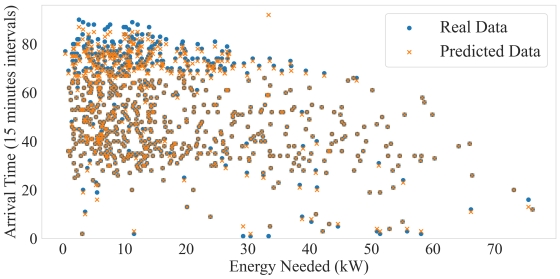

(b) Energy needed based on arrival time

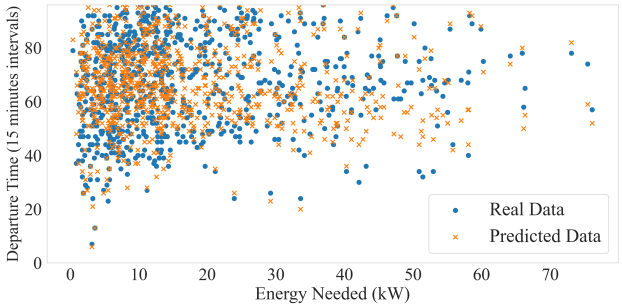

(c) Energy needed based on departure time

Figure 5.8 EVs behavior prediction in cluster 5 for a specific day

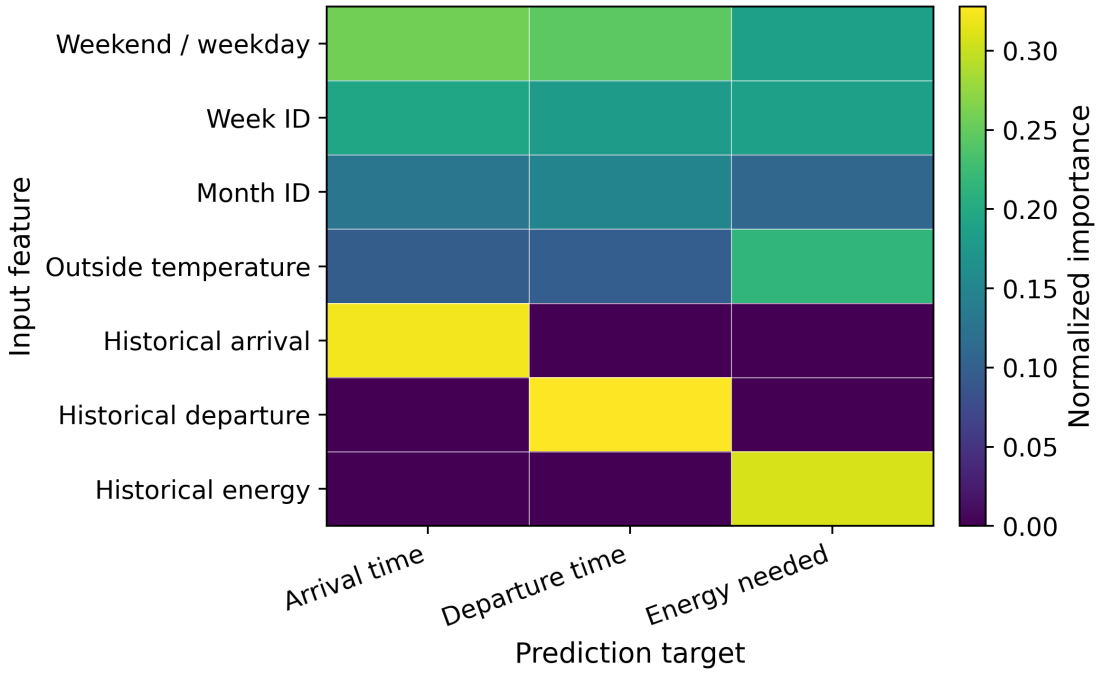

Figure 5.9 Normalized feature importance extracted from the TFT variable selection networks for the three prediction tasks.

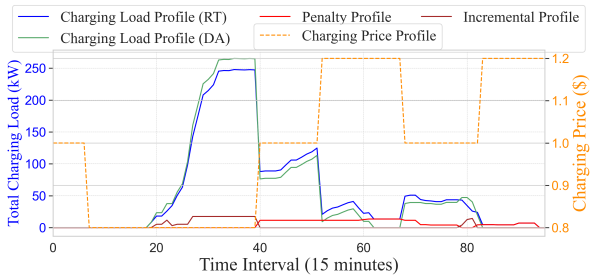

(a) Cluster 1

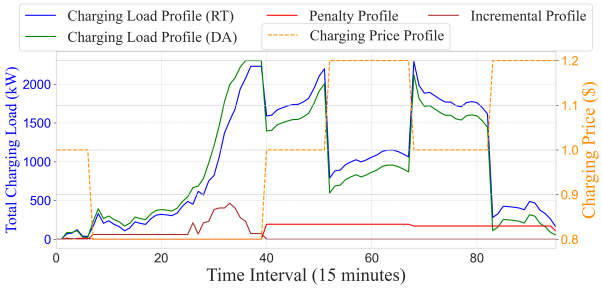

(b) Cluster 2

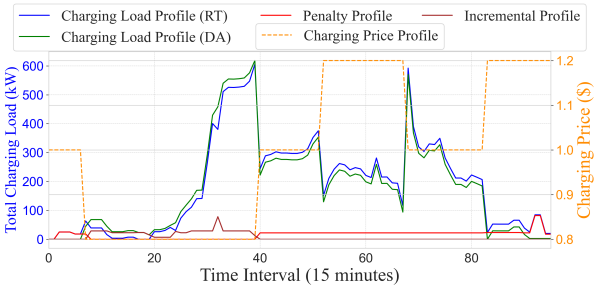

(c) Cluster 3

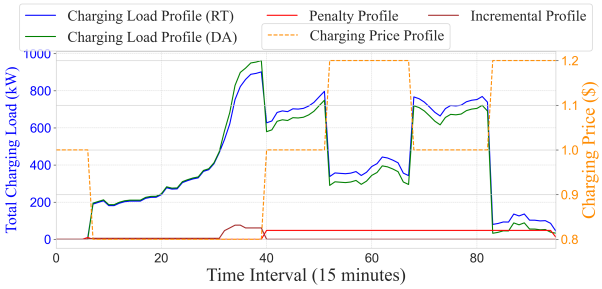

(d) Cluster 4

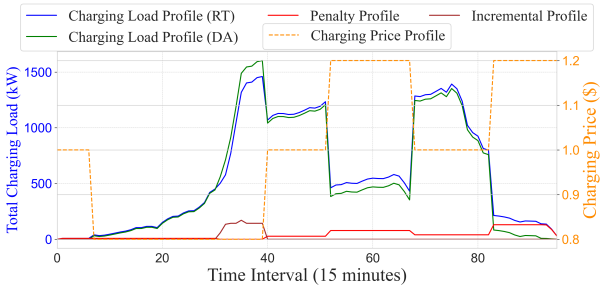

(e) Cluster 5

Figure 5.10 Charging Profiles in SC1

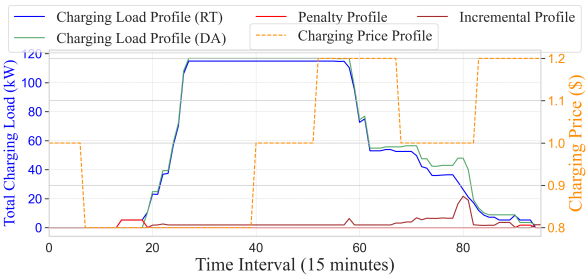

(a) Cluster 1

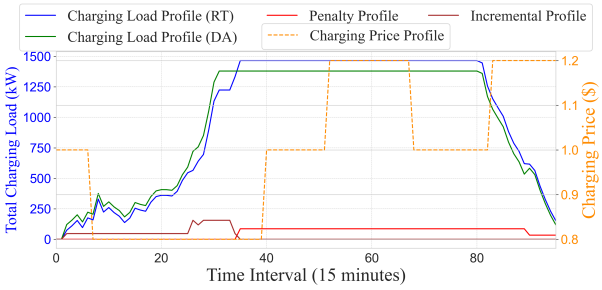

(b) Cluster 2

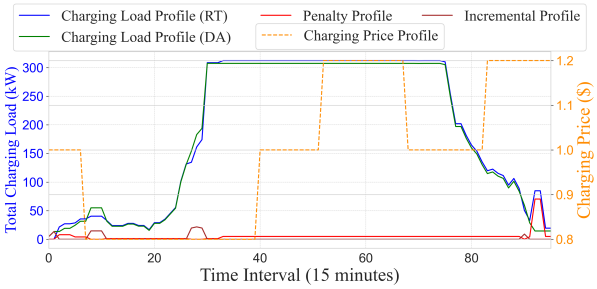

(c) Cluster 3

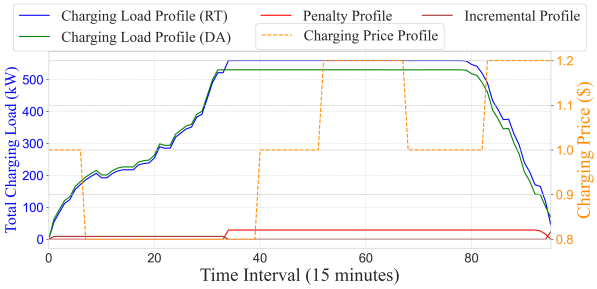

(d) Cluster 4

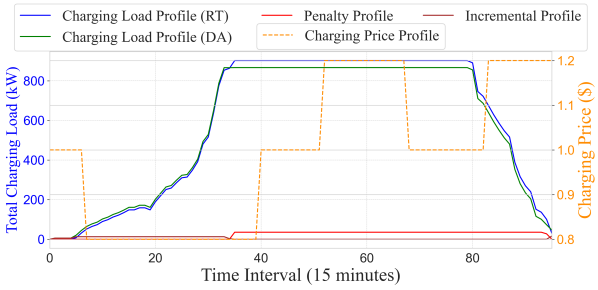

(e) Cluster 5

Figure 5.11 Charging Profiles in SC2

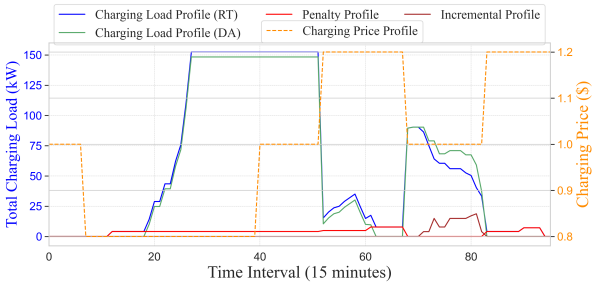

(a) Cluster 1

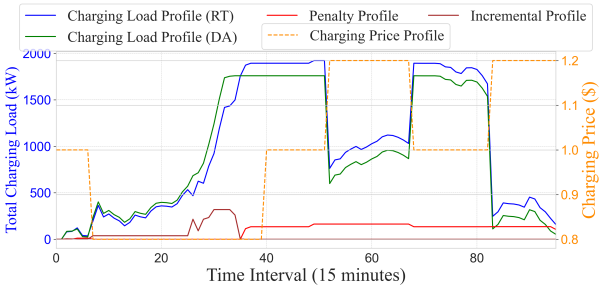

(b) Cluster 2

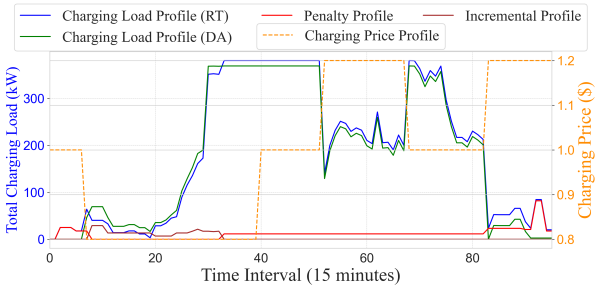

(c) Cluster 3

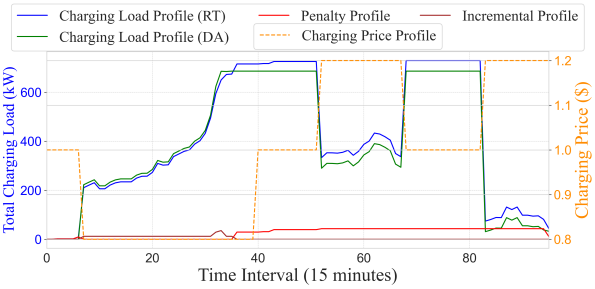

(d) Cluster 4

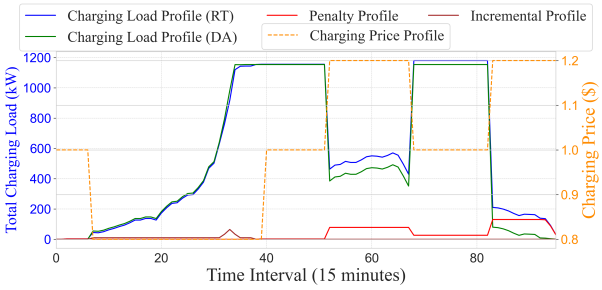

(e) Cluster 5

Figure 5.12 Charging Profiles in SC3

CHAPTER 6 ARTICLE 3: TRI-LEVEL EV CHARGING COORDINATION VIA URGENCY-AWARE PROPORTIONAL ALLOCATOR AND LEARNING-AUGMENTED ADMM

Authors: Arian Shah Kamrani, Hanane Dagdougui

Submitted on September 4th, 2025 at *IEEE Transactions on Transportation Electrification*, under review.

Contributions: Conception of the work's idea, literature review, design of experiments, implementation of the code, conducting the experiments, analysis of the results, and writing.

6.1 Introduction

The large-scale integration of electric vehicles (EVs) into distribution networks introduces many challenges related to the grid safety and infrastructure capacity in power systmes [155]. As EV number increases, traditional centralized control becomes impractical due to privacy concerns, computational complexity, and communication issues. These challenges have motivated the use of distributed optimization techniques. Among them, the alternating direction method of multipliers (ADMM) can be implemented for hierarchical coordination and decomposes complicated optimization problems into smaller sub-problems [156]. While centralized approaches require full system knowledge and costly communication infrastructure, in ADMM, each agent solves local problems and gradually reaches a global consensus through an iterative process with only limited communication [157]. Although classical ADMM formulations have shown strong performance for convex power system problems [158, 159], their practical implementation still needs accurate penalty parameter tuning and may suffer from slow convergence in complex scenarios [160]. Recent works have explored adaptive weighting [161], asynchronous communication [162], and learning-augmented variants [163] to improve robustness and speed in the ADMM iterative process. Motivated by these developments, in [72], a single-loop ADMM is developed to solve the hierarchical EV charging management, including a distribution system operator (DSO) at the top layer, EV aggregators (EVAs) at the middle layer, and EV charging stations at the bottom layer. Charging cost minimization at the EV charging stations level, peak load shaving at the EVAs level, and voltage regulation at the DSO level have been considered in this work. Authors in [164] propose a distributed real-time optimization framework based on an improved ADMM algorithm for coordinating large-scale EV charging with wind power integration. The improved ADMM

extends classical two-block ADMM to a multi-block setting by allowing parallel updates of separable variables subject to a global coupling constraint. In [165], a hierarchical ADMM-based system is designed to coordinate EV charging across a DSO, EVAs, and virtual groups (VGs) of EVs. To manage the complexity of their proposed framework, which integrates EVs with stochastic charging behavior, the authors propose a deadline-differentiated threshold charging policy that prioritizes the EV charging mechanism based on the energy needed and the departure time of EVs. In [166], an ADMM-based planning method for integrating EV charging stations and photovoltaic systems into distribution networks under uncertainty is proposed. A peer-to-peer transactive energy market is introduced, where a decentralized algorithm ensures privacy-preserving energy trading and convergence of the planning model. Simulation results show that the method reduces PV curtailment, avoids unnecessary network expansion, and regulates EV charging through optimal pricing and network charges. Authors in [167] propose a decentralized ADMM-based scheduling framework for EV charging that considers grid constraints. The framework considers real-time pricing, valley filling, and peak shaving to control EV consumption behavior. Although recent studies have advanced the ADMM framework for EV charging coordination, its computational demands remain an important challenge. Most existing methods still rely on per-EV decision variables, which leads to complex optimization and slower solving times. While strategies such as adaptive weighting and learning-based warm starts can improve convergence speed [168], they often neglect the cost of solving each iteration. The mentioned limitations illustrate that we need approaches that not only reduce the number of iterations but also simplify the structure of local subproblems to achieve faster and more scalable coordination across hierarchical layers.

The ADMM scalability also depends on how EVs are grouped and dispatched within hierarchical frameworks. Clustering has been widely used in EV charging management frameworks to group EVs with similar behavioral patterns. In [169], the authors propose a hierarchical charging framework based on clustering mobile charging robots (MCRs). Within each MCR, with the help of clustering, localized scheduling is conducted to facilitate multi-objective dispatch and real-time coordination. In [170], EV user participation in V2G scheduling is introduced through an evaluation model and an optimal cluster scheduling strategy. The strategy considers multiple indicators such as declared dispatch power, user credit, battery degradation, and participation frequency to estimate the reliability and value of each EV. In [171], the authors propose a charging model for an EV fleet where EVs are grouped based on their battery state of charge (SoC). Clustering based on SoC allows the operator to manage large fleets efficiently and make the charging scheduling process more scalable. While previous work has considered clustering schemes for energy dispatch, a gap remains in this domain. Fixed clustering strategies often generalize EV behavior across time, while there is variability

in EVs' charging patterns, such as arrival/departure times and the energy needed, from month to month or even day to day. This motivates the need for considering dynamic clustering methods in EV charging to capture the temporal dynamics of real-world EV sessions within hierarchical structures.

To address the challenges of coordinating large-scale EV charging under a decentralized structure, this work introduces a tri-level ADMM framework that integrates dynamic clustering, urgency-aware dispatch, and machine learning application for warm starting the optimization. The proposed architecture reduces the computational burden from two perspectives. First, the use of the urgency-aware proportional allocator (UAPA) facilitates local energy scheduling by proportionally distributing available charging power among EVs according to their urgency factors. Second, it reduces the required ADMM iterations via machine learning–augmented ADMM (ML-ADMM) initialization. The key contributions of this work are summarized as follows:

- A tri-level ADMM framework is proposed to coordinate EV charging across clusters, EVAs, and the DSO. The framework comprises distinct objectives at each level: peak demand mitigation at the grid level, electricity cost minimization at the EVA level, and reliable and battery-conscious charging at the local cluster level, utilizing real data.
- Dynamic clustering is applied for each EVA to group EVs based on the different days of the week pattern of EV owners' behaviour (arrival time, departure time, and laxity), which makes the EVs' charging more manageable. Dynamic means clusters are re-formed each day because the set of EVs changes daily.
- A novel UAPA is proposed at the cluster level, which replaces per-EV trajectory optimization with a single aggregate decision variable. This reduces computational complexity while preserving alignment with individual charging needs, based on the urgency of charging.
- A learning-augmented prediction mechanism is developed for both EVA and DSO levels to predict primal and dual ADMM variables. This mechanism accelerates convergence in distributed optimization frameworks, significantly reducing the number of iterations and communication overhead.

6.2 system description

The proposed hierarchical EV charging coordination framework consists of three levels, as illustrated in Fig. 6.1. At the top layer, the DSO considers grid-level objectives such as peak

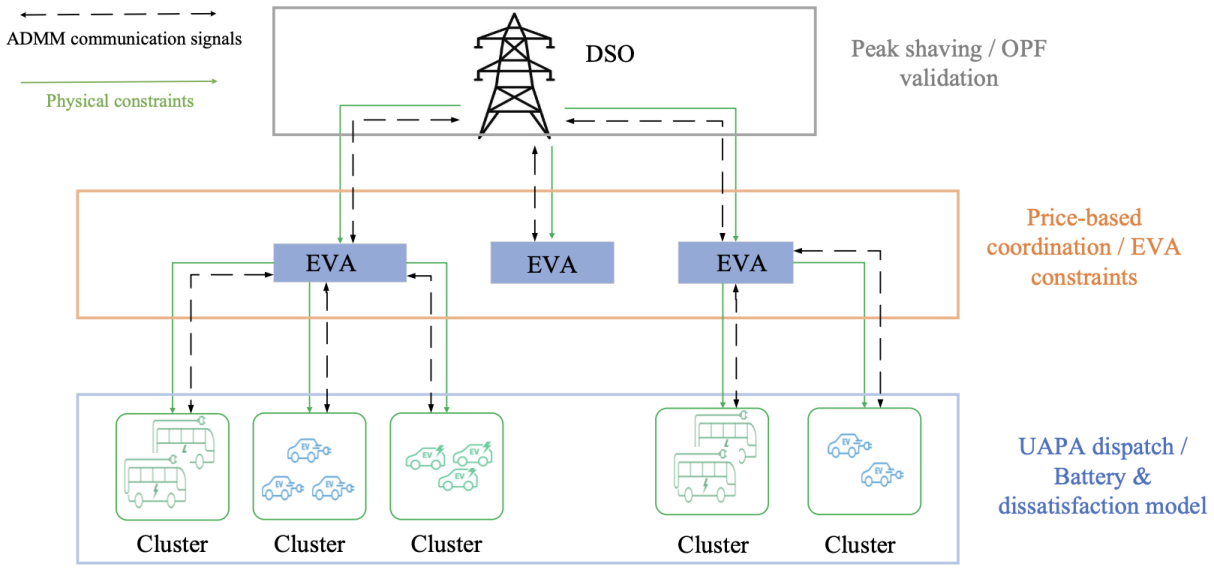

Figure 6.1 Overview of the proposed tri-level EV charging coordination framework.

shaving and power flow validation. EVAs at the middle level coordinate aggregate power profiles from clusters, subject to dynamic pricing and local capacity constraints. At the bottom layer, EV clusters make charging decisions locally, guided by daily usage characteristics and behavioral patterns. These clusters are dynamically formed to capture temporal and behavioral patterns in EV usage.

Within each cluster, a novel UAPA control energy allocation method is proposed for EVs, considering the urgency of charging sessions. This local mechanism reduces computational complexity of charging management by avoiding per-EV trajectory optimization, instead using a single decision variable per cluster. The coordination across all levels is achieved using an ADMM optimization scheme, where consensus and dual variables are exchanged between layers. This structure is further enhanced by a learning-augmented method, which significantly accelerates convergence by reducing the number of required iterations.

6.3 Problem Formulation

6.3.1 Clusters

To manage a large number of EV charging sessions related to an EVA and break them into smaller groups, we use a clustering strategy that groups similar sessions into clusters. The resulting clusters serve as the fundamental optimization units within each EVA.

Session Collection and Characterization For each EVA i, let $\mathcal{Q}_i$ denote the set of charging session requests from EV owners on a given day. Each session $q \in \mathcal{Q}_i$ is characterized by the tuple $\gamma_{i,q} = (t^{\text{in}}_{i,q}, t^{\text{out}}_{i,q}, e_{i,q}, r^{\max}_{i,q})$, where:

- $t^{\text{in}}_{i,q}$, $t^{\text{out}}_{i,q}$: arrival and departure time slots.
- $e_{i,q}$: required energy demand (kWh).
- $r^{\max}_{i,q}$: maximum charging rate (kW).

Assumption: We assume that the tuple $\gamma_{i,q}$ is known before optimization, which allows clustering and scheduling to be performed in advance.

We extract several features from each session to capture its temporal and power-related characteristics. The *ArrivalSlot* and *DepartureSlot* illustrate the session's start and end times based on 15-minute intervals. The difference between these two defines the *DurationSlots*, which shows the number of available time slots for the charging process. The *RequiredSlots* is computed as:

$$\text{RequiredSlots}_{i,q} := \frac{e_{i,q}}{r^{\max}_{i,q} \cdot \delta_t}, \tag{6.1}$$

where $e_{i,q}$ is the energy demand of session q at EVA i, $r^{\max}_{i,q}$ is the maximum charging rate of the EV, and δ_t is the time duration of each slot. This value shows the number of time slots needed to meet the energy demand of session q. Based on this, we define the *Laxity* of session q as the excess time available for scheduling, given by:

$$\text{Laxity}_{i,q} := \max\left\{0,\ \text{DurationSlots}_{i,q} - \text{RequiredSlots}_{i,q}\right\}. \tag{6.2}$$

Each charging session is then mapped to a feature vector:

$$\begin{aligned}\mathbf{x}_{i,q} := \Big[&\text{Laxity}_{i,q},\ \text{ArrivalSlot}_{i,q},\\ &\text{DepartureSlot}_{i,q} \Big]^\top \in \mathbb{R}^3,\end{aligned} \tag{6.3}$$

which contains the key dimensions for clustering. All vectors $\mathbf{x}_{i,q}$ are standardized using z-score normalization, where each feature component is transformed as:

$$\tilde{x}^{(f)}_{i,q} = \frac{x^{(f)}_{i,q} - \mu^{(f)}}{\sigma^{(f)}}, \tag{6.4}$$

with $\mu^{(f)}$ and $\sigma^{(f)}$ indicating the mean and standard deviation of feature f computed over all sessions.

Dynamic Clustering using HDBSCAN To group sessions based on their similarities, we apply the hierarchical density-based spatial clustering of applications with noise (HDBSCAN) algorithm independently for each EVA. This clustering process is performed once per day for each new set of charging session requests, which is why we consider it a dynamic clustering approach. Unlike K-Means, HDBSCAN does not require the number of clusters to be specified in advance and can identify clusters of varying densities. Also, HDBSCAN can automatically detect outliers [172].

Let $j \in \mathcal{C}_i$ index the identified clusters under EVA i, and define $\mathcal{Q}_{i,j} \subseteq \mathcal{Q}_i$ as the set of sessions assigned to cluster j. These clusters represent the smallest coordinated charging units in our hierarchical framework.

Algorithm 4 Clustering of EV Sessions Using HDBSCAN

Require: EV session dataset $\mathcal{Q}_i$ for each EVA i on a given day
Ensure: Clustered groups $\mathcal{Q}_{i,j}$ across all EVAs
for all session $q \in \mathcal{Q}_i$ **do**
    Compute *RequiredSlots* and *Laxity* using Equations (6.1) and (6.2)
    Construct feature vector $\mathbf{x}_{i,q}$ as defined in Equation (6.3)
end for
Normalize all $\mathbf{x}_{i,q}$ using z-score standardization (Equation (6.4))
for all EVA i **do**
    Apply HDBSCAN to $\{\mathbf{x}_{i,q}\}_{q \in \mathcal{Q}_i}$
    Assign cluster label j to each session q
    Form clusters $\mathcal{Q}_{i,j} \subseteq \mathcal{Q}_i$
end for

Cluster-Level Optimization Model The objective of each cluster is to minimize dissatisfaction and charging violations to promote battery health.

The following constraints are applied for all $i \in \mathcal{I}$, $j \in \mathcal{C}_i$, $q \in \mathcal{Q}_{i,j}$, and $\tau \in \mathcal{T}$:

$$\text{P1:} \quad \min_{\{r_{i,j,q,\tau}\}} \quad \sum_{q \in \mathcal{Q}_{i,j}} \left(c_d \cdot \max\left\{0,\ e_{i,j,q} - \sum_{\tau=t^{\text{in}}_{i,j,q}}^{t^{\text{out}}_{i,j,q}} r_{i,j,q,\tau} \right\} + \ c_h \cdot \sum_{\tau \in \mathcal{T}} r^2_{i,j,q,\tau} \right) \tag{6.5a}$$

$$P_{i,j,\tau} = \sum_{q \in \mathcal{Q}_{i,j}} r_{i,j,q,\tau} \tag{6.5b}$$

$$\underline{P}_{i,j} \leq P_{i,j,\tau} \leq \overline{P}_{i,j} \tag{6.5c}$$

$$0 \leq r_{i,j,q,\tau} \leq r^{\max}_{i,j,q} \tag{6.5d}$$

$$r_{i,j,q,\tau} = 0, \quad \forall \tau < t^{\text{in}}_{i,j,q} \text{ or } \tau > t^{\text{out}}_{i,j,q} \tag{6.5e}$$

$$\sum_{\tau=t^{\text{in}}_{i,j,q}}^{t^{\text{out}}_{i,j,q}} r_{i,j,q,\tau} \cdot \delta_t \geq \hat{e}^{\min}_{i,j,q} \tag{6.5f}$$

The objective function contains two terms, the first term penalizes unmet energy, while the r^2 term is a quadratic cost that limit very high charging rates and promotes smoother charging profiles which is good for EV owners battery health. Here, $r_{i,j,q,\tau}$ is the charging power of the session q at time slot τ, and $\boldsymbol{P}_{i,j} = \{P_{i,j,\tau}\}_{\tau \in \mathcal{T}}$ denotes the cluster's total load profile. $\overline{P}_{i,j}$ and $\underline{P}_{i,j}$ indicate the maximum and minimum allowable charging power at cluster j within EVA i, and $\hat{e}^{\min}_{i,j,q}$ illustrates the desired amount of energy to be delivered to session q by its departure time.

6.3.2 EVA

Each EVA seeks to minimize its total energy purchasing cost from the DSO over the scheduling horizon in order to maximize its benefit $\mathcal{T}$:

$$\text{P2:} \quad \min_{\{P_{i,\tau}\}} \quad \sum_{\tau \in \mathcal{T}} c_{i,\tau} \cdot P_{i,\tau} \tag{6.6a}$$

To evaluate this cost, the total charging power of EVA i at time slot τ is computed as the sum of cluster-level consumptions:

$$P_{i,\tau} = \sum_{j \in \mathcal{C}_i} P_{i,j,\tau} \tag{6.6b}$$

To ensure feasible operation, the total EVA-level charging demand must respect its infrastructure capacity:

$$P_{i,\tau} \leq \overline{P}_{i,\tau} \tag{6.6c}$$

Here, $\mathcal{C}_i$ denotes the set of clusters under EVA i, $c_{i,\tau}$ is the electricity price signal, and $\overline{P}_{i,\tau}$ is the maximum available power for EVA i at time τ.

6.3.3 Distribution network

DSO-Level Optimization Model DSO, in general, seeks to ensure the reliable operation of the distribution network and control the EVAs' power consumption on each bus. In this framework, the DSO's objective is to minimize the sum of the daily peak power consumption across all EVAs. Let $\mathcal{I}$ be the set of all EVAs.

$$\text{P3:} \quad \min \quad \lambda_{\text{peak}} \cdot \sum_{i \in \mathcal{I}} \max_{\tau \in \mathcal{T}} P_{i,\tau} \tag{6.7a}$$

The DSO captures the charging profiles of each EVA $\{\mathbf{P}_i\}_{i \in \mathcal{I}}$, and this profile must satisfy the physical and operational constraints of the power distribution network. In this work, the distribution network is modeled as a radial system consisting of a set of buses $\mathcal{B}$ and distribution lines $\mathcal{L}$. Let $\mathcal{D}(b)$ denote the set of child nodes (downstream buses) of bus b. We adopt a branch-flow formulation, as in [173], to model the power flow dynamics.

All equations below are enforced for every bus b, line (b, b'), and time slot τ.

$$P_{\kappa(b),\tau} - \sum_{b' \in \mathcal{D}(b)} \Big(P_{bb',\tau} + R_{bb'}\, I^2_{bb',\tau} \Big) + P^G_{b,\tau} = P^D_{b,\tau} + \sum_{i : b(i) = b} P_{i,\tau}, \tag{6.7b}$$

$$Q_{\kappa(b),\tau} - \sum_{b' \in \mathcal{D}(b)} \Big(Q_{bb',\tau} + X_{bb'}\, I^2_{bb',\tau} \Big) + Q^G_{b,\tau} = Q^D_{b,\tau}, \tag{6.7c}$$

$$P^G_{b,\tau} = Q^G_{b,\tau} = 0, \tag{6.7d}$$

$$V^2_{b',\tau} \cdot I^2_{bb',\tau} = P^2_{bb',\tau} + Q^2_{bb',\tau}, \tag{6.7e}$$

$$V^2_{b,\tau} - 2\Big(R_{bb'} P_{bb',\tau} + X_{bb'} Q_{bb',\tau} \Big) + \Big(R^2_{bb'} + X^2_{bb'} \Big) I^2_{bb',\tau} = V^2_{b',\tau}, \tag{6.7f}$$

$$\underline{V}^2 \leq V^2_{b,\tau} \leq \overline{V}^2, \tag{6.7g}$$

$$0 \leq I^2_{bb',\tau} \leq \overline{I}^2_{bb'}. \tag{6.7h}$$

In the above equations, $P_{bb',\tau}$ and $Q_{bb',\tau}$ represent the active and reactive power flows from bus b to its child bus b', respectively.$P^D_{b,\tau}$ and $Q^D_{b,\tau}$ denote non-EV active and reactive power demands at bus b. $P^G_{b,\tau}$ and $Q^G_{b,\tau}$ represent controllable generation at bus b. $I^2_{bb',\tau}$ is the squared current magnitude on line (b, b'), and $V^2_{b,\tau}$ is the squared voltage magnitude at bus b. The parameters $R_{bb'}$ and $X_{bb'}$ indicate the resistance and reactance of line (b, b'), while $\underline{V}^2$, $\overline{V}^2$, and $\overline{I}^2_{bb'}$ denote the lower and upper voltage bounds and the maximum allowable current on line (b, b'), respectively. The mapping $b(i)$ associates each EVA i to its connected bus.

To achieve a computationally feasible convex model, we apply a second-order cone programming (SOCP) relaxation of the non-convex equality in Equation (6.7e).

$$\sqrt{P^2_{bb',\tau} + Q^2_{bb',\tau}} \leq V_{b',\tau} \cdot I_{bb',\tau}, \tag{6.7i}$$

This relaxation guarantees convexity. The overall problem, including this SOCP constraint, can be solved efficiently using convex optimization solvers.

6.3.4 Hierarchical ADMM-Based Decomposition

The centralized problem that minimizes the aggregate objective of all clusters, EVAs, and the DSO is formulated as:

$$\begin{aligned} \text{P4:} \quad \min_{\{r_{i,j,q,\tau},\, P_{i,j,\tau},\, P_{i,\tau}\}} \quad & \sum_{i\in\mathcal{I}} \sum_{j\in\mathcal{C}_i} \sum_{q\in\mathcal{Q}_{i,j}} \\ \Bigg(c_d \cdot \max\Bigg\{0,\, e_{i,j,q} - \sum_{\tau=t^{\text{in}}_{i,j,q}}^{t^{\text{out}}_{i,j,q}} r_{i,j,q,\tau}\Bigg\} \quad & + c_h \cdot \sum_{\tau\in\mathcal{T}} r^2_{i,j,q,\tau} \Bigg) \\ + \sum_{i\in\mathcal{I}} \sum_{\tau\in\mathcal{T}} c_{i,\tau}\, P_{i,\tau} \quad & + \lambda_{\text{peak}} \cdot \sum_{i\in\mathcal{I}} \max_{\tau\in\mathcal{T}} P_{i,\tau} \end{aligned} \tag{8}$$

s.t. Constraints (6.5b)–(6.5f), (6.6b)–(6.6c), (6.7b)–(6.7i).

To allow distributed coordination across the tri-level EV charging framework, we adopt a hierarchical ADMM-based decomposition method that preserves privacy, reduces computational complexity, and permits parallel updates.

ADMM Reformulation

Auxiliary consensus variables are introduced to decouple local and global decisions across agents. Specifically, for each cluster (i, j), let $\hat{\mathbf{p}}_{i,j}$ denote the consensus copy of the local

charging profile $\mathbf{P}_{i,j}$, and for each EVA i, let $\hat{\mathbf{P}}_i$ represent the consensus copy of its aggregate power allocation $\mathbf{P}_i$. Using these, we define $\mathbf{z}_i := \sum_{j\in\mathcal{C}_i} \hat{\mathbf{p}}_{i,j}$ as the total consensus power profile of EVA i, and $\mathbf{z} := \sum_{i\in\mathcal{I}} \hat{\mathbf{P}}_i$ as the system-wide aggregate consensus power. We introduce scaled dual variables $\mathbf{u}_i$ and $\mathbf{v}$ for the EVA–cluster and DSO–EVA couplings, respectively. The corresponding augmented Lagrangian is formulated below.

The following constraints apply for all $i \in \mathcal{I}$ and $j \in \mathcal{C}_i$.

$$\begin{aligned}\mathcal{L}_\rho = &\sum_i \sum_j \mathrm{P1}_{i,j}(\mathbf{P}_{i,j}) + \sum_i \mathrm{P2}_i(\mathbf{P}_i) + \mathrm{P3}(\mathbf{P}) \\ &+ \sum_i \frac{\rho}{2} \left\| \sum_j \hat{\mathbf{p}}_{i,j} - \hat{\mathbf{P}}_i + \mathbf{u}_i \right\|_2^2 + \frac{\rho}{2} \left\| \sum_i \hat{\mathbf{P}}_i - \mathbf{P} + \mathbf{v} \right\|_2^2 .\end{aligned} \tag{6.9}$$

Cluster-level update

$$\mathbf{P}_{i,j}^{k+1} := \arg\min_{\mathbf{P}_{i,j}} \quad \mathrm{P1}_{i,j}(\mathbf{P}_{i,j}) + \frac{\rho}{2} \left\| \mathbf{P}_{i,j} - \hat{\mathbf{p}}_{i,j}^k \right\|_2^2 . \tag{6.10}$$

EVA-level update

$$\mathbf{P}_i^{k+1} := \arg\min_{\mathbf{P}_i} \quad \mathrm{P2}_i(\mathbf{P}_i) + \frac{\rho}{2} \left\| \sum_j \hat{\mathbf{p}}_{i,j}^{k+1} - \hat{\mathbf{P}}_i + \mathbf{u}_i^k \right\|_2^2 . \tag{6.11}$$

DSO-level update

$$\mathbf{P}^{k+1} := \arg\min_{\mathbf{P}} \ \mathrm{P3}(\mathbf{P}) + \frac{\rho}{2} \left\| \sum_i \hat{\mathbf{P}}_i^{k+1} - \mathbf{P} + \mathbf{v}^k \right\|_2^2 . \tag{6.12}$$

Consensus variable updates

$$\hat{\mathbf{p}}_{i,j}^{k+1} = \mathbf{P}_{i,j}^{k+1}, \tag{6.13}$$

$$\hat{\mathbf{P}}_i^{k+1} = \mathbf{P}_i^{k+1}, \tag{6.14}$$

$$\hat{\mathbf{P}}^{k+1} = \mathbf{P}^{k+1}. \tag{6.15}$$

Dual variable updates

$$\mathbf{u}_i^{k+1} = \mathbf{u}_i^k + \left(\sum_j \hat{\mathbf{p}}_{i,j}^{k+1} - \hat{\mathbf{P}}_i^{k+1} \right), \tag{6.16}$$

$$\mathbf{v}^{k+1} = \mathbf{v}^k + \left(\sum_i \hat{\mathbf{P}}_i^{k+1} - \hat{\mathbf{P}}^{k+1} \right). \tag{6.17}$$

Stopping Criteria The ADMM iteration terminates when both the primal and dual residuals fall below predefined tolerances. Specifically, we define the *primal residuals* as the

mismatch between local and consensus variables:

$$\mathbf{r}_{\text{pri}}^{k+1} := \begin{bmatrix} \sum_j \hat{\mathbf{p}}_{i,j}^{k+1} - \hat{\mathbf{P}}_i^{k+1} \\ \sum_i \hat{\mathbf{P}}_i^{k+1} - \hat{\mathbf{P}}^{k+1} \end{bmatrix}, \tag{6.18}$$

and the *dual residuals* as the change in consensus variables between iterations:

$$\mathbf{r}_{\text{dual}}^{k+1} := \begin{bmatrix} \rho\left(\hat{\mathbf{P}}_i^{k+1} - \hat{\mathbf{P}}_i^{k}\right) \\ \rho\left(\hat{\mathbf{P}}^{k+1} - \hat{\mathbf{P}}^{k}\right) \end{bmatrix}. \tag{6.19}$$

The algorithm stops when:

$$\left\|\mathbf{r}_{\text{pri}}^{k+1}\right\|_2 \leq \epsilon_{\text{pri}}, \quad \left\|\mathbf{r}_{\text{dual}}^{k+1}\right\|_2 \leq \epsilon_{\text{dual}}, \tag{6.20}$$

where ϵ_{pri} and ϵ_{dual} are pre-specified tolerances that control the convergence threshold.

Convergence and Remarks

Under standard assumptions that P1, P2, and P3 are convex, continuous, and proper, the ADMM procedure guarantees convergence to the global optimum.

6.3.5 Urgency-Aware Proportional Allocator (UAPA)

To make the system more scalable and reduce computational complexity, we introduce the UAPA at the cluster level. This method offers a simplified, convex approximation of the original cluster-level problem described in Section 6.3.1, where individual EV charging profiles $r_{i,j,q,\tau}$ were directly optimized. Instead of solving for each EV's charging trajectory, UAPA introduces a single decision variable $\mathbf{P}_{i,j} = \{P_{i,j,\tau}\}_{\tau \in \mathcal{T}}$ that represents the aggregate load profile of cluster j under EVA i. Then, individual EV allocations are calculated through a proportional dispatch mechanism based on urgency scores. This mechanism significantly reduces the number of decision variables and increases the scalability of the framework.

Each EV $q \in \mathcal{Q}_{i,j}$ is assigned an urgency score that computes how critical its energy demand is relative to its availability and maximum charging rate:

$$\omega_{i,j,q} := \frac{\hat{e}_{i,j,q}^{\min}}{(t_{i,j,q}^{\text{out}} - t_{i,j,q}^{\text{in}}) \cdot r_{i,j,q}^{\max}}, \tag{6.21}$$

which shows the average energy demand per unit of allowable charging capacity over the session window.

Algorithm 5 Tri-Level ADMM-Based Charging Coordination

$k \leftarrow 1$
Initialize primal, consensus, and dual variables
repeat
  for all EVA $i \in \mathcal{I}$ **in parallel do**
    for all Cluster $j \in \mathcal{C}_i$ **in parallel do**
      Update cluster profile via (6.10)
    end for
    Update consensus variables via (6.13)
    Aggregate $\mathbf{z}_i^{k+1} := \sum_j \hat{\mathbf{p}}_{i,j}^{k+1}$
    Update EVA profile via (6.11)
    Update consensus via (6.14)
    Update dual variable $\mathbf{u}_i$ via (6.16)
  end for
  Aggregate $\mathbf{z}^{k+1} := \sum_i \hat{\mathbf{P}}_i^{k+1}$
  Update DSO profile via (6.12)
  Update consensus via (6.15)
  Update dual variable $\mathbf{v}$ via (6.17)
  Compute residuals via (6.18) and (6.19)
  $k \leftarrow k + 1$
until stopping condition (6.20) is met

Let $\chi_{i,j,q,\tau} \in \{0, 1\}$ be a binary indicator such that

$$\chi_{i,j,q,\tau} = \begin{cases} 1, & \text{if } \tau \in [t_{i,j,q}^{\text{in}}, t_{i,j,q}^{\text{out}}], \\ 0, & \text{otherwise,} \end{cases} \tag{6.22}$$

which encodes the availability of EV q at time τ.

Using this mask, we define the raw urgency-weighted allocation matrix:

$$A_{i,j}[\tau, q] = \omega_{i,j,q} \cdot \chi_{i,j,q,\tau}. \tag{6.23}$$

Each row of this matrix is normalized to produce a soft allocation weight:

$$W_{i,j}[\tau, q] = \frac{A_{i,j}[\tau, q]}{\sum\limits_{q'} A_{i,j}[\tau, q'] + \varepsilon}, \tag{6.24}$$

where ε is a small constant to avoid division by zero when no EVs are present.

The per-EV charging profile is derived by proportionally mapping the cluster-level aggregate variable using normalized urgency-based weights:

$$\tilde{r}_{i,j,q,\tau} = W_{i,j}[\tau, q] \cdot P_{i,j,\tau}. \tag{6.25}$$

To respect per-EV charging rate limits, this preliminary value is clipped:

$$\hat{r}_{i,j,q,\tau} = \min\left\{\tilde{r}_{i,j,q,\tau},\, r^{\max}_{i,j,q}\right\}. \tag{6.26}$$

The total energy delivered to each EV is computed as:

$$\hat{e}_{i,j,q} := \sum_{\tau \in \mathcal{T}} \delta_t \cdot \hat{r}_{i,j,q,\tau}. \tag{6.27}$$

Despite the simplified allocation mechanism in UAPA, it remains essential to ensure that each EV receives its minimum required energy by departure time:

$$\hat{e}_{i,j,q} \geq \hat{e}^{\min}_{i,j,q}. \tag{6.28}$$

Note: While the UAPA scheme may not meet all energy requirements on the first attempt, we address this with a simple and logical repair process. If the energy delivered to any EV, $\hat{e}_{i,j,q}$, falls below its minimum required level $\hat{e}^{\min}_{i,j,q}$, the algorithm slightly adjusts the urgency weights and re-runs the allocation. This ensures that all energy needs are eventually met. Moreover, it does not compromise the convex structure of the problem.

Binary Feasibility Repair To ensure that Equation (6.28) is satisfied, we adopt an iterative binary feasibility check. If any EV fails to meet its energy requirement, its urgency score is doubled:

$$\omega_{i,j,q} \leftarrow 2 \cdot \omega_{i,j,q} \quad \text{if } \hat{e}_{i,j,q} < \hat{e}^{\min}_{i,j,q}, \tag{6.29}$$

and the allocation is repeated. This process continues until all EVs satisfy their minimum energy or a maximum retry count is reached.

Finally, the cluster-level objective function under UAPA becomes:

$$\text{P1: } \min_{\{\mathbf{P}_{i,j}\}} \sum_{q \in \mathcal{Q}_{i,j}} c_d \cdot \left(e_{i,j,q} - \hat{e}_{i,j,q}\right)^2 + c_h \cdot \sum_{\tau \in \mathcal{T}} P^2_{i,j,\tau}. \tag{6.30}$$

Remark Although individual EV charging stress is not individually modeled in the UAPA scheme, the cluster-level term $\sum_\tau P^2_{i,j,\tau}$ helps as a convex surrogate that penalizes high variability in aggregate charging profiles. Since per-EV allocations are derived through linear projections of the cluster-level decision variable(i.e., $\hat{r}_{i,j,q,\tau} \propto P_{i,j,\tau}$).

Algorithm 6 UAPA with Binary Feasibility Repair

Require: Cluster data $\mathcal{Q}_{i,j}$, session parameters $\{\hat{e}^{\min}_{i,j,q}, r^{\max}_{i,j,q}, t^{\text{in}}_{i,j,q}, t^{\text{out}}_{i,j,q}\}$, and aggregate decision $\mathbf{P}_{i,j} = \{P_{i,j,\tau}\}$
Ensure: Per-EV charging profiles $\hat{r}_{i,j,q,\tau}$, delivered energies $\hat{e}_{i,j,q}$

repeat
  for all EV $q \in \mathcal{Q}_{i,j}$ **do**
    Compute urgency score $\omega_{i,j,q}$ via Eq. (6.21)
    for all Time slot $\tau \in \mathcal{T}$ **do**
      Compute availability mask $\chi_{i,j,q,\tau}$ via Eq. (6.22)
      Compute raw weight $A_{i,j}[\tau, q]$ via Eq. (6.23)
    end for
  end for
  for all Time slot $\tau \in \mathcal{T}$ **do**
    Normalize weights $W_{i,j}[\tau, q]$ via Eq. (6.24)
    for all EV $q \in \mathcal{Q}_{i,j}$ **do**
      Compute $\tilde{r}_{i,j,q,\tau}$, clip to $\hat{r}_{i,j,q,\tau}$ via Eq. (6.26)
    end for
  end for
  feasible $\leftarrow$ `True`
  for all EV $q \in \mathcal{Q}_{i,j}$ **do**
    Compute $\hat{e}_{i,j,q}$ via Eq. (6.27)
    if $\hat{e}_{i,j,q} < \hat{e}^{\min}_{i,j,q}$ **then**
      Boost urgency $\omega_{i,j,q} \leftarrow 2 \cdot \omega_{i,j,q}$
      feasible $\leftarrow$ `False`
    end if
  end for
until feasible = `True` or max retries reached
Compute objective P1 via Eq. (6.30)

6.3.6 Learning-Augmented ADMM at the EVA and DSO Levels

While there is scalable coordination in the tri-level ADMM framework among clusters, EVAs, and the DSO, the convergence rate may still remain slow in large-scale settings due to delays in the communication between agents' consensus. To accelerate convergence, we introduce a machine learning–augmented warm-start mechanism applied at both the EVA and DSO levels, inspired by the ML-ADMM paradigm in [160].

The UAPA already reduces per-iteration computational complexity by minimizing the number of decision variables at the cluster level. In contrast, ML-ADMM focuses on reducing the number of ADMM iterations by providing high-quality initializations for the primal and dual variables involved in the EVA–DSO and EVA–cluster consensus couplings.

Why Not at the Cluster Level?

ML-ADMM is not applied at the cluster level because the UAPA mechanism already reduces the high-dimensional per-EV optimization problem to a low-dimensional convex formulation over aggregate cluster profiles $\boldsymbol{P}_{i,j}$. Additionally, since power flow calculations and coordination tasks occur at the DSO and EVA layers, warm-starting these layers is significantly more impactful in reducing iteration count and improving overall system performance.

Learning-Augmented Neural Network Initialization for ADMM

To enhance convergence of the hierarchical ADMM algorithm, we introduce deep neural networks (DNNs) to predict warm-start values for primal and dual variables at the EVA and DSO levels.

Learning Targets At each ADMM iteration k, the EVA and DSO subproblems (Equations (6.11) and (6.12)) require solving for:

$$\mathbf{P}_i \in \mathbb{R}^{|\mathcal{T}|}, \quad \mathbf{u}_i \in \mathbb{R}^{|\mathcal{T}|} \quad \text{(EVA level)}, \tag{6.31}$$

$$\mathbf{P} \in \mathbb{R}^{|\mathcal{T}|}, \quad \mathbf{v} \in \mathbb{R}^{|\mathcal{T}|} \quad \text{(DSO level)}. \tag{6.32}$$

We aim to predict initializations:

$$\mathbf{y}_i^{\text{EVA}} = \left[\mathbf{P}_i^{\text{init}},\ \mathbf{u}_i^{\text{init}}\right], \tag{6.33}$$

$$\mathbf{y}^{\text{DSO}} = \left[\mathbf{P}^{\text{init}},\ \mathbf{v}^{\text{init}}\right]. \tag{6.34}$$

Feature Construction

EVA-level inputs: The feature vector $\mathbf{x}_i^{\text{EVA}} \in \mathbb{R}^d$ includes:

- Number of clusters $|\mathcal{C}_i|$
- Number of EVs in each cluster
- Electricity prices $\{c_{i,\tau}\}_{\tau \in \mathcal{T}}$
- Aggregated urgency scores $\sum_{j,q} \omega_{i,j,q}$

DSO-level inputs: The input vector $\mathbf{x}^{\text{DSO}} \in \mathbb{R}^{d'}$ includes:

- Electricity price profile $\{\pi_\tau\}$

- Forecasted non-EV base load $\{P^D_{b,\tau}\}$
- Number of EVs in each EVA

Deep Neural Network Architecture Each predictor is a fully connected deep neural network $M : \mathbb{R}^d \to \mathbb{R}^m$, where:

$$\mathbf{y} = M(\mathbf{x}) = \pi(W_{i+1}\mathbf{h}_i + \mathbf{b}_{i+1}), \tag{6.35}$$

with intermediate layers defined as:

$$\mathbf{h}_1 = \pi(W_1\mathbf{x} + \mathbf{b}_1), \tag{6.36}$$
$$\mathbf{h}_j = \pi(W_j\mathbf{h}_{j-1} + \mathbf{b}_j), \quad j = 2, \ldots, i. \tag{6.37}$$

Here, $\mathbf{x} \in \mathbb{R}^d$ is the input feature vector, $\mathbf{y} \in \mathbb{R}^m$ is the predicted output (primal and dual initialization), $W_j \in \mathbb{R}^{d_j \times d_{j-1}}$ are trainable weight matrices, $\mathbf{b}_j \in \mathbb{R}^{d_j}$ are bias vectors, and $\pi(\cdot)$ is a non-linear activation function such as ReLU.

Loss Function and Training Each model is trained using mean squared error (MSE) loss:

$$\min_{\theta} \sum_{(\mathbf{x},\mathbf{y})\in\mathcal{T}_{\text{train}}} \|M(\mathbf{x};\theta) - \mathbf{y}\|_2^2, \tag{6.38}$$

where $\theta = \{W_j, \mathbf{b}_j\}$ denotes the network parameters.

Integration into ADMM At test time, the predicted values replace standard flat initializations:

$$\mathbf{P}_i^{(0)} \leftarrow \hat{\mathbf{P}}_i^{\text{init}}, \quad \mathbf{u}_i^{(0)} \leftarrow \hat{\mathbf{u}}_i^{\text{init}}, \tag{6.39}$$
$$\mathbf{P}^{(0)} \leftarrow \hat{\mathbf{P}}^{\text{init}}, \quad \mathbf{v}^{(0)} \leftarrow \hat{\mathbf{v}}^{\text{init}}. \tag{6.40}$$

These values are injected into Equations (6.11), (6.12), (6.16), and (6.17), accelerating convergence by reducing the number of iterations required to reach consensus.

6.4 Case study

To evaluate the performance of the proposed hierarchical ADMM coordination framework, all simulations were performed locally on a laptop with an M2 chip and 16 GB of unified memory,

Algorithm 7 Learning-Augmented Initialization for ADMM

Require: EVA features $\mathbf{x}_i^{\text{EVA}}$, DSO features $\mathbf{x}^{\text{DSO}}$, trained networks $M^{\text{EVA}}, M^{\text{DSO}}$
Ensure: Warm-started variables: $\mathbf{P}_i^{(0)}, \mathbf{u}_i^{(0)}, \mathbf{P}^{(0)}, \mathbf{v}^{(0)}$
1: **for all** EVA $i \in \mathcal{I}$ **do**
2: Form EVA-level input features as in Section 6.3.6
3: Predict $[\mathbf{P}_i^{\text{init}}, \mathbf{u}_i^{\text{init}}] \leftarrow M^{\text{EVA}}(\mathbf{x}_i^{\text{EVA}})$
4: **end for**
5: Construct DSO input features as per Section 6.3.6
6: Predict $[\mathbf{P}^{\text{init}}, \mathbf{v}^{\text{init}}] \leftarrow M^{\text{DSO}}(\mathbf{x}^{\text{DSO}})$
7: Inject $\mathbf{P}_i^{(0)} \leftarrow \mathbf{P}_i^{\text{init}}$, $\mathbf{u}_i^{(0)} \leftarrow \mathbf{u}_i^{\text{init}}$ into (6.11), (6.16)
8: Inject $\mathbf{P}^{(0)} \leftarrow \mathbf{P}^{\text{init}}$, $\mathbf{v}^{(0)} \leftarrow \mathbf{v}^{\text{init}}$ into (6.12), (6.17)

running macOS Ventura.

6.4.1 Network and Load Configuration

The IEEE 33-bus and 118-bus test systems are adopted to represent the power distribution network, implemented via the Pandapower toolbox and solved using CVXPY. In both networks, a total of five aggregation buses, located at buses 3, 7, 12, 20, and 26, are selected as EVAs. Base non-EV load profiles are extracted from [174] and randomly assigned to buses. Finally, the charging transactions have been assigned to EVAs based on their proximity in geographical location.

6.4.2 EV Dataset and Learning Augmented ADMM

Dataset

The EV charging dataset is obtained during one week in 2024 from real-world transactions from public charging stations located on Montreal Island. These records capture individual charging sessions, including arrival and departure times, power limits, and requested energy. Also, the location-based information, such as latitude and longitude, for each charging transaction is available. For simulation purposes, the data is structured over a 96-slot horizon, corresponding to a 24-hour period with 15-minute resolution.

ML-Augmented Dataset for Warm-Starting ADMM

To construct the learning-augmented ADMM dataset, we simulate classical ADMM runs over six consecutive days with real EV session data. For each day, the full tri-level optimization framework is executed to convergence under cold-start initialization. At convergence, the final

primal and dual variables from both the EVA-level and DSO-level subproblems are extracted and stored as the target output vectors y defined in Section 6.3.6.

The corresponding input features x, also defined in Section 6.3.6, capture characteristics from both the EVA coordination network and the grid-level distribution network. These include cluster composition, pricing signals, urgency statistics, consensus variables, and non-EV base load.

This yields a labeled dataset $\{(x^{(n)}, y^{(n)})\}$ used to train neural networks that predict warm-start values for ADMM. On the seventh day, the trained models generate predictions $\hat{y}$ from observed features x. These results are then injected as initializations for the primal and dual variables at both the EVA and DSO levels.

6.4.3 Simulation Parameters

The objective function in each subproblem includes three additive terms: a dissatisfaction cost weighted by $c_d = 1000$, a charging volatility penalty with $c_h = 1$, and a peak demand regularization term at the DSO level with $\lambda_{\text{peak}} = 1$. These coefficients are selected to reflect both the physical priorities of EV charging and the numerical characteristics of the optimization problem. Among the competing objectives, ensuring that EVs reach their desired state of charge by departure is the most critical practical requirement. However, the dissatisfaction term operates on the energy gap between requested and delivered values, which tends to be numerically smaller than power or peak-related quantities. To ensure this smaller but essential component has sufficient influence in the optimization, a larger weight c_d is applied. In contrast, the charging violation indicator and peak-shaving objectives involve quantities of larger scale and smoother dynamics, allowing them to be effectively captured with smaller weights. Finally, the penalty parameter of ADMM is set to $\rho = 0.5$ and the stopping criterion is based on a tolerance of 10^{-2} for both ϵ_{pri} and ϵ_{dual}.

To accelerate convergence, the machine learning-augmented ADMM module employs two separate fully connected deep neural networks: one at the EVA level and one at the DSO level. The EVA-level model is shared across all EVAs and receives the input vector x_i^{EVA}, similarly, the DSO-level model takes system-level input x^{DSO}, also defined in Section 6.3.6.

Each neural network consists of two hidden layers with 64 and 32 neurons, respectively. ReLU activation functions are utilized and both models are trained using the Adam optimizer with a learning rate of 10^{-3} and a batch size of 32. Training is performed over 200 epochs using labeled data generated from historical ADMM trajectories, as described in Section 6.3.6. These predictions are then used to warm-start the primal and dual variables in the EVA-DSO

Table 6.1 Number of clusters per EVA across different days.

Day	EVA 1	EVA 2	EVA 3	EVA 4	EVA 5
Day 1	3	3	2	2	2
Day 2	2	2	3	3	2
Day 3	2	2	2	5	2
Day 4	5	2	4	2	2
Day 5	2	2	2	4	2
Day 6	3	3	3	2	2
Day 7	2	2	4	4	2

Table 6.2 Comparison of daily peak, charging cost, energy delivered, and squared power sum for each EVA under the proposed and uncontrolled strategies.

EVA	Peak (kW)		Cost ($)		Energy Delivered (kWh)		$\sum_t P_{i,t}^2$	
	Proposed	Uncontrolled	Proposed	Uncontrolled	Proposed	Uncontrolled	Proposed	Uncontrolled
1	58.59	106.20	456.34	476.49	547.22	553.62	92704.98	123541.08
2	59.51	120.82	194.32	216.31	268.13	270.74	39624.29	64890.52
3	278.80	467.16	2372.25	2621.32	2915.37	2946.44	2131708.66	2880545.36
4	151.99	212.24	1599.26	1719.56	1945.92	1975.90	923961.98	1094079.08
5	73.19	115.65	237.57	259.94	287.30	297.43	46417.36	73734.00

consensus coupling, reducing the number of ADMM iterations required for convergence.

6.5 Results

6.5.1 Clustering

EVs are grouped into clusters based on their charging characteristics to be managed more effectively. Table 6.1 illustrates the number of clusters formed per EVA across a sample week. As shown, the number of clusters changes across both days and EVAs. For instance, EVA 1 ranges from 2 to 5 clusters depending on the day, while EVA 3 shows cluster counts between 2 and 4. This variation highlights the dynamic nature of the clustering approach because EVs' arrival times, charging needs, and departure deadlines change from day to day; hence, the way EVs are grouped should also be changed. By updating the clusters daily, the system adapts to these shifts in flexibility, allowing it to coordinate charging in a way that stays both detailed and efficient.

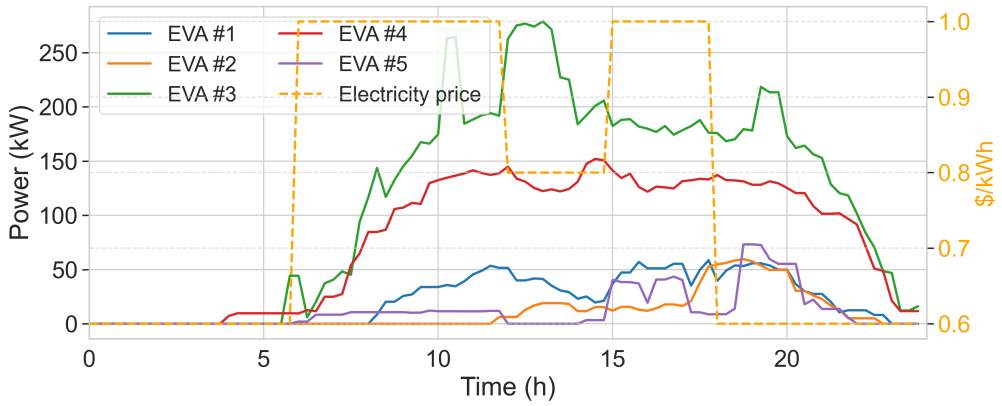

Figure 6.2 Daily EVA charging profiles under the proposed UAPA strategy with electricity price overlay.

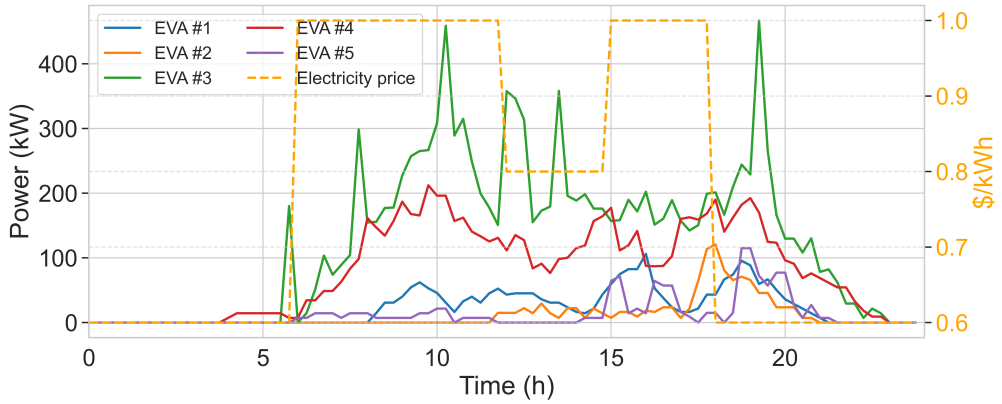

Figure 6.3 Uncontrolled charging profiles without coordination, showing higher peaks and disregard for pricing.

6.5.2 Proposed Hierarchical ADMM Framework

To demonstrate the superiority of the proposed hierarchical framework, we have compared its results with those of uncontrolled charging for one sample day in the IEEE 33-bus test case. In uncontrolled charging, EVs are charged at the maximum charging rate until they are fully charged upon arrival at the station. Figs 6.2 and 6.3 present the daily aggregate charging profiles for each EVA under the proposed coordination and an uncontrolled baseline. In the uncontrolled scenario, the EVAs' charging profiles exhibit volatility peaks due to the maximum charging rate that exists in this scenario, which negatively impacts battery lifespans and grid constraints. Moreover, the charging process typically occurs during the on-peak period, when the electricity price is at its highest value.

Table 6.2 summarizes four critical metrics for each EVA: peak power, total charging cost,

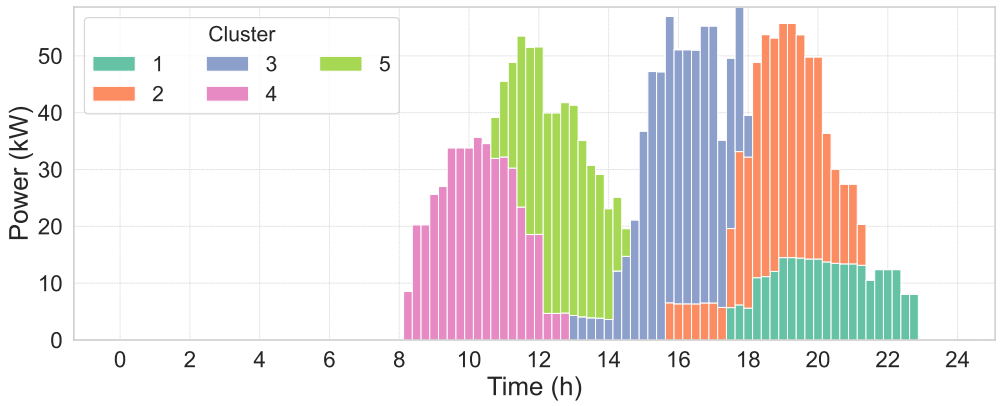

Figure 6.4 Cluster-wise charging breakdown for EVA 1.

energy delivered, and the sum of squared charging power as the charging stress indicator. The proposed method help to reduce peak values across all EVAs. For instance, EVA #1's peak drops from 106.2 kW to 58.59 kW, while EVA #4 and EVA #5 see similar reductions of 28.4% and 36.4%, respectively.

Charging cost also decreased under the proposed coordination due to avoidance of high-price charging intervals. EVA #2, for example, pays $194.32 under the proposed strategy compared to $216.31 in the uncontrolled case, yielding a 10.2% cost reduction. Despite these savings, energy demands are fully met in both approaches; the delivered energy remains identical for all EVAs, with only slight variations.

Battery health is indirectly considered in this work through the reduced charging stress indicator. The sum of squared power, $\sum_t P_{i,t}^2$, is notably lower under the proposed framework. EVA #1 fall from 123541.08 to 92704.98, while EVA #3 sees a drop of over 700000 units in this metric.

Two sample EVAs are chosen to illustrate the shares of clusters in this framework. Fig. 6.4 and Fig. 6.5 present the power allocation breakdown among different clusters within EVA 1 and EVA 3, respectively. In Fig. 6.4, EVA 1 is composed of five clusters, which show distinct profile patterns. For instance, cluster 4 charges primarily during morning hours, while cluster 1 and cluster 2 consist of EVs that are mainly charging during the evening and night. In contrast, Fig. 6.5 shows the cluster contributions for EVA 3, where the charging profiles are distributed across the entire day, and all clusters remain active throughout the day time. Moreover, the majority of charging transactions are belong to cluster 4.

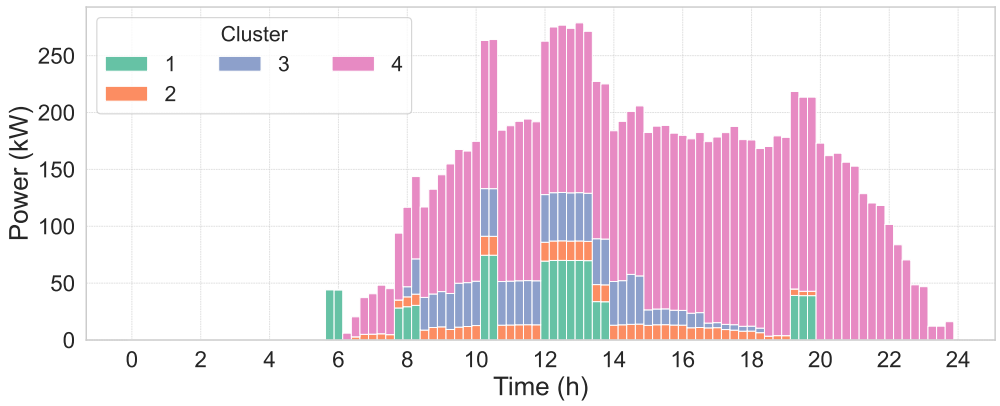

Figure 6.5 Cluster-wise charging breakdown for EVA 3.

6.5.3 UAPA Vs Per EV

Here, we demonstrate the superiority and effectiveness of the UAPA dispatch by comparing it with a per EV scenario, where we have a decision variable for every single EV in the charging process across all EVAs. Here, the comparison is based on two aspects: first, the simulation time, and second, the objective function terms.

UAPA Vs Per EV Simulation Time Result

Table 6.3 Computation Time (in seconds) for UAPA and Per-EV Optimization Across Test Systems and EV Penetration Levels

EV Penetration	**IEEE 33-Bus**		**IEEE 118-Bus**	
	UAPA	Per-EV	UAPA	Per-EV
100%	234	2574	260	3150
75%	232	1771	251	2180
50%	238	1033	255	1148
25%	229	540	251	561

Table 6.3 indicates the computational advantages of the proposed UAPA strategy compared to the traditional Per-EV optimization across various EV penetration levels and network sizes. In the IEEE 33-bus system, UAPA reduces computation time from 2574 seconds to 234 seconds at 100% EV penetration—a 91% reduction. Similar trends are observed for lower penetrations: 86.9%, 77.0%, and 57.6% reductions at 75%, 50%, and 25% penetration levels, respectively. In the larger IEEE 118-bus system, UAPA achieves comparable efficiency gains. At 100% penetration, the computation time drops from 3150 to 260 seconds—a 91.7% improvement. Even at 75%, 50%, and 25% penetration, UAPA reduces runtime by 88.5%,

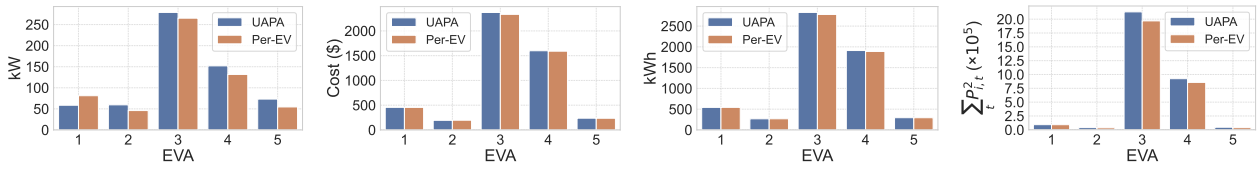

Figure 6.6 Comparison of EVA-level performance under UAPA and Per-EV optimization strategies. (a) Daily peak power per EVA. (b) Daily charging cost. (c) Total energy delivered. (d) Charging stress indicator measured by $\sum_t P_{i,t}^2$.

77.8%, and 55.3%, respectively. These results confirm that UAPA maintains low computation times across all EV penetration levels by relying on a single aggregated variable per cluster, unlike Per-EV optimization, whose complexity grows with the number of EVs.

UAPA Vs Per EV Optimization Result

Here, as a sample, the result of optimization in the 33-bus scenario with 100% EV penetration is presented. Fig. 6.6 compares EVA-level performance under the proposed UAPA method and the conventional Per-EV optimization approach. Overall, the results across the two strategies are very similar, while there is a minor variation depending on cluster characteristics and the UAPA charging mechanism. Notably, in the UAPA scheme, results show a slight increase in peak power consumption for most EVAs. For instance, the peak load for EVA 2 increases from 45.96 kW to 59.51 kW, and EVA 4 sees a rise from 131.65 kW to 151.99 kW. However, this increase also brings a slight improvement in overall energy delivery. As an example, EVA 3 receives 2828.89 kWh under UAPA, compared to 2779.91 kWh with the Per-EV optimization approach. This trade-off reflects UAPA's urgency-aware mechanism, which enhances user satisfaction by better fulfilling energy needs, even if it slightly elevates peak loads.

In terms of charging cost (Fig. 6.6b), the results remain very close. EVA 2, for instance, sees its cost decrease from \$196.49 (Per-EV) to \$194.32 (UAPA), while other EVAs maintain nearly identical cost profiles. Regarding charging stress, as measured by the indicator $\sum_t P_{i,t}^2$ in Fig. 6.6d, the Per-EV strategy performs slightly better due to its higher control precision. For EVA 5, the stress indicator is 38,449.94 under Per-EV and increases to 46,417.36 under UAPA. This difference is expected given that UAPA optimizes over aggregate cluster profiles rather than individual EVs.

The aggregated EVA charging profiles obtained using the proposed UAPA-based method are compared against those from the Per-EV optimization baseline in Fig. 6.7. As observed,

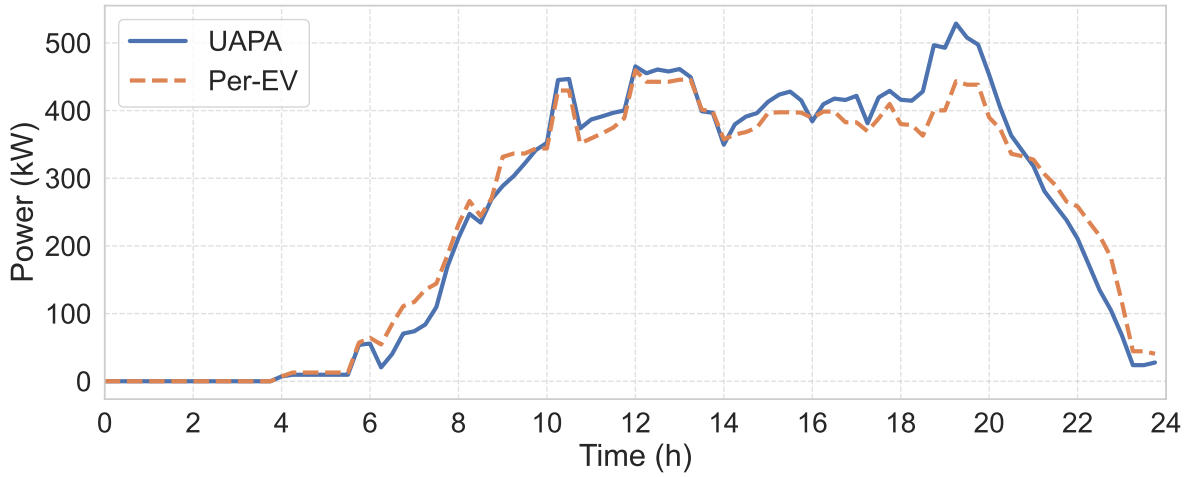

Figure 6.7 Comparison of total EVA aggregate charging profiles under UAPA and Per-EV optimization strategies.

both profiles exhibit highly similar charging patterns and peaks throughout the 24-hour horizon. Numerically, the cosine similarity between the two trajectories is 99.52%, while the coefficient of determination (R^2 score) is 96.44%. These results confirm that UAPA produces nearly identical aggregate charging outcomes as the more computationally intensive Per-EV optimization.

6.5.4 Learning Augmented ADMM

To compare the performance of the classical ADMM and learning augmented ADMM, two scenarios are implemented on the IEEE 33-bus and 118-bus test systems, where in the first scenario the optimization is solved with classical ADMM with cold-start while in the second scenario primal and dual variables were predicted using ML method and the optimization is run based on these predictions.

Table 6.4 Number of Iterations for Classical vs. ML-ADMM Across Test Systems and EV Penetration Levels

EV Penetration	**IEEE 33-Bus**		**IEEE 118-Bus**	
	ADMM	ML-ADMM	ADMM	ML-ADMM
100%	298	82	334	91
75%	281	78	318	85
50%	266	75	301	88
25%	268	77	294	84

Table 6.4 presents the number of ADMM iterations required to reach convergence under

classical and learning-augmented ADMM. Also, four different EV penetration levels and two sample networks are taken into account. For instance, in the IEEE 118-bus system with full EV penetration, classical ADMM requires 334 iterations to converge, while the learning-augmented ADMM achieves convergence in just 91 iterations. Similar improvements are observed at lower penetration levels and in the 33-bus system, where, at 25% penetration, the number of iterations drops by 71.27%. These findings demonstrate the benefit of warm-starting the ADMM algorithm with predicted primal and dual variables in large-scale hierarchical coordination frameworks.

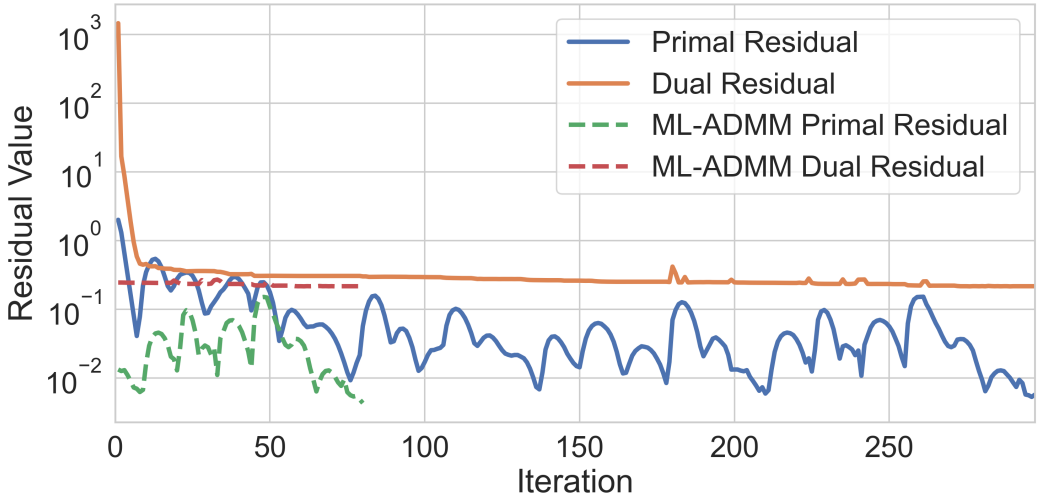

Figure 6.8 Comparison of residuals in classical ADMM and ML-augmented ADMM for EVA–DSO coordination.

Fig. 6.8 illustrates the 100% penetration in the 33 bus test case system convergence behavior of the classical ADMM versus the learning-augmented ADMM between EVAs and the DSO. The classical ADMM dual residuals exhibit a slow but consistent decay over the iterations, whereas the primal residual displays a clear oscillatory behavior. In contrast, in the ML-ADMM, the residuals start from a more favorable initialization, near the terminal values of the classical run, and reach convergence within a fraction of the iteration count.

6.6 Conclusion

This work presents a scalable and hierarchical EV charging coordination framework based on a tri-level ADMM architecture. This framework integrates dynamic clustering, UAPA, and machine learning–augmented for acceleration in the charging management. The optimization decomposes the problem across clusters, EVAs, and the DSO, which enables distributed

coordination with low communication overhead and full privacy preservation. The proposed UAPA mechanism at the cluster-level eliminates the need for per-EV control and introduces a single aggregate profile per cluster, which significantly reduces computational burden while preserving service quality.

Extensive simulations on IEEE 33- and 118-bus systems with real-world EV data confirm the advantages of the proposed charging approach. Compared to per-EV optimization, the UAPA method reduces computational time up to 91% while having a small deviation in the daily charging pattern. Compared to uncontrolled charging, the framework reduces daily peak power consumption by 44.8% and reduces the electricity costs by 10.2% across EVAs. Moreover, the integration of machine learning and ADMM helps warm start the optimization at the EVA and DSO layers. The result indicates this integration can reduce the number of ADMM iterations needed for convergence by more than 70%. Overall, this framework offers a practical and scalable solution for charging networks with high EV penetration under grid and electricity market constraints.

Future work can focus on two key extensions. First, the proposed framework can be enhanced to account for uncertainty in EV owners' behavior and electricity prices, and solved with robust or stochastic optimization techniques. This would improve coordination reliability in real-world implementation. Second, the ML-ADMM module in this framework is based on a simple neural network, which can be further advanced by using attention-based or sequence-aware learning models to reduce the number of iterations needed for convergence even further.

CHAPTER 7 CONCLUSION

7.1 Summary of Works

This thesis presents hierarchical frameworks for charging management of EVs. Each layer represents a main stakeholder in this structure. At the top level, DSO observes the state of the grid. At the middle level, EVAs manage their EV fleet, considering the electricity price and constraints from both EVs and the grid. Finally, EVs are at the lower level of this structure and act as end users with individual charging needs. First work introduced an MADRL framework to control RT charging management of EVs. In this framework, EVAs act as RL agents and determine the optimal purchasing power based on the signal they receive from DSO and EVs. Also, fairness and grid safety have been considered at the distribution level to ensure the applicability of the framework in the real-world. In the second work, the focus is on clustering charging ports and predicting the behavior of EV owners using TFT in each cluster. Then, a DA-RT framework for charging management of EVs is introduced to minimize the charging cost and procurement in RT while satisfying the EV owners' departure SoC. In the third work, a DA ADMM-based structure is introduced for distributed EV charging, which consists of EV clusters, EVAs, and DSO. At the cluster level, a heuristic UAPA mechanism is presented, which is much faster than per-EV optimization, as it only has one decision variable, which is determined based on the priority of charging of EVs. Moreover, at the EVA and DSO level, a learning-augmented model is established to reduce the iteration counts needed for convergence.

7.2 Limitations

First, the frameworks focus on the electricity distribution system but do not account for broader energy system couplings, such as heating, hydrogen, or V2G with renewable uncertainty. In practice, EV charging will interact with other distributed energy resources and demand-response programs. Extending the frameworks to multi-energy integration and co-optimization remains a promising but challenging direction.

Second, observability and measurement assumptions in these frameworks may not always be accessible. For instance, the RL framework assumes per-agent state observability, and the tri-level ADMM assumes cluster-level and aggregator-level power profiles are measurable and enforceable; DA–RT scheduling assumes accurate forecasting of flexibility and EV departure times. However, shared infrastructure and privacy constraints may cause challenges that

hinder precise state estimation or control execution. In such cases, the coordination mechanism should be able to operate under partial observability, which can introduce delay or non-optimal control strategies.

Third, each framework relies on modular decomposition assumptions, whether treating agents as independently controlled nodes in the first work, clustering EV ports by usage patterns in the second work, or partitioning control hierarchies into clusters, EVAs, and DSO layers in the third work.

These assumptions simplify the problem formulation but they may neglect strong coupling effects between clusters or EVAs, such as shared feeders, overlapping EV user participation, or global constraints that link otherwise independent components. In practice, not considering these interactions could lead to suboptimal decisions or infeasibility under boundary case conditions.

7.3 Future Research

There are four research directions to continue in this line of work:

1. *Integrate electricity market signals and uncertainty into decision-making.* Electricity market entities play a pivotal role in the EV charging architecture. In the ADMM structure, local energy markets can be added to the distributed framework in order to determine the marginal prices and dynamic tariffs. Clusters can submit bids or flexibility offers, taking into account the grid constraints. In the DA-RT framework, uncertainty from demand fluctuation, and price deviation can be better handled through stochastic optimization or scenario-based planning. Considering probabilistic scenarios in the DA planning can improve robustness, and RT corrections would ensure feasibility.

2. *Improve adaptivity through transfer learning and meta-learning.* In both the forecasting and RL-based approaches, current models are trained separately for each region or agent. To reduce training time and improve generalization, transfer learning techniques could be used to tune the hyperparameters of the models across clusters or stations. Likewise, meta-learning could be explored to develop generalized policy or prediction models that quickly adapt to new EV behavior patterns, station layouts, or pricing schemes. Including transfer and meta learning in these frameworks is highly useful when expansion to new regions or stations is needed.

3. *Deploy and evaluate controllers in real-world environments.* The proposed frameworks have demonstrated promising results in simulation; however, real-world implementation

remains an essential next step of this work. Simulation environments simplify many of the practical challenges, such as sensor malfunctions, communication delays, or deviations from expected user behavior. Hence, to improve the practicality of the proposed frameworks, it is important to model these factors in frameworks.

4. *Life-cycle and sustainability-aware optimization.* While the proposed frameworks present short-term objectives such as electricity cost reduction, load balancing, and user satisfaction, further research is needed to integrate life-cycle considerations and long-term sustainability aspects into EV charging coordination. For instance, although the tri-level ADMM framework accounts for battery degradation through a simple penalty term, a more comprehensive model could include dynamic modeling of battery health over extended usage cycles. Likewise, the RL-based RT controller could be extended to learn policies that take into account environmental impact. Some techniques, such as prioritizing low-carbon charging periods and balancing cost with battery longevity, could be examined. By taking these aspects into account, charging strategies can evolve from purely cost-based solutions into tools that actively support long-term sustainability goals. This would help to align electric mobility with the broader vision of a cleaner energy future.

REFERENCES

[1] A. Kwilinski, O. Lyulyov, and T. Pimonenko, "Reducing transport sector co2 emissions patterns: Environmental technologies and renewable energy," *Journal of Open Innovation: Technology, Market, and Complexity*, vol. 10, no. 1, p. 100217, 2024.

[2] S. Wanniarachchi, K. Hewage, C. Wirasinghe, G. Chhipi-Shrestha, H. Karunathilake, and R. Sadiq, "Transforming road freight transportation from fossils to hydrogen: Opportunities and challenges," *International Journal of Sustainable Transportation*, vol. 17, no. 5, pp. 552–572, 2023.

[3] L. Brodnicke, F. Kachirayil, P. Gabrielli, G. Sansavini, and R. McKenna, "Transforming decentralized energy systems: Flexible ev charging and its impact across urbanization degrees," *Applied Energy*, vol. 384, p. 125303, 2025.

[4] C. B. Saner, A. Trivedi, and D. Srinivasan, "A cooperative hierarchical multi-agent system for ev charging scheduling in presence of multiple charging stations," *IEEE Transactions on Smart Grid*, vol. 13, no. 3, pp. 2218–2233, 2022.

[5] S. Mateen, M. Amir, A. Haque, and F. I. Bakhsh, "Ultra-fast charging of electric vehicles: A review of power electronics converter, grid stability and optimal battery consideration in multi-energy systems," *Sustainable Energy, Grids and Networks*, vol. 35, p. 101112, 2023.

[6] Y. Zheng, Y. Wang, and Q. Yang, "Two-phase operation for coordinated charging of electric vehicles in a market environment: From electric vehicle aggregators' perspective," *Renewable and Sustainable Energy Reviews*, vol. 171, p. 113006, 2023.

[7] Y. Zhang, Q. Yang, D. An, D. Li, and Z. Wu, "Multistep multiagent reinforcement learning for optimal energy schedule strategy of charging stations in smart grid," *IEEE Transactions on Cybernetics*, vol. 53, no. 7, pp. 4292–4305, 2022.

[8] W. Wang and L. Wu, "A semi-decentralized real-time charging scheduling scheme for large ev parking lots considering uncertain ev arrival and departure," *IEEE Transactions on Smart Grid*, 2024.

[9] S. S. K. Madahi, H. Nafisi, H. A. Abyaneh, and M. Marzband, "Co-optimization of energy losses and transformer operating costs based on smart charging algorithm for plug-

in electric vehicle parking lots," *IEEE Transactions on Transportation Electrification*, vol. 7, no. 2, pp. 527–541, 2020.

[10] M. Ahrabi, M. Abedi, H. Nafisi, M. A. Mirzaei, B. Mohammadi-Ivatloo, and M. Marzband, "Evaluating the effect of electric vehicle parking lots in transmission-constrained ac unit commitment under a hybrid igdt-stochastic approach," *International Journal of Electrical Power & Energy Systems*, vol. 125, p. 106546, 2021.

[11] M. A. Gharibi, H. Nafisi, H. Askarian-abyaneh, and A. Hajizadeh, "Deep learning framework for day-ahead optimal charging scheduling of electric vehicles in parking lot," *Applied Energy*, vol. 349, p. 121614, 2023.

[12] S. Khan, B. Brandherm, and A. Swamy, "Electric vehicle user behavior prediction using learning-based approaches," in *2020 IEEE Electric Power and Energy Conference (EPEC)*. IEEE, 2020, pp. 1–5.

[13] P. V. Dahiwale, Z. H. Rather, and I. Mitra, "A comprehensive review of smart charging strategies for electric vehicles and way forward," *IEEE Transactions on Intelligent Transportation Systems*, 2024.

[14] A. Shahkamrani, H. Askarian-Abyaneh, H. Nafisi, and M. Marzband, "A framework for day-ahead optimal charging scheduling of electric vehicles providing route mapping: Kowloon case study," *Journal of Cleaner Production*, vol. 307, p. 127297, 2021.

[15] C. Schade, P. Aliasghari, R. Egging-Bratseth, and C. Pfister, "Least cost vehicle charging in a smart neighborhood considering uncertainty and battery degradation," *Batteries*, vol. 11, no. 3, p. 104, 2025.

[16] X. Yang, T. Cui, H. Wang, and Y. Ye, "Multiagent deep reinforcement learning for electric vehicle fast charging station pricing game in electricity-transportation nexus," *IEEE Transactions on Industrial Informatics*, vol. 20, no. 4, pp. 6345–6355, 2024.

[17] Q. Kang, J. Wang, M. Zhou, and A. C. Ammari, "Centralized charging strategy and scheduling algorithm for electric vehicles under a battery swapping scenario," *IEEE Transactions on Intelligent Transportation Systems*, vol. 17, no. 3, pp. 659–669, 2015.

[18] N. I. Nimalsiri, C. P. Mediwaththe, E. L. Ratnam, M. Shaw, D. B. Smith, and S. K. Halgamuge, "A survey of algorithms for distributed charging control of electric vehicles in smart grid," *IEEE Transactions on Intelligent Transportation Systems*, vol. 21, no. 11, pp. 4497–4515, 2019.

[19] B. Wang, D. Zhao, P. Dehghanian, Y. Tian, and T. Hong, "Aggregated electric vehicle load modeling in large-scale electric power systems," *IEEE Transactions on Industry Applications*, vol. 56, no. 5, pp. 5796–5810, 2020.

[20] A. Jain and S. Bhullar, "Operating modes of grid integrated pv-solar based electric vehicle charging system-a comprehensive review," *e-Prime-Advances in Electrical Engineering, Electronics and Energy*, vol. 8, p. 100519, 2024.

[21] P. A. Gunkel, C. Bergaentzlé, I. G. Jensen, and F. Scheller, "From passive to active: Flexibility from electric vehicles in the context of transmission system development," *Applied Energy*, vol. 277, p. 115526, 2020.

[22] I. Diahovchenko, A. Chuprun, and Z. Čonka, "Assessment and mitigation of the influence of rising charging demand of electric vehicles on the aging of distribution transformers," *Electric power systems research*, vol. 221, p. 109455, 2023.

[23] H. Wang, F. Guo, and A. Sivakumar, "Analysing the impact of electric vehicle charging on households: An interrelated load profile generation approach," *Energy and Buildings*, vol. 335, p. 115558, 2025.

[24] A. A. El-Fergany, "Reviews on load flow methods in electric distribution networks," *Archives of Computational Methods in Engineering*, pp. 1–15, 2024.

[25] A. F. Soofi, R. Bayani, and S. D. Manshadi, "Analyzing power quality implications of high level charging rates of electric vehicle within distribution networks," in *2021 IEEE Transportation Electrification Conference & Expo (ITEC)*. IEEE, 2021, pp. 684–689.

[26] T.-Z. Ang, M. Salem, M. Kamarol, H. S. Das, M. A. Nazari, and N. Prabaharan, "A comprehensive study of renewable energy sources: Classifications, challenges and suggestions," *Energy strategy reviews*, vol. 43, p. 100939, 2022.

[27] N. Kumar, V. Saxena, B. Singh, and B. K. Panigrahi, "Power quality improved grid-interfaced pv-assisted onboard ev charging infrastructure for smart households consumers," *IEEE Transactions on Consumer Electronics*, vol. 69, no. 4, pp. 1091–1100, 2023.

[28] A. Dutta, S. Ganguly, and C. Kumar, "Coordinated control scheme for ev charging and volt/var devices scheduling to regulate voltages of active distribution networks," *Sustainable Energy, Grids and Networks*, vol. 31, p. 100761, 2022.

[29] K. Prakash, M. Ali, M. Siddique, A. Karmaker, C. Macana, D. Dong, and H. Pota, "Bi-level planning and scheduling of electric vehicle charging stations for peak shaving and congestion management in low voltage distribution networks," *Computers and Electrical Engineering*, vol. 102, p. 108235, 2022.

[30] T. Xie, Y. Su, G. Zhang, K. Zhang, H. Li, and R. Wang, "Optimizing peak-shaving cooperation among electric vehicle charging stations: A two-tier optimal dispatch strategy considering load demand response potential," *International Journal of Electrical Power & Energy Systems*, vol. 162, p. 110228, 2024.

[31] J. Li, G. Wang, X. Wang, and Y. Du, "Smart charging strategy for electric vehicles based on marginal carbon emission factors and time-of-use price," *Sustainable Cities and Society*, vol. 96, p. 104708, 2023.

[32] S.-W. Park, K.-S. Cho, G. Hoefter, and S.-Y. Son, "Electric vehicle charging management using location-based incentives for reducing renewable energy curtailment considering the distribution system," *Applied Energy*, vol. 305, p. 117680, 2022.

[33] T. Yuvaraj, K. Devabalaji *et al.*, "Minimizing the electric vehicle charging stations impact in the distribution networks by simultaneous allocation of dg and dstatcom with considering uncertainty in load," *Energy Reports*, vol. 10, pp. 1796–1817, 2023.

[34] A. L. S. de Sa, P. S. Lavieri, Y.-T. Cheng, E. Hajhashemi, and G. J. Oliveira, "Modelling driver's response to demand management strategies for electric vehicle charging in australia," *Energy Research & Social Science*, vol. 103, p. 103218, 2023.

[35] Y. Song, L. Shangguan, and G. Li, "Simulation analysis of flexible concession period contracts in electric vehicle charging infrastructure public-private-partnership (evci-ppp) projects based on time-of-use (tou) charging price strategy," *Energy*, vol. 228, p. 120328, 2021.

[36] J.-S. Park, S. Hussain, J.-O. Lee, B. H. Kim, and Y.-S. Kim, "Time-of-use (tou) electricity rate for vehicle-to-grid (v2g) to minimize a charging station capacity," *International Journal of Electrical Power & Energy Systems*, vol. 161, p. 110209, 2024.

[37] Z. Zhao and C. K. Lee, "Dynamic pricing for ev charging stations: A deep reinforcement learning approach," *IEEE Transactions on Transportation Electrification*, vol. 8, no. 2, pp. 2456–2468, 2021.

[38] T. M. Aljohani, A. F. Ebrahim, and O. A. Mohammed, "Dynamic real-time pricing mechanism for electric vehicles charging considering optimal microgrids energy management system," *IEEE Transactions on Industry Applications*, vol. 57, no. 5, pp. 5372–5381, 2021.

[39] J. Hu, C. Ye, Y. Ding, J. Tang, and S. Liu, "A distributed mpc to exploit reactive power v2g for real-time voltage regulation in distribution networks," *IEEE Transactions on Smart Grid*, vol. 13, no. 1, pp. 576–588, 2021.

[40] Y. Zheng, Z. Shao, and L. Jian, "The peak load shaving assessment of developing a user-oriented vehicle-to-grid scheme with multiple operation modes: The case study of shenzhen, china," *Sustainable Cities and Society*, vol. 67, p. 102744, 2021.

[41] X. Li, Y. Tan, X. Liu, Q. Liao, B. Sun, G. Cao, C. Li, X. Yang, and Z. Wang, "A cost-benefit analysis of v2g electric vehicles supporting peak shaving in shanghai," *Electric Power Systems Research*, vol. 179, p. 106058, 2020.

[42] A. Tchagang and Y. Yoo, "V2b/v2g on energy cost and battery degradation under different driving scenarios, peak shaving, and frequency regulations," *World Electric Vehicle Journal*, vol. 11, no. 1, p. 14, 2020.

[43] ElaadNL, "Ev charging sessions dataset - the netherlands," Accessed July 2025, 2020, https://www.elaad.nl/research/.

[44] Z. J. Lee, T. Li, and S. H. Low, "ACN-Data: Analysis and applications of an open ev charging dataset," in *Proceedings of the Tenth International Conference on Future Energy Systems (e-Energy '19)*, 2019, pp. 139–149.

[45] V.-H. Bui, A. Hussain, S. Zarrabian, P. M. Kump, and W. Su, "Clustering-based optimal operation of charging stations under high penetration of electric vehicles," *Sustainable Energy, Grids and Networks*, vol. 36, p. 101178, 2023.

[46] L. Xu, X. Gu, and Z. Song, "Optimal charging for large-scale heterogeneous electric vehicles: A novel paradigm based on learning and backward clustering," *Applied Energy*, vol. 382, p. 125232, 2025.

[47] H. Jahangir, S. S. Gougheri, B. Vatandoust, M. A. Golkar, A. Ahmadian, and A. Hajizadeh, "Plug-in electric vehicle behavior modeling in energy market: A novel deep learning-based approach with clustering technique," *IEEE Transactions on Smart Grid*, vol. 11, no. 6, pp. 4738–4748, 2020.

[48] T. Xie, X. Yun, G. Zhang, H. Li, K. Zhang, and R. Wang, "Charging station cluster load prediction: Spatiotemporal multi-graph fusion technology," *Renewable and Sustainable Energy Reviews*, vol. 206, p. 114855, 2024.

[49] M. Jasiński, E. Jasińska, Z. Leonowicz, M. Jasiński, M. Gono, L. Martirano, M. Y. Shih, and R. Gono, "K-mean algorithm to support energy future decision for household with pv and ev," in *2024 IEEE International Conference on Environment and Electrical Engineering and 2024 IEEE Industrial and Commercial Power Systems Europe (EEEIC/I&CPS Europe)*. IEEE, 2024, pp. 1–4.

[50] Y. Mudgal, R. Tiwari, N. Krishnan, and A. A. Téllez, "Advanced cluster-based load forecasting and peak demand management for electric vehicle charging networks," *IEEE Access*, 2025.

[51] D. M. Saputra, D. Saputra, and L. D. Oswari, "Effect of distance metrics in determining k-value in k-means clustering using elbow and silhouette method," in *Sriwijaya international conference on information technology and its applications (SICONIAN 2019)*. Atlantis Press, 2020, pp. 341–346.

[52] M. F. Elahe, M. A. Kabir, S. H. Mahmud, and R. Azim, "Factors impacting short-term load forecasting of charging station to electric vehicle," *Electronics*, vol. 12, no. 1, p. 55, 2022.

[53] C. Wu, H. Han, and S. Gao, "Feedback-driven real-time forecasting method for the arrival times of electric vehicles," *Electric Power Systems Research*, vol. 228, p. 110077, 2024.

[54] M. Boulakhbar, M. Farag, K. Benabdelaziz, M. Zazi, M. Maaroufi, and T. Kousksou, "Electric vehicles arrival and departure time prediction based on deep learning: the case of morocco," in *2022 2nd International Conference on Innovative Research in Applied Science, Engineering and Technology (IRASET)*. IEEE, 2022, pp. 1–8.

[55] S. Wang, C. Zhuge, C. Shao, P. Wang, X. Yang, and S. Wang, "Short-term electric vehicle charging demand prediction: A deep learning approach," *Applied Energy*, vol. 340, p. 121032, 2023.

[56] A. Orzechowski, L. Lugosch, H. Shu, R. Yang, W. Li, and B. H. Meyer, "A data-driven framework for medium-term electric vehicle charging demand forecasting," *Energy and AI*, vol. 14, p. 100267, 2023.

[57] P. K. Bhat, Z. Wu, and B. Chen, "Long trip charging planning of battery electric vehicle considering vehicle waiting time forecast at fast charging stations: A mixed-integer dynamic programming approach," *IEEE Access*, 2025.

[58] D. Kim, H. G. Shim, and J. S. Eo, "A machine learning method for ev range prediction with updates on route information and traffic conditions," in *Proceedings of the AAAI Conference on Artificial Intelligence*, vol. 36, no. 11, 2022, pp. 12 545–12 551.

[59] Y. Chen, Z. Tang, Y. Cui, W. Rao, and Y. Li, "Electric vehicle charging demand prediction model based on spatiotemporal attention mechanism," *Energies*, vol. 18, no. 3, p. 687, 2025.

[60] S. Makaremi, "A multi-output deep learning model for energy demand and port availability forecasting in ev charging infrastructure," *Energy*, vol. 317, p. 134582, 2025.

[61] H. Guo, L. Chen, Z. Wang, and L. Li, "Day-ahead prediction of electric vehicle charging demand based on quadratic decomposition and dual attention mechanisms," *Applied Energy*, vol. 381, p. 125198, 2025.

[62] R. Luo, Y. Zhang, Y. Zhou, H. Chen, L. Yang, J. Yang, and R. Su, "Deep learning approach for long-term prediction of electric vehicle (ev) charging station availability," in *2021 IEEE International Intelligent Transportation Systems Conference (ITSC)*. IEEE, 2021, pp. 3334–3339.

[63] M. Baza, M. Pazos-Revilla, A. Sherif, M. Nabil, A. J. Aljohani, M. Mahmoud, and W. Alasmary, "Privacy-preserving and collusion-resistant charging coordination schemes for smart grids," *IEEE Transactions on Dependable and Secure Computing*, vol. 19, no. 4, pp. 2226–2243, 2021.

[64] J. C. Mukherjee and A. Gupta, "A review of charge scheduling of electric vehicles in smart grid," *IEEE Systems Journal*, vol. 9, no. 4, pp. 1541–1553, 2014.

[65] T. Rahman, Y. Xu, and Z. Qu, "Continuous-domain real-time distributed admm algorithm for aggregator scheduling and voltage stability in distribution network," *IEEE Transactions on Automation Science and Engineering*, vol. 19, no. 1, pp. 60–69, 2021.

[66] R. Zdunek, A. Grobelny, J. Witkowski, and R. I. Gnot, "On–off scheduling for electric vehicle charging in two-links charging stations using binary optimization approaches," *Sensors*, vol. 21, no. 21, p. 7149, 2021.

[67] C. Li, L. Zhang, Z. Ou, Q. Wang, D. Zhou, and J. Ma, "Robust model of electric vehicle charging station location considering renewable energy and storage equipment," *Energy*, vol. 238, p. 121713, 2022.

[68] J. Wüst, M. J. Booysen, and J. Bekker, "Comparison of optimisation techniques for the electric vehicle scheduling problem," *Smart Cities*, vol. 8, no. 3, p. 85, 2025.

[69] B. Ahmadi and E. Shirazi, "A heuristic-driven charging strategy of electric vehicle for grids with high ev penetration," *Energies*, vol. 16, no. 19, p. 6959, 2023.

[70] V. Lazari and A. Chassiakos, "Multi-objective optimization of electric vehicle charging station deployment using genetic algorithms," *Applied Sciences*, vol. 13, no. 8, p. 4867, 2023.

[71] W. Du, J. Ma, and W. Yin, "Orderly charging strategy of electric vehicle based on improved pso algorithm," *Energy*, vol. 271, p. 127088, 2023.

[72] S. Kiani, K. Sheshyekani, and H. Dagdougui, "Admm-based hierarchical single-loop framework for ev charging scheduling considering power flow constraints," *IEEE Transactions on Transportation Electrification*, vol. 10, no. 1, pp. 1089–1100, 2023.

[73] J. Shanmuganathan, A. A. Victoire, G. Balraj, and A. Victoire, "Deep learning lstm recurrent neural network model for prediction of electric vehicle charging demand," *Sustainability*, vol. 14, no. 16, p. 10207, 2022.

[74] N. Klungsida, P. Maneechot, N. Butploy, and K. Khiewwan, "Forecasting energy consumption from ev station charging using rnn, lstm and gru neural network," *Journal of Renewable Energy and Smart Grid Technology*, vol. 19, no. 1, pp. 1–6, 2024.

[75] B. Aljafari, P. R. Jeyaraj, A. C. Kathiresan, and S. B. Thanikanti, "Electric vehicle optimum charging-discharging scheduling with dynamic pricing employing multi agent deep neural network," *Computers and Electrical Engineering*, vol. 105, p. 108555, 2023.

[76] Q. Xing, Y. Xu, Z. Chen, Z. Zhang, and Z. Shi, "A graph reinforcement learning-based decision-making platform for real-time charging navigation of urban electric vehicles," *IEEE Transactions on Industrial Informatics*, vol. 19, no. 3, pp. 3284–3295, 2022.

[77] Z. Zhang, Y. Wan, J. Qin, W. Fu, and Y. Kang, "A deep rl-based algorithm for coordinated charging of electric vehicles," *IEEE Transactions on Intelligent Transportation Systems*, vol. 23, no. 10, pp. 18 774–18 784, 2022.

[78] V.-H. Bui and W. Su, "Real-time operation of distribution network: A deep reinforcement learning-based reconfiguration approach," *Sustainable energy technologies and assessments*, vol. 50, p. 101841, 2022.

[79] F. L. Da Silva, C. E. Nishida, D. M. Roijers, and A. H. R. Costa, "Coordination of electric vehicle charging through multiagent reinforcement learning," *IEEE Transactions on Smart Grid*, vol. 11, no. 3, pp. 2347–2356, 2019.

[80] H. Li, Z. Wan, and H. He, "Constrained ev charging scheduling based on safe deep reinforcement learning," *IEEE Transactions on Smart Grid*, vol. 11, no. 3, pp. 2427–2439, 2019.

[81] K. Wang, H. Wang, Z. Yang, J. Feng, Y. Li, J. Yang, and Z. Chen, "A transfer learning method for electric vehicles charging strategy based on deep reinforcement learning," *Applied Energy*, vol. 343, p. 121186, 2023.

[82] S. Orfanoudakis, V. Robu, E. M. Salazar, P. Palensky, and P. P. Vergara, "Scalable reinforcement learning for large-scale coordination of electric vehicles using graph neural networks," *Communications Engineering*, vol. 4, no. 1, p. 118, 2025.

[83] S. Gu, K. Qian, and Y. Yang, "Optimization of electric vehicle charging and discharging strategies considering battery health state: A safe reinforcement learning approach," *World Electric Vehicle Journal*, vol. 16, no. 5, p. 286, 2025.

[84] A. S. Kamrani, A. Dini, H. Dagdougui, and K. Sheshyekani, "Multi-agent deep reinforcement learning with online and fair optimal dispatch of ev aggregators," *Machine Learning with Applications*, vol. 19, p. 100620, 2025.

[85] J. Bai, T. Ding, W. Jia, S. Zhu, L. Bai, and F. Li, "Online rectangle packing algorithm for swapped battery charging dispatch model considering continuous charging power," *IEEE Transactions on Automation Science and Engineering*, vol. 21, no. 1, pp. 320–331, (2024).

[86] Z. Bao, Z. Hu, and A. Mujeeb, "A novel electric vehicle aggregator bidding method in electricity markets considering the coupling of cross-day charging flexibility," *IEEE Transactions on Transportation Electrification*, pp. 1–1, (2024).

[87] S. S. K. Madahi, A. S. Kamrani, and H. Nafisi, "Overarching sustainable energy management of PV integrated EV parking lots in reconfigurable microgrids using generative adversarial networks," *IEEE Transactions on Intelligent Transportation Systems*, vol. 23, no. 10, pp. 19 258–19 271, (2022).

[88] C. Qi, C.-C. Liu, X. Lu, L. Yu, and M. W. Degner, "Transactive energy for EV owners and aggregators: Mechanism and algorithms," *IEEE Transactions on Sustainable Energy*, vol. 14, no. 3, pp. 1849–1865, (2023).

[89] R. Jin, Y. Zhou, C. Lu, and J. Song, "Deep reinforcement learning-based strategy for charging station participating in demand response," *Applied Energy*, vol. 328, p. 120140, (2022).

[90] S. Kiani, K. Sheshyekani, and H. Dagdougui, "An extended state space model for aggregation of large-scale evs considering fast charging," *IEEE Transactions on Transportation Electrification*, pp. 1–1, 2022.

[91] Y. Zhang, X. Rao, C. Liu, X. Zhang, and Y. Zhou, "A cooperative EV charging scheduling strategy based on double deep q-network and prioritized experience replay," *Engineering Applications of Artificial Intelligence*, vol. 118, p. 105642, (2023).

[92] T. Ding, Z. Zeng, J. Bai, B. Qin, Y. Yang, and M. Shahidehpour, "Optimal electric vehicle charging strategy with markov decision process and reinforcement learning technique," *IEEE Transactions on Industry Applications*, vol. 56, no. 5, pp. 5811–5823, (2020).

[93] E. O. Arwa and K. A. Folly, "Reinforcement learning techniques for optimal power control in grid-connected microgrids: A comprehensive review," *IEEE Access*, vol. 8, pp. 208 992–209 007, (2020).

[94] H. M. Abdullah, A. Gastli, and L. Ben-Brahim, "Reinforcement learning based EV charging management systems–a review," *IEEE Access*, vol. 9, pp. 41 506–41 531, (2021).

[95] Y. Cao, H. Wang, D. Li, and G. Zhang, "Smart online charging algorithm for electric vehicles via customized actor–critic learning," *IEEE Internet of Things Journal*, vol. 9, no. 1, pp. 684–694, (2022).

[96] Y. Zhang, Q. Yang, D. An, D. Li, and Z. Wu, "Multistep multiagent reinforcement learning for optimal energy schedule strategy of charging stations in smart grid," *IEEE Transactions on Cybernetics*, vol. 53, no. 7, pp. 4292–4305, (2023).

[97] C. Zhang, Y. Liu, F. Wu, B. Tang, and W. Fan, "Effective charging planning based on deep reinforcement learning for electric vehicles," *IEEE Transactions on Intelligent Transportation Systems*, vol. 22, no. 1, pp. 542–554, 2021.

[98] Q. Wang, Z. Chen, Y. Zhou, Z. Liu, and Z. Peng, "Real-time monitoring and optimization of machine learning intelligent control system in power data modeling technology," *Machine Learning with Applications*, vol. 18, p. 100584, (2024).

[99] A. B. Sediq, R. H. Gohary, R. Schoenen, and H. Yanikomeroglu, "Optimal tradeoff between sum-rate efficiency and jain's fairness index in resource allocation," *IEEE Transactions on Wireless Communications*, vol. 12, no. 7, pp. 3496–3509, (2013).

[100] M. Hupez, J.-F. Toubeau, Z. De Grève, and F. Vallée, "A new cooperative framework for a fair and cost-optimal allocation of resources within a low voltage electricity community," *IEEE Transactions on Smart Grid*, vol. 12, no. 3, pp. 2201–2211, (2021).

[101] A. Hussain and P. Musilek, "Fairness and utilitarianism in allocating energy to evs during power contingencies using modified division rules," *IEEE Transactions on Sustainable Energy*, vol. 13, no. 3, pp. 1444–1456, (2022).

[102] S. Poudel, M. Mukherjee, R. Sadnan, and A. P. Reiman, "Fairness-aware distributed energy coordination for voltage regulation in power distribution systems," *IEEE Transactions on Sustainable Energy*, vol. 14, no. 3, pp. 1866–1880, (2023).

[103] D. Wu, N. Radhakrishnan, and S. Huang, "A hierarchical charging control of plug-in electric vehicles with simple flexibility model," *Applied Energy*, vol. 253, p. 113490, (2019).

[104] C. B. Saner, A. Trivedi, and D. Srinivasan, "A cooperative hierarchical multi-agent system for EV charging scheduling in presence of multiple charging stations," *IEEE Transactions on Smart Grid*, vol. 13, no. 3, pp. 2218–2233, (2022).

[105] S. Kiani, K. Sheshyekani, and H. Dagdougui, "Admm-based hierarchical single-loop framework for ev charging scheduling considering power flow constraints," *IEEE Transactions on Transportation Electrification*, pp. 1–1, 2023.

[106] M. H. Amini, P. McNamara, P. Weng, O. Karabasoglu, and Y. Xu, "Hierarchical electric vehicle charging aggregator strategy using dantzig-wolfe decomposition," *IEEE Design & Test*, vol. 35, no. 6, pp. 25–36, (2018).

[107] Y. Zheng, Y. Song, D. J. Hill, and K. Meng, "Online distributed MPC-based optimal scheduling for ev charging stations in distribution systems," *IEEE Transactions on Industrial Informatics*, vol. 15, no. 2, pp. 638–649, (2019).

[108] D. Paudel and T. K. Das, "A deep reinforcement learning approach for power management of battery-assisted fast-charging EV hubs participating in day-ahead and real-time electricity markets," *Energy*, vol. 283, p. 129097, (2023).

[109] C. Yuan, M. A. A. Forhad, R. Bansal, A. Sidorova, and M. V. Albert, "Multi-agent dual level reinforcement learning of strategy and tactics in competitive games," *Results in Control and Optimization*, vol. 16, p. 100471, (2024).

[110] R. K. Jain, D.-M. W. Chiu, W. R. Hawe *et al.*, "A quantitative measure of fairness and discrimination," *Eastern Research Laboratory, Digital Equipment Corporation, Hudson, MA*, vol. 21, (1984).

[111] S. Boyd and L. Vandenberghe, *Convex optimization*. Cambridge university press, (2004).

[112] T. M. Aljohani, A. Ebrahim, and O. Mohammed, "Real-time metadata-driven routing optimization for electric vehicle energy consumption minimization using deep reinforcement learning and markov chain model," *Electric Power Systems Research*, vol. 192, p. 106962, (2021).

[113] M. Dorokhova, Y. Martinson, C. Ballif, and N. Wyrsch, "Deep reinforcement learning control of electric vehicle charging in the presence of photovoltaic generation," *Applied Energy*, vol. 301, p. 117504, (2021).

[114] T. T. Nguyen, N. D. Nguyen, and S. Nahavandi, "Deep reinforcement learning for multiagent systems: A review of challenges, solutions, and applications," *IEEE Transactions on Cybernetics*, vol. 50, no. 9, pp. 3826–3839, (2020).

[115] B. Wang, Y. Tang, Y. Huang, and T. Wang, "Power system emergency control strategy based on severely disturbed units identification and STGCN-DDQN," *Electric Power Systems Research*, vol. 226, p. 109903, (2024).

[116] A. Sharma and V. Thangaraj, "Intelligent service placement algorithm based on DDQN and prioritized experience replay in IoT-Fog computing environment," *Internet of Things*, vol. 25, p. 101112, (2024).

[117] X. Yan, Y. Xu, X. Xing, B. Cui, Z. Guo, and T. Guo, "Trustworthy network anomaly detection based on an adaptive learning rate and momentum in iiot," *IEEE Transactions on Industrial Informatics*, vol. 16, no. 9, pp. 6182–6192, (2020).

[118] H. Iiduka, "Appropriate learning rates of adaptive learning rate optimization algorithms for training deep neural networks," *IEEE Transactions on Cybernetics*, vol. 52, no. 12, pp. 13 250–13 261, (2022).

[119] D. Zhang, Z. Fu, and L. Zhang, "An improved ts algorithm for loss-minimum reconfiguration in large-scale distribution systems," *Electric Power Systems Research*, vol. 77, no. 5, pp. 685–694, (2007).

[120] OpenEI, "Commercial and residential hourly load profiles for all tmy3 locations in the united states," https://openei.org/doe-opendata/dataset/commercial-and-residential-hourly-load-profiles-for-all-tmy3-locations-in-the-united-states, October (2014).

[121] F. Braeuer, "Load profile data of 50 industrial plants in Germany for one year," Jun. (2020).

[122] R. D. Zimmerman, C. E. Murillo-Sánchez, and R. J. Thomas, "Matpower: Steady-state operations, planning, and analysis tools for power systems research and education," *IEEE Transactions on Power Systems*, vol. 26, no. 1, pp. 12–19, (2011).

[123] H. Van Hasselt, A. Guez, and D. Silver, "Deep reinforcement learning with double q-learning," in *Proceedings of the AAAI conference on artificial intelligence*, vol. 30, no. 1, (2016).

[124] R. Lowe, Y. I. Wu, A. Tamar, J. Harb, O. Pieter Abbeel, and I. Mordatch, "Multi-agent actor-critic for mixed cooperative-competitive environments," *Advances in neural information processing systems*, vol. 30, (2017).

[125] J. Schulman, F. Wolski, P. Dhariwal, A. Radford, and O. Klimov, "Proximal policy optimization algorithms," *arXiv preprint arXiv:1707.06347*, (2017).

[126] J. E. G. Bustos, C. Baeza, B. B. Schiele, V. Rivera, B. Masserano, M. E. Orchard, C. Burgos-Mellado, and A. Perez, "A novel data-driven framework for driving range prognostics in electric vehicles," *Engineering Applications of Artificial Intelligence*, vol. 142, p. 109925, 2025.

[127] R. Azarafshar and W. N. Vermeulen, "Electric vehicle incentive policies in canadian provinces," *Energy Economics*, vol. 91, p. 104902, 2020.

[128] EnergyRates.ca, "An overview of public ev charging in canada," 2024, accessed: 2024-12-03.

[129] M. A. Gharibi, H. Nafisi, H. Askarian-abyaneh, and A. Hajizadeh, "Deep learning framework for day-ahead optimal charging scheduling of electric vehicles in parking lot," *Applied Energy*, vol. 349, p. 121614, 2023.

[130] E. Yaghoubi, E. Yaghoubi, A. Khamees, D. Razmi, and T. Lu, "A systematic review and meta-analysis of machine learning, deep learning, and ensemble learning approaches in predicting ev charging behavior," *Engineering Applications of Artificial Intelligence*, vol. 135, p. 108789, 2024.

[131] X. Wu, L. Yao, Y. Yu, X. Jiang, R. Wu, and G. Gong, "Heterogeneous aggregation and control modeling for electric vehicles with random charging behaviors," *IEEE Transactions on Sustainable Energy*, vol. 14, no. 1, pp. 525–536, 2023.

[132] H. Zhao, X. Yan, and H. Ren, "Quantifying flexibility of residential electric vehicle charging loads using non-intrusive load extracting algorithm in demand response," *Sustainable Cities and Society*, vol. 50, p. 101664, 2019.

[133] A. Corsetti, R. Castro, C. Geyken, and A. Mohan, "Commercial ev fleet smart charging for cost reduction and renewables integration: a case study in germany," *Journal of Energy Storage*, vol. 100, p. 113765, 2024.

[134] V.-H. Bui, A. Hussain, S. Zarrabian, P. M. Kump, and W. Su, "Clustering-based optimal operation of charging stations under high penetration of electric vehicles," *Sustainable Energy, Grids and Networks*, vol. 36, p. 101178, 2023.

[135] A. Nespoli, E. Ogliari, and S. Leva, "User behavior clustering based method for ev charging forecast," *IEEE Access*, vol. 11, pp. 6273–6283, 2023.

[136] A. S. Khwaja, B. Venkatesh, and A. Anpalagan, "Performance analysis of lstms for daily individual ev charging behavior prediction," *IEEE Access*, vol. 9, pp. 154 804–154 814, 2021.

[137] A. Ahmadian, V. Ghodrati, and R. Gadh, "Artificial deep neural network enables one-size-fits-all electric vehicle user behavior prediction framework," *Applied Energy*, vol. 352, p. 121884, 2023.

[138] J. Liu, G. Lin, C. Rehtanz, S. Huang, Y. Zhou, and Y. Li, "Data-driven intelligent ev charging operating with limited chargers considering the charging demand forecasting," *International Journal of Electrical Power & Energy Systems*, vol. 141, p. 108218, 2022.

[139] Q. Wang, C. Huang, C. Wang, K. Li, and N. Xie, "Joint optimization of bidding and pricing strategy for electric vehicle aggregator considering multi-agent interactions," *Applied Energy*, vol. 360, p. 122810, 2024.

[140] H. Jahangir, S. S. Gougheri, B. Vatandoust, M. A. Golkar, A. Ahmadian, and A. Hajizadeh, "Plug-in electric vehicle behavior modeling in energy market: A novel deep learning-based approach with clustering technique," *IEEE Transactions on Smart Grid*, vol. 11, no. 6, pp. 4738–4748, 2020.

[141] A.-M. Koufakis, E. S. Rigas, N. Bassiliades, and S. D. Ramchurn, "Offline and online electric vehicle charging scheduling with v2v energy transfer," *IEEE Transactions on Intelligent Transportation Systems*, vol. 21, no. 5, pp. 2128–2138, 2020.

[142] D. Choudhary, R. N. Mahanty, and N. Kumar, "Demand management of plug-in electric vehicle charging station considering bidirectional power flow using deep reinforcement learning," *Engineering Applications of Artificial Intelligence*, vol. 139, p. 109585, 2025.

[143] M. Majidpour, C. Qiu, P. Chu, H. R. Pota, and R. Gadh, "Forecasting the ev charging load based on customer profile or station measurement?" *Applied energy*, vol. 163, pp. 134–141, 2016.

[144] B. Vatandoust, A. Ahmadian, M. A. Golkar, A. Elkamel, A. Almansoori, and M. Ghaljehei, "Risk-averse optimal bidding of electric vehicles and energy storage aggregator in day-ahead frequency regulation market," *IEEE Transactions on Power Systems*, vol. 34, no. 3, pp. 2036–2047, 2019.

[145] J. MacQueen *et al.*, "Some methods for classification and analysis of multivariate observations," in *Proceedings of the fifth Berkeley symposium on mathematical statistics and probability*, vol. 1, no. 14. Oakland, CA, USA, 1967, pp. 281–297.

[146] V. Kaverinskiy, I. Chaikovsky, A. Mnevets, T. Ryzhenko, M. Bocharov, and K. Malakhov, "Scalable clustering of complex ecg health data: Big data clustering analysis with umap and hdbscan," *Computation*, vol. 13, no. 6, p. 144, 2025.

[147] Z. Ahmed, B. Issac, and S. Das, "Ok-nb: An enhanced optics and k-naive bayes classifier for imbalance classification with overlapping," *IEEE Access*, vol. 12, pp. 57 458–57 477, 2024.

[148] E. Schubert, J. Sander, M. Ester, H. P. Kriegel, and X. Xu, "Dbscan revisited, revisited: why and how you should (still) use dbscan," *ACM Transactions on Database Systems (TODS)*, vol. 42, no. 3, pp. 1–21, 2017.

[149] A. Nazir, A. K. Shaikh, A. S. Shah, and A. Khalil, "Forecasting energy consumption demand of customers in smart grid using temporal fusion transformer (tft)," *Results in Engineering*, vol. 17, p. 100888, 2023.

[150] B. Lim, S. Arık, N. Loeff, and T. Pfister, "Temporal fusion transformers for interpretable multi-horizon time series forecasting," *International Journal of Forecasting*, vol. 37, no. 4, pp. 1748–1764, 2021.

[151] D. Li, Y. Tan, Y. Zhang, S. Miao, and S. He, "Probabilistic forecasting method for mid-term hourly load time series based on an improved temporal fusion transformer model," *International Journal of Electrical Power & Energy Systems*, vol. 146, p. 108743, 2023.

[152] A. Vaswani, "Attention is all you need," *Advances in Neural Information Processing Systems*, 2017.

[153] P. J. Rousseeuw, "Silhouettes: A graphical aid to the interpretation and validation of cluster analysis," *Journal of Computational and Applied Mathematics*, vol. 20, pp. 53–65, 1987.

[154] A. Shahkamrani, H. Askarian-abyaneh, H. Nafisi, and M. Marzband, "A framework for day-ahead optimal charging scheduling of electric vehicles providing route mapping: Kowloon case study," *Journal of Cleaner Production*, vol. 307, p. 127297, 2021.

[155] J. Jaworski, N. Zheng, M. Preindl, and B. Xu, "Vehicle-to-grid fleet service provision considering nonlinear battery behaviors," *IEEE Transactions on Transportation Electrification*, vol. 10, no. 2, pp. 2945–2955, 2024.

[156] A. Maneesha and K. S. Swarup, "A survey on applications of alternating direction method of multipliers in smart power grids," *Renewable and Sustainable Energy Reviews*, vol. 152, p. 111687, 2021.

[157] S. Huang, Q. Wu, Y. Guo, X. Chen, B. Zhou, and C. Li, "Distributed voltage control based on admm for large-scale wind farm cluster connected to vsc-hvdc," *IEEE Transactions on Sustainable Energy*, vol. 11, no. 2, pp. 584–594, 2019.

[158] S.-W. Lin and C.-C. Chu, "Optimal distributed admm-based control for frequency synchronization in isolated ac microgrids," *IEEE Transactions on Industry Applications*, vol. 59, no. 2, pp. 2458–2472, 2022.

[159] F. Shen, S. Lin, J. Wei, S. Huang, Q. Wu, Y. Shen, L. Zhu, P. Wang, and B. Wang, "Distributed dynamic tariff for congestion management in distribution networks considering temporal–spatial coordination of electric vehicles," *IEEE Transactions on Transportation Electrification*, vol. 10, no. 3, pp. 7358–7373, 2024.

[160] T. W. Mak, M. Chatzos, M. Tanneau, and P. Van Hentenryck, "Learning regionally decentralized ac optimal power flows with admm," *IEEE Transactions on Smart Grid*, vol. 14, no. 6, pp. 4863–4876, 2023.

[161] X. Chen, Q. Yang, H. Wang, Y. Zeng, and B. Deng, "Adaptive admm-based high-quality fast imaging algorithm for short-range mmw mimo-sar systems," *IEEE Transactions on Antennas and Propagation*, vol. 71, no. 11, pp. 8925–8935, 2023.

[162] Z. Guo, P. Pinson, Q. Wu, S. Chen, Q. Yang, and Z. Yang, "An asynchronous online negotiation mechanism for real-time peer-to-peer electricity markets," *IEEE transactions on power systems*, vol. 37, no. 3, pp. 1868–1880, 2021.

[163] W. Tang, W. Zhao, T. Qian, B. Zhao, Z. Lin, and Y. Xin, "Learning-accelerated asynchronous decentralized optimization for integrated transmission and distribution systems over lossy networks," *Sustainable Energy, Grids and Networks*, vol. 31, p. 100724, 2022.

[164] Y. Hu, M. Zhang, K. Wang, and D. Wang, "Optimization of orderly charging strategy of electric vehicle based on improved alternating direction method of multipliers," *Journal of Energy Storage*, vol. 55, p. 105483, 2022.

[165] L. Cai, G. Guo, and D. Wu, "A cooperative multi-agent charging scheduling by regrouping evs with differentiated deadlines," *IEEE Transactions on Intelligent Transportation Systems*, 2025.

[166] H. Yao, Y. Xiang, C. Gu, and J. Liu, "Optimal planning of distribution systems and charging stations considering pv-grid-ev transactions," *IEEE transactions on smart grid*, 2024.

[167] A. I. Aygun, M. S. Hasan, A. Joshi, and S. Kamalasadan, "An optimal hybrid management of electric vehicle fleet charging and load scheduling in active electric distribution system," *IEEE Transactions on Industry Applications*, 2024.

[168] A. Rajaei, O. Arowolo, and J. L. Cremer, "Learning-accelerated admm for stochastic power system scheduling with numerous scenarios," *IEEE Transactions on Sustainable Energy*, 2025.

[169] Z. Zhang, Z. Y. Dong, and C. Yip, "A new charging scheme based on mobile charging robots cluster: A three-level coordinated perspective," *IEEE Transactions on Industrial Informatics*, vol. 20, no. 4, pp. 6900–6912, 2024.

[170] H. Yue, Q. Zhang, X. Zeng, W. Huang, L. Zhang, and J. Wang, "Optimal scheduling strategy of electric vehicle cluster based on index evaluation system," *IEEE Transactions on Industry Applications*, vol. 59, no. 1, pp. 1212–1221, 2022.

[171] K. Šepetanc and H. Pandžić, "A cluster-based model for charging a single-depot fleet of electric vehicles," *IEEE Transactions on Smart Grid*, vol. 12, no. 4, pp. 3339–3352, 2021.

[172] A. K. Mishra and B. Das, "A novel density based clustering approach for electricity theft detection," *IEEE Transactions on Industry Applications*, pp. 1–12, 2025.

[173] M. E. Baran and F. F. Wu, "Optimal capacitor placement on radial distribution systems," *IEEE Transactions on power Delivery*, vol. 4, no. 1, pp. 725–734, 2002.

[174] New York Independent System Operator (NYISO), "Historical load profile," https://www.nyiso.com/load-data, 2024, [Online; accessed 2-Mar-2025].

[175] W. Wang, Z. Han, M. Alazab, T. R. Gadekallu, X. Zhou, and C. Su, "Ultra super fast authentication protocol for electric vehicle charging using extended chaotic maps," *IEEE Transactions on Industry Applications*, vol. 58, no. 5, pp. 5616–5623, 2022.

[176] X. Yang, D. Niu, L. Sun, Z. Ji, J. Zhou, K. Wang, and Z. Siqin, "A bi-level optimization model for electric vehicle charging strategy based on regional grid load following," *Journal of Cleaner Production*, vol. 325, p. 129313, 2021.

[177] H. Dagdougui, F. Bagheri, H. Le, and L. Dessaint, "Neural network model for short-term and very-short-term load forecasting in district buildings," *Energy and Buildings*, vol. 203, p. 109408, 2019.

[178] S. S. Karimi Madahi, H. Nafisi, H. Askarian Abyaneh, and M. Marzband, "Co-optimization of energy losses and transformer operating costs based on smart charging algorithm for plug-in electric vehicle parking lots," *IEEE Transactions on Transportation Electrification*, vol. 7, no. 2, pp. 527–541, 2021.

[179] F. Tuchnitz, N. Ebell, J. Schlund, and M. Pruckner, "Development and evaluation of a smart charging strategy for an electric vehicle fleet based on reinforcement learning," *Applied Energy*, vol. 285, p. 116382, 2021.

[180] S.-A. Amamra and J. Marco, "Vehicle-to-grid aggregator to support power grid and reduce electric vehicle charging cost," *IEEE Access*, vol. 7, pp. 178 528–178 538, 2019.

[181] B. Khaki, C. Chu, and R. Gadh, "Hierarchical distributed framework for ev charging scheduling using exchange problem," *Applied Energy*, vol. 241, pp. 461–471, 2019.

[182] Z. Xu, W. Su, Z. Hu, Y. Song, and H. Zhang, "A hierarchical framework for coordinated charging of plug-in electric vehicles in china," *IEEE Transactions on Smart Grid*, vol. 7, no. 1, pp. 428–438, 2016.

[183] C. B. Saner, A. Trivedi, and D. Srinivasan, "A cooperative hierarchical multi-agent system for ev charging scheduling in presence of multiple charging stations," *IEEE Transactions on Smart Grid*, vol. 13, no. 3, pp. 2218–2233, 2022.

[184] J. Singh and R. Tiwari, "Real power loss minimisation of smart grid with electric vehicles using distribution feeder reconfiguration," *IET Generation, Transmission & Distribution*, vol. 13, no. 18, pp. 4249–4261, 2019.

[185] S. M. Bagher Sadati, J. Moshtagh, M. Shafie-khah, A. Rastgou, and J. P. Catalão, "Operational scheduling of a smart distribution system considering electric vehicles parking lot: A bi-level approach," *International Journal of Electrical Power and Energy Systems*, vol. 105, pp. 159–178, 2019.

[186] G. Irisarri, X. Wang, J. Tong, and S. Mokhtari, "Maximum loadability of power systems using interior point nonlinear optimization method," *IEEE transactions on Power Systems*, vol. 12, no. 1, pp. 162–172, 1997.

[187] V. Farahani, B. Vahidi, and H. A. Abyaneh, "Reconfiguration and capacitor placement simultaneously for energy loss reduction based on an improved reconfiguration method," *IEEE Transactions on power systems*, vol. 27, no. 2, pp. 587–595, 2011.

[188] S. Shafiee, M. Fotuhi-Firuzabad, and M. Rastegar, "Investigating the impacts of plug-in hybrid electric vehicles on power distribution systems," *IEEE transactions on smart grid*, vol. 4, no. 3, pp. 1351–1360, 2013.

[189] C. E. V. Database, 2022, data retrieved from ev-database.org, :https://ev-database.org/.

[190] G. Chrysanidis, D. Kosmanos, A. Argyriou, and L. Maglaras, "Stochastic optimization of electric vehicle charging stations," in *2019 IEEE SmartWorld, Ubiquitous Intelligence and Computing, Advanced and Trusted Computing, Scalable Computing and Communications, Cloud and Big Data Computing, Internet of People and Smart City Innovation (SmartWorld/SCALCOM/UIC/ATC/CBDCom/IOP/SCI)*, 2019, pp. 1–7.

APPENDIX A ARTICLE 4: A TWO-STAGE OPTIMIZATION FRAMEWORK FOR ELECTRIC VEHICLE FLEET DAY-AHEAD CHARGING MANAGEMENT

Authors: Arian Shah Kamrani, Hanane Dagdougui

Submitted on March 15st, 2023 and accepted on May 6rd, 2023 at *IEEE 11th International Conference on Smart Energy Grid Engineering (SEGE).*

Contributions: Conception of the work's idea, implementation of the code, conducting the experiments, analysis of the results, and writing.

A.1 Introduction

The ever-increasing interest in using Electric Vehicles (EVs), due to less pollution and lower charging cost compared to fossil-fueled vehicles, has caused the high penetration of EVs in the power grid [175]. The increased penetration of uncontrolled EVs in terms of charging will lead to some challenges related to power quality control, increased peak-valley difference in the distribution network, line congestion, power grid loss, and voltage deviation [176]. The smart charging of EVs is essential, as it can bring significant techno-economical benefits such as peak load reduction, energy efficiency, and integration of distributed energy resources [177]. In [178], centralized charging coordination has been performed for an EV fleet with the aim of power reducing grid electricity loss and increasing transformer lifespan. In this paper, the Sirjan power grid is used as the grid network and EV uncertainties are modeled as a normal distribution. Authors in [87] implemented a method for coordinated fleet charging of EVs in a re-configurable network. The purpose of this paper is to reduce the cost of charging and network losses by observing the optimal power flow (OPF) restrictions and reducing the aging costs of distribution cables and transformers. Authors in [179] proposed a charging coordination system based on Reinforcement Learning using an artificial neural network as a function approximator. With this method, they were able to reduce the variance of the total load by 65% in comparison with uncontrolled charging. In [180], a day-ahead and real-time framework for smart charging of EVs has been introduced, which aims to reduce the cost of EV charging and control the voltage and frequency of the grid with the help of vehicle-to-grid (V2G) technology. A standard IEEE 33-node distribution network with five EV charging stations is used to demonstrate the effectiveness of the proposed system. Authors in [90] proposed an extended state-space model for large-scale EV aggregation with the aim of

frequency regulation and peak load shaving in power systems. The proposed model improves the flexibility of the EV aggregator by enabling EVs to participate in ancillary services with both regular and fast charging/discharging rates.

In the former cited papers, all required data from dispersed EVs is received by a central entity such as a distribution system operator (DSO) that coordinates the charging demand via a communication network. Subsequently, the optimal charging profiles are sent to the EVs [154]. However, such centralized approaches have the following main problems: (I) As EV owners must communicate sensitive information with the central coordinator, their privacy is at risk (e.g. arrival and departure times as well as their battery energy level and capacity). (II) When EV penetration level increases in the grid, the curse of dimensionality occurs. (III) vulnerability to a single point of failure, i.e. if the central coordinator faces any problems, the whole system breaks down [181]. In order to improve computations, privacy issues and communications, hierarchical and distributed methods have recently received more attention. In [182] a three-level plug-in EV charging strategy is proposed with the aim of jointly optimizing system load profile and charging costs while satisfying customer charging requirements. This paper examines its framework at three levels: provincial level, municipal level, and charging station level in China. Authors in [183] presented a cooperative hierarchical multi-agent system, they proposed an EV charging scheduling strategy in order to minimize the demand and energy charges while meeting the EV users' energy requirements and satisfying the system security constraints. To validate the proposed methodology, a series of case studies on 33-bus and 118-bus distribution test feeders were analyzed. In [184], a two-stage optimization framework has been proposed. EV charging in the first stage is scheduled to minimize battery degradation and filling valleys, and in the second stage, an optimal solution to the distribution feeder reconfiguration has been found with the aim of reducing network electrical losses. A bi-level framework is presented for the operational scheduling of a DSO with EV parking lots and renewable energy sources (RES) in [185]. DSO's profit is maximized at the upper level by minimizing the cost of power purchased from the wholesale market. At the lower level, the profit maximization of EV parking lot owners is investigated by considering many factors such as the cost of battery depreciation and cost of payment to EV owners because of participation in the V2G interaction. In the aforementioned works, different hierarchical frameworks have been investigated. However, to the best of the authors' knowledge, no article has considered smart charging of EVs, while taking into account OPF constraints as well as EV owners' privacy simultaneously.

In this paper, we present an optimal two-stage approach for smart charging of EVs, which takes into account the benefits of EV owners, DSO, and EV aggregators simultaneously. At the upper stage, which considers the benefit of DSO, an OPF is done by the DSO based

on the data sent by aggregators and the maximum power consumption is sent as set-point signals at each time interval to each aggregator specifically. At the lower stage, based on the constraints obtained in the upper stage and with the aim of reducing the charging electricity purchase of each aggregator as well as satisfying EV owners' comfort (desirable departure SoC), optimization is done at each aggregator level. In general, the contributions of this work can be summarized as follows:

- A two-stage semi-private framework for EV smart charging has been introduced, which considers the constraints related to the power grid OPF.
- Unlike uncontrolled charging, the interests of all stakeholders (EV owners, DSO, EV aggregators) are considered in this framework by reducing the cost of purchasing electricity for aggregators, reaching the desirable departure SoC for EV owners, and satisfying OPF constraints as well as grid peak shaving.
- Computational time has decreased compared to the centralized mode, despite the fact that the optimal solution is the same in both architectures.

A.2 Proposed Framework

In this framework, a semi-private two-stage charging of EVs is introduced. This framework is comprised of two stages, and at the lower stage, EV fleet smart charging takes place. Therefore, each EV owner's information is shared only with its related aggregator, and it is not shared with DSO or any other aggregator, which is why we call the framework semi-private. In this work, the goal is to introduce an algorithm for EV charging in order to meet the restrictions related to the power grid and user satisfaction (desirable final SoC), as well as cost reduction of EV charging. The proposed two-stage method scheme is shown in Fig A.1. As shown in this figure, based on EV information prediction in each aggregator (arrival time, departure time and initial State of charge (SoC)), the amount of cumulative energy consumption at each aggregator is calculated and sent to the DSO (specific information for each EV is not sent to DSO).

Taking into account the information sent from each aggregator, an optimal power flow is run at the upper stage, which provides set-point load profiles to each aggregator, and these set-point signals are sent to aggregators as shown in Fig A.1. This signal is actually the maximum amount of power that DSO can provide to each aggregator in day-ahead scheduling. Finally, based on the information sent from the DSO, electricity market, and information of EVs, fleet smart charging is performed at the lower stage with the aim of reducing the cost

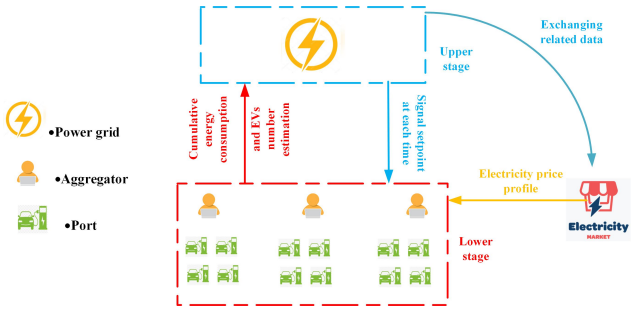

Figure A.1 Proposed method scheme.

of charging, while ensuring user satisfaction at each aggregator. From the DSO perspective, power set-point calculation ensures that the network constraints are always satisfied even when there are multiple EV fleet charging transactions across the distribution system. From the data privacy point of view, the EV aggregator does not need power system data to satisfy the security limits while scheduling EVs. Similarly, the DSO agent does not receive the individual EV-related data such as arrival/departure time, rated power, battery capacity, and SoC, but only the aggregated schedules, which is anonymized data.

A.3 Problem formulation

A.3.1 Upper-stage: maximum power set-point evaluation by DSO

As mentioned in Section A.2, in order to perform the smart charging of EVs, there must be a coordination between EV aggregators and DSO. At the upper stage, DSO calculates a parameter named maximum set-point power at each time interval upon the request of each aggregator in order to ensure that the network constraints are satisfied while scheduling EV fleet charging. DSO evaluates the maximum power set-point at each time interval by solving the following optimization problem:

$$OF_1 = \max_{I_c, V_b, \delta_b, (b,j) \in \mathcal{B}, \mathcal{C}, \mathcal{I}} P_i^{max}(t) \tag{A.1}$$

$$\text{s.t. } P_{bj} = y_{bj} \left(V_b^2 \cos\left(\theta_{bj}\right) - V_b V_j \cos\left(\delta_b - \delta_j - \theta_{bj}\right) \right) \tag{A.2}$$

$$Q_{bj} = y_{bj} \left(V_b^2 \sin\left(\theta_{bj}\right) - V_b V_j \sin\left(\delta_b - \delta_j - \theta_{bj}\right) \right) \tag{A.3}$$

$$\sum_{j: y_{bj} \neq 0} P_{bj} = \frac{P_b^g(t) - \left(P_b^d(t) + P_i^{max}(t) \right)}{S_{base}} \tag{A.4}$$

$$\sum_{j:y_{bj}\neq 0} Q_{bj} = \frac{Q_b^g(t) - Q_b^d(t)}{S_{base}} \tag{A.5}$$

$$\underline{V_b} \leq V_b \leq \overline{V_b} \tag{A.6}$$

$$\underline{\delta_b} \leq \delta_b \leq \overline{\delta_b} \tag{A.7}$$

$$I_c \leq \overline{I_c} \tag{A.8}$$

$$\sqrt{P_{bj}^2 + Q_{bj}^2} \leq \bar{S}_{bj}/S_{base} \tag{A.9}$$

Introducing the notations in this section, I_b is the current at each branch, $V_b\angle\delta_b$ is the per-unit complex voltage at bus j, and $y_{bj}\angle\theta_{bj}$ is the per-unit series admittance between buses b and j. S_{base} is the kVA base for per-unit calculations. $P_{bj}\,(Q_{bj})$ is the per-unit real (reactive) power flow from bus b to bus j.$P_b^g(t)\,(Q_b^g(t))$ and $P_b^d(t)\,\left(Q_b^d(t)\right)$ are the kW (kVAr) real (reactive) power generation and demand, excluding the EV load, at bus b for time interval t, respectively. Indices *(b,j)*, t and i correspond to the bus, time interval, and the bus to which the EV aggregator is connected respectively. $\mathcal{B}$, $\mathcal{I}$, and $\mathcal{C}$ is the set of Buses in the distribution system, the bus to which the EV aggregator is connected, and the distribution network branches respectively.

Equation A.1 is the objective function that aims to calculate the maximum power set-point that DSO can provide to each aggregator. The constraints A.2- A.5 are the OPF equations. Equation A.6 is the voltage magnitude, equation A.7 is the voltage angle, equation A.8 is the current magnitude, and equation A.9 is the apparent power flow constraints. Since the upper-stage problem is a special case of the maximum loadability problem, the interior point method is used for efficiency as suggested in [186].

A.3.2 Lower-stage: EV aggregators and EV owners charging cost reduction

At the lower stage, the goal is to reduce EV fleet charging costs in each aggregator, taking into account the limitations obtained from the upper-stage optimization and EV user preferences. As a result, the optimal solution is obtained by solving the following optimization problem at each aggregator level:

$$OF_{2i} = \min_{n,i\in\mathcal{I}} \; E_i^{agg}(t).pr(t) \tag{A.10}$$

$$\underline{SoC}_{n,i} \leqslant SoC_{n,i}(t) \leqslant \overline{SoC}_{n,i} \tag{A.11}$$

$$p_{n,i}(t) \leqslant \overline{\gamma}_{c_{n,i}} \tag{A.12}$$

$$p_i^{agg}(t) \leqslant \ P_i^{max}(t) \tag{A.13}$$

$$SoC_{n,i}^{des} \leqslant SoC_{n,i}^{dep} \tag{A.14}$$

Introducing the notations in this section, $E_i^{agg}(t)$ and $pr(t)$ are the energy consumption and electricity price at aggregator i. $SoC_{n,i}(t)$ and $p_{n,i}(t)$ are the SoC and power injection to the EV number n at aggregator i at each time interval. $\overline{\gamma}_{c_{n,i}}$ is the upper bound for the rate of charge of each EV battery at aggregator i. $p_i^{agg}(t)$ is the aggregator i power consumption and $p_i^{max}(t)$ is the maximum power set-point calculated in the upper-stage optimization problem. $\underline{SoC}_{n,i}$ and $\overline{SoC}_{n,i}$ are maximum and minimum acceptable SoC for EV number n at aggregator i which are 20% and 100% in this work. Finally, $SoC_{n,i}^{des}$ and $SoC_{n,i}^{dep}$ are each EV's desired and departure SoC at aggregator i, respectively.

Equation A.10 is the objective function that aims to minimize the charging cost of each aggregator. Equation A.11 guarantees that in each time interval, SoC of each EV is between the maximum and minimum allowed value for that particular EV. In A.12, the condition related to the maximum charging rate at each time interval is checked, equation A.13 satisfies the DSO constraint which is obtained from the upper stage, and finally, equation A.14 guarantees the EV user's satisfaction condition at the departure time.

Table A.1 Various types of EV and their key parameters

Type	Segment	Vehicle	Penetration level	E_c(kWh/mile)	BC(kWh)
PHEV	1	Compact sedan	20%	0.26	10.4
	2	Mid-size sedan	30%	0.3	12
	3	Mid-size SUV	30%	0.38	15.2
	4	Full-size SUV	20%	0.46	18.4
BEV	A/B (small vehicles)	BMW i3 120 Ah I	50%	0.26	42.2
	C (medium vehicles)	Kia e-Niro	10%	0.28	64
	D (large vehicles)	Tesla Model 3 Long Range Performance	24%	0.27	75
	E+ (Executive and luxury vehicles)	Tesla Model X Long Range	16%	0.35	100

A.4 Case study

In order to demonstrate the efficiency of the proposed framework, a modified IEEE 33-bus network has been used, and different types of load profiles mentioned in [187] have been randomly assigned to the network nodes. Fig A.2 shows the location of aggregators on the

IEEE 33-bus network. As shown in this figure, three aggregators are placed in buses 8, 22, and 32 with estimated capacities of 75, 75, and 150 respectively for day-ahead planning. Most EVs today fall into two main categories, plug-in hybrid electric vehicles(PHEVs) and Battery electric vehicles (BEVs). Information about different types of PHEVs [188] and BEVs [189] and their market share [190] is given in TABLE A.1. Considering the uncertainty related to the behavior of EV owners, EV mobility data are assumed to follow a Gaussian characteristic. The mean and standard deviations for the arrival time of EVs in aggregator1, aggregator2, and aggregator3 are (12h00, 1h00),(11h00, 2h00), and (9h00, 2h00) respectively. Moreover, The mean and standard deviations for the departure time of EVs in aggregator1, aggregator2, and aggregator3 are (18h00, 2h00),(18h00, 1h00), and (16h00, 2h00) respectively. Also, initial SoC level distributions for all EVs are (50%, 10%), respectively. The desired departure SOC is set to 100%. Moreover, the SAE J1772-2017 standard defines four levels of charging: AC Level 1, AC Level 2, DC Level 1, and DC Level 2. To ensure flexibility, at the upper stage, an additional 10% of the cumulative energy consumption sent by the aggregator to the DSO during EV presence at the stations is taken into account for each aggregator. This is because only the aggregators know the arrival and departure times of EVs, and flexibility is required. In this study, it is assumed at the lower level that EVs use a single-phase connection to the grid with a maximum charging power of 19.2 kW, (EVs use ac-level 2 charging). Finally, a real-time pricing scheme is used for energy management of EV charging as given in [87].

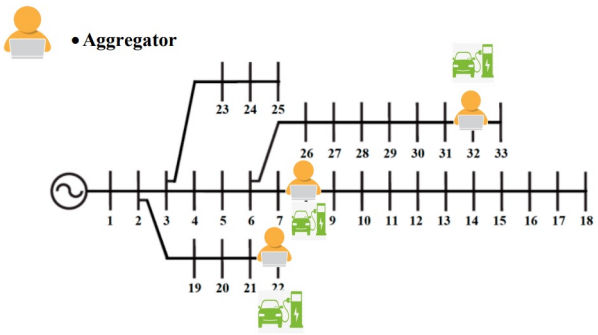

Figure A.2 Location of aggregators on the IEEE 33-bus network.

A.5 Simulation results

A.5.1 Charging management

In this section, the results of optimization are analyzed. For the purpose of comparison, two scenarios of uncontrolled charging and smart charging are considered. In the uncontrolled

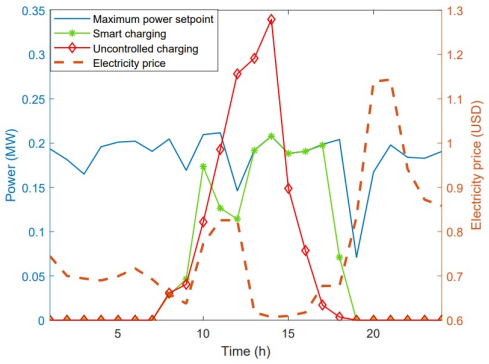

(a) Aggregator 1

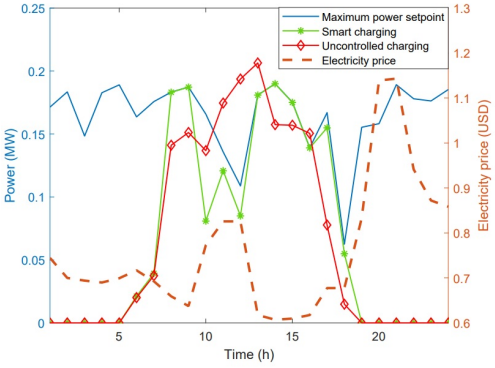

(b) Aggregator 2

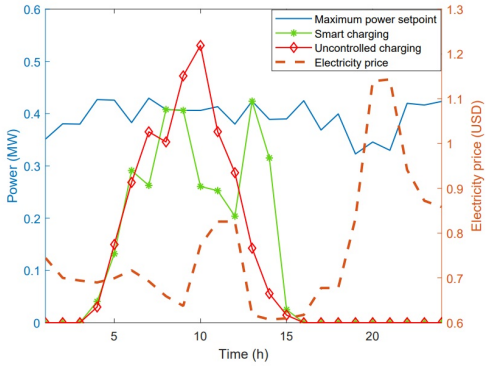

(c) Aggregator 3

Figure A.3 Aggregators' load profiles.

charging scenario, each EV is charged at a fixed rate of 15 kW as soon as it reaches the charging port. In the smart charging scenario, the charging rate of EVs in each aggregator at each time interval can be different according to the objective functions mentioned in Section A.3. The load profiles of the three mentioned aggregators in different scenarios, as well as the electricity price profile are shown in Fig A.3. In this figure, three periods of electricity pricing are used: 1) on-peak (between 19 to 22), 2) mid-peak (between 10 to 13), and 3) off-peak (the rest of the day). The maximum power set-point in these figures is obtained from the upper-stage optimization, which is explained in section A.3. This profile indicates the maximum power capacity that DSO can provide to each aggregator at each time interval.

In Fig A.3, it can be seen that in all aggregators, the restrictions related to the maximum power set-point are satisfied in the smart charging scenario, and the power consumption of each aggregator does not exceed its corresponding limit in all time intervals. It can also be seen in this scenario that during off-peak periods, aggregators prefer to use all the capacity they have and charge EVs. According to the restrictions related to user preference (desirable final SoC) and EVs' departure time, aggregators may have to charge EVs during mid-peak. For instance, in aggregator 1, because the standard deviation in arrival time is less than the other two aggregators, it can be seen that EVs reach the charging ports almost simultaneously. As a result, a more severe situation prevails in the uncontrolled charging scenario, and we see a significant peak of charging in this scenario. Moreover, in Fig A.3, it can be observed that EV aggregators prefer to charge EV batteries up to the desired SoC before entering the on-peak period, to avoid charging EVs during this period. Finally, in the uncontrolled charging scenario, the aggregators' power consumption is higher than the permissible limit in some hours and exceeds the maximum power set-point, which leads to the violation of the restrictions related to the upper stage, and causes the OPF not to be established in the power network.

In Fig A.4, the electricity price and daily load profile of the entire power grid are shown in different scenarios. As can be depicted in this figure, in the uncontrolled charging scenario, the peak of the network has increased more compared to the smart charging scenario. It can also be seen that in the smart charging scenario, charging of EVs is mainly done during the off-peak period, whereas in the uncontrolled charging scenario, most of the charging is done in the Mid-peak period. TABLE A.2 demonstrates the comparison between the results of these two scenarios. It can be seen that the cost of charging, as well as network peak in smart charging have decreased compared to uncontrolled charging by 5.31% and 4.90% respectively. Moreover, contrary to smart charging, load flow restrictions are not satisfied in the uncontrolled charging mode. Furthermore, The random EV charging process is shown in Fig A.5. In this figure, the charging process of PHEVs is shown using dashed lines and as

can be seen, due to their lower battery capacity, their charging process is faster than BEVs, whose charging process is displayed by solid lines.

Table A.2 Comparison Between Two Scenarios

Scenario	Charging Cost	Peak of the Network (MW)	OPF Validity
Smart charging	416.21	2.91	Yes
Uncontrolled charging	439.57	3.06	No

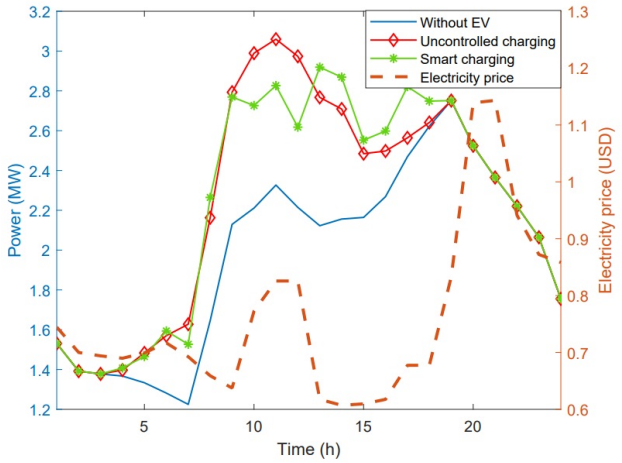

Figure A.4 Network load profile.

A.5.2 Centralized vs. proposed hierarchical method

In order to show the advantage of the proposed hierarchical method compared to the centralized method, optimization was done once again with the centralized method (both OPF and charging were done at the level of DSO), and the optimal charging profile in the network, in this case, was exactly the same as the optimal profile in the hierarchical mode. From the processing time viewpoint, time per iteration in the optimization process was analyzed in two centralized and proposed hierarchical modes for the first 20 iterations. For the centralized method average time per iteration is 90.99 seconds however for the proposed hierarchical method this time is 65.72 seconds. The simulation was done on an Intel(R) Core(TM) i7-8565u@ 1.80 GHz laptop using the MATLAB optimization toolbox.

A.6 Conclusion

In this paper, a two-stage framework for smart charging of EVs was presented, which simultaneously considers the interests of DSO, EV aggregators, and EV owners. For the

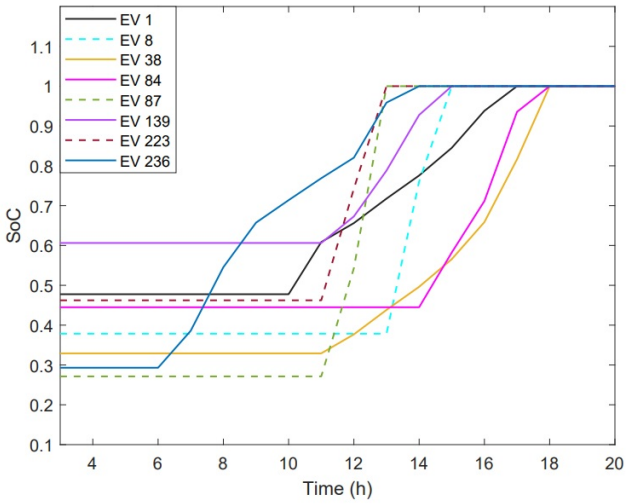

Figure A.5 Random EVs charging process.

purpose of privacy, the information of EVs is first sent to DSO in a cumulative form by EV aggregators. Then, following the calculations performed by DSO at the upper stage, taking into account the limitations of the power network, power set-point signals are sent to each aggregator. At the lower stage, smart charging of EV fleets is performed in aggregators with the aim of reducing charging costs and respecting EV owners' preferences, taking into account upper-stage constraints. The proposed framework was implemented on the IEEE 33-bus network and the results showed that the cost of charging and the peak of the network have decreased by 5.31% and 4.90% respectively compared to uncontrolled charging. Moreover, unlike uncontrolled charging, in this case all the restrictions related to the OPF in the power network are satisfied. Finally, the computation time of the proposed hierarchical framework was compared with the centralized scheme and it showed the superiority of the proposed hierarchical method. For future work, distributed optimization can be investigated in which the privacy of EV owners is fully respected.